

AMERICAN UNIVERSITY OF BEIRUT

EFFECT OF LOADING RATE, TEMPERATURE AND
ADHESIVE BONDLINE THICKNESS ON THE
MECHANICAL RESPONSE OF DISSIMILAR CFRP-STEEL
SINGLE LAP JOINTS BONDED WITH FLEXIBLE
ADHESIVE

by
MOHAMAD JAMAL AL ZEENNI

A thesis
submitted in partial fulfillment of the requirements
for the degree of Master of Engineering
to the Department of Mechanical Engineering
of the Maroun Semaan Faculty of Engineering and Architecture
at the American University of Beirut

Beirut, Lebanon
December 2021

AMERICAN UNIVERSITY OF BEIRUT

EFFECT OF LOADING RATE, TEMPERATURE AND
ADHESIVE BONDLINE THICKNESS ON THE
MECHANICAL RESPONSE OF DISSIMILAR CFRP-STEEL
SINGLE LAP JOINTS BONDED WITH FLEXIBLE
ADHESIVE

by
MOHAMAD JAMAL AL ZEENNI

Approved by:

Ramsey F. Hamade

Dr. Ramsey Hamade, Professor
Department of Mechanical Engineering

Advisor

Mu'tasem

Dr. Mu'Tasem Shehadeh, Associate Professor
Department of Mechanical Engineering

Member of Committee

Walid Saad

Dr. Walid Saad, Associate Professor
Department of Chemical Engineering and Advanced Energy

Member of Committee

Ilige Hage

Dr. Ilige Hage, Assistant Professor
Notre Dame University-Louaize

Member of Committee

Date of thesis defense: December 14, 2021

AMERICAN UNIVERSITY OF BEIRUT

THESIS RELEASE FORM

Student Name: Al Zeenni Mohamad Jamal
Last First Middle

I authorize the American University of Beirut, to: (a) reproduce hard or electronic copies of my thesis; (b) include such copies in the archives and digital repositories of the University; and (c) make freely available such copies to third parties for research or educational purposes:

- As of the date of submission
- One year from the date of submission of my dissertation.
- Two years from the date of submission of my dissertation.
- Three years from the date of submission of my dissertation.



04/01/2022

Signature

Date

ACKNOWLEDGEMENTS

I would like first to express my sincere gratitude for my advisor, Dr. Ramsey Hamadeh, for his guidance and advice throughout the course of writing this thesis. I would also like to extend this gratitude for the thesis committee, Dr. Mu'Tasem Shehadeh, Dr. Walid Saad and Dr. Ilige Hage, for their constructive criticism and insightful comments.

Finally, I would like to thank my family and friends for their continuous motivation and encouragement.

ABSTRACT OF THE THESIS OF

Mohamad Jamal Al Zeenni for

Master of Engineering

Major: Mechanical Engineering

Title: Effect of Loading Rate, Temperature and Adhesive Bondline Thickness on the Mechanical Response of Dissimilar CFRP-Steel Single Lap Joints Bonded with Flexible Adhesive

The impressive properties of composite materials have allowed their integration in various structural and light weight applications. This large dependence on composites has resulted in multiple situations where bonding with other materials is required. Of the possible bonding mechanisms, adhesive bonding offers significant advantages such as eliminating stress concentration sites and the ability to bond brittle material. Single lap joints are considered a simple and efficient joining configuration that allows the bonding of two materials along an adhesive overlap. Consequently, analyzing the performance of single lap joints that incorporate composites bonded to different materials is highly important.

The performance of dissimilar CFRP-Steel single lap joints was investigated under variable operating conditions (testing temperature, loading rate) and adhesive bondline thickness. All joints were fabricated using a simple mold design that allowed the production of consistent lap joints with precise bondline thickness. Experimental results showed a general decrease in single lap joint shear strength at elevated temperatures; however, the strain rate effect was more evident upon increasing the temperature within the adhesive's heat resistance range resulting in enhanced single lap joint shear strength. Furthermore, analysis of variance (ANOVA) results show that testing temperature has a larger contribution to the lap shear strength compared to the loading rate. On the other hand, the lap shear strength decreased progressively with the increase in bondline thickness.

Finally, a material characterization process was performed to extract the hyperelastic parameters of the flexible adhesive under study, particularly Mooney-Rivlin and Neo-Hookean parameters. A hyperelastic numerical model was then established and showed impressive accuracy in replicating the experimental and analytical results for a selected case study of operating conditions.

TABLE OF CONTENTS

ACKNOWLEDGEMENTS	1
ABSTRACT	2
ILLUSTRATIONS	6
TABLES	8
ABBREVIATIONS	10
INTRODUCTION	12
1.1. Motivation and Research Questions	13
1.2. Methodology	16
LITERATURE REVIEW	17
2.1. Adhesion	17
2.1.1. Mechanical Interlocking	17
2.1.2. Adsorption	18
2.1.3. Diffusion	18
2.1.4. Electrostatic Theory	19
2.2. Adhesive Types.....	19
2.2.1. MS Polymer Adhesives	20
2.2.2. Epoxy Adhesives	21
2.2.3. Polyurethane Adhesives.....	23
2.2.4. Acrylic Adhesives.....	24
2.3. Hyperelasticity	25

2.4. Related Work	26
ANALYTICAL MODELS	30
3.1. Volkersen Model.....	31
3.2. Goland and Reissner Model.....	34
EXPERIMENTAL VARIABLES	36
4.1. Temperature	37
4.2. Loading Rate.....	38
4.3. Adhesive Thickness	39
EXPERIMENTAL TESTING	41
5.1. Material Characterization	41
5.1.1. Adhesive Material.....	41
5.1.2. Adherend Material	43
SINGLE LAP JOINT FABRICATION AND TESTING	45
6.1. Dimensions	45
6.2. Surface Treatment.....	46
6.2. Mold Preparation	47
6.4. Single Lap Joint Bonding	48
6.5. Testing	50
EXPERIMENTAL RESULTS	52
7.1. Impact of Testing Temperature and Loading Rate	52

7.1.1. ANOVA Study.....	53
7.2. Impact of Adhesive Thickness.....	55
7.3. Failure Modes	56
7.3.1. Tested Samples Failure Modes	57
NUMERICAL MODELING	60
8.1. Numerical Results.....	65
8.1.1. Stress Distribution.....	65
8.1.2. Force-Displacement Curves.....	84
8.2. Numerical Results Discussion	87
CONCLUSION	88
APPENDIX	89
REFERENCES	91

ILLUSTRATIONS

1. Various lap joint configurations : (a) single lap joint, (b) double lap joint, (c) tapered lap joint, (d) scarf joint, (e) butt joint, (f) single strap joint, (g) double strap joint.	13
2. Adhesive bonding utilized in the Airbus A380. [11].....	15
3. Composite usage in various commercial aircraft. [12].....	16
4. Proposed experimental and numerical study.	16
5. The mechanical interlocking mechanism.	18
6. The adsorption theory showing the van der Waals attracting forces.....	18
7. Interdiffusion of molecules between adhesive and adherend material.	19
8. The electron transfer between adhesive and adherend at the interface.....	19
9. MS polymer chemical structure having a polyether group in the polymeric backbone and two active dimethoxy silane groups. [20].....	20
10. The general synthesis of epoxy resin.	22
11. The general synthesis of polyurethane. [26].....	23
12. The chemical structure of two acrylic monomers: (a) methyl methacrylate [30] and (b) acrylic acid [18].....	25
13. Difference in shear stress distribution predicted by classical analysis and analysis that consider zero shear stress at overlap ends. [57].....	31
14. Single lap joint configuration to derive the Volkersen model. (a) Parameters of the Volkersen model (b) Elemental diagram.	32
15. The parameters and SLJ configuration of Goland and Reissner model.	34
16. Stress distribution along bondline for stiff and ductile adhesives. [63].....	37
17. Lap-shear strength as a function of adhesive's ductility and strength. [65]	38
18. Shear and normal stress improvement with increased strain rate for a selected epoxy resin. [71]	39
19. Stress distribution in (a) thick bondline and (b) thin bondline single lap joint. [44].....	40
20. (a) ASTM D638 dimensions (b) Fully cured bulk MS polymer sample.	42
21. MS polymer: Three stress-strain response curves coplotted (Loading rate = 50 mm/min; Testing temperature = 25°C).	42

22. The Hounsfield H100KS universal tensile testing machine mounted with an environmental chamber and laser extensometer.	43
23. Single lap joint configuration with letter codes representing geometrical dimensions.	45
24. Sandblasted steel samples.	47
25. Dimensions and CAD model of the fabricated mold with a 3.26 mm step size.	48
26. Top (a) and side (b) views of the machined mold.	48
27. Placement of SLJ adherends and adhesive material on the fabricated mold.	49
28. Bonding process of one single lap joint sample.	49
29. Uniform adhesive bondline thickness along the overlap length.	50
30. Various fabricated single lap joints.	50
31. Tensile testing of a SLJ specimen placed in the environmental chamber.	51
32. Effect of operating conditions on the average shear strength of the adhesively bonded single lap joints.	53
33. Average shear strength as a function of adhesive thickness with standard error bars.	55
34. Various failure modes of FRP adhesive bonded joints. [27]	56
35. Modelled SLJ specimen.	63
36. The applied boundary conditions on the modeled SLJ specimen.	64
37. Meshing of the SLJ model with a higher mesh density in the overlap region.	64
38. Centerline (red) selected to extract the stress distributions	65

TABLES

Table

1. Various applications of MS polymer adhesives and sealants. [19]	21
2. Various applications of epoxy adhesives. [22] [24] [25].....	22
3. Various applications of polyurethane adhesives.....	24
4. Various applications of acrylic adhesives.....	25
5. Results obtained from literature for single lap joints tested under different testing conditions and composed of different material combinations.	29
6. AMS 55 material properties.....	43
7. CFRP adherend material properties.....	44
8. Steel adherend material properties.....	44
9. Dimensions of the fabricated SLJ joints.....	46
10. ANOVA analysis performed on the tested samples.	54
11. Surface morphology of the tested joints after failure.	58
12. Surface morphology of the tested joints with different adhesive bondline thickness.....	59
13. Hyperelastic parameters obtained after the fitting process.	63
14. Numerical results (Neo-Hookean and Mooney-Rivlin models) obtained for 0.76mm adhesive bondline thickness, where the maximum experimental force is applied for the selected joints.	66
15. Numerical results (Neo-Hookean and Mooney-Rivlin models) obtained for 1mm adhesive bondline thickness, where the maximum experimental force is applied for the selected joints.	72
16. Numerical results (Neo-Hookean and Mooney-Rivlin models) obtained for 1.2mm adhesive bondline thickness, where the maximum experimental force is applied for the selected joints.	78
17. Numerical force-displacement curves coplotted with the experimental results for the selected joints having a 0.76mm adhesive bondline thickness.	84
18. Numerical force-displacement curves coplotted with the experimental results for the selected joints having a 1mm adhesive bondline thickness.	85
19. Numerical force-displacement curves coplotted with the experimental results for the selected joints having a 1.2mm adhesive bondline thickness.	86

20. Experimental testing summary for single lap joints tested under variable testing temperature and loading rate.....	89
21. Experimental testing summary for single lap joints fabricated with different bondline thicknesses.	90

ABBREVIATIONS

SLJ: Single lap joint

CFRP: Carbon fiber reinforced polymer

P: Force per unit width

h: Adhesive thickness

G_a : Adhesive shear modulus

E: Young's modulus

$E_{a,1}$: Young's modulus of adherend 1

t_1 : Thickness of adherend 1

$E_{a,2}$: Young's modulus of adherend 2

t_2 : Thickness of adherend 2

l: Overlap length

c: Half overlap length

σ_1 : Axial stress in upper adherend

σ_2 : Axial stress in lower adherend

ε_1 : Axial strain in upper adherend

ε_2 : Axial strain in lower adherend

τ : Shear stress

δ : Relative horizontal displacement between upper and lower adherend

γ_s : Shear strain

E_{11} : Longitudinal Young's modulus

ν_{12} : In – plane Poisson's ratio

ρ : Density

ν : Poisson's ratio

L_1 : Length of adherend 1

L_2 : Length of adherend 2

Partial SS: Partial sum of squares

df: Degrees of freedom

MS: Mean square

F: Ratio between mean square of independent variable and mean square of the residual

U: Strain energy potential

\bar{I}_1 : First deviatoric strain invariant

\bar{I}_2 : Second deviatoric strain invariant

C_{ij} & D_i : Hyperelastic material parameters

J_{el} : Elastic volume ratio

J: Total volume ratio

λ_i : Principal stretches

CHAPTER 1

INTRODUCTION

Composite materials have been extensively integrated in modern structures due to their weight savings, durability, and design flexibility. These properties have made composites perfect candidates for usage in aerospace and automobile applications. This large dependence on composites, has resulted in an increasing need for bonding with different materials. Typical joining methods include riveting, bolting, welding, and brazing. In comparison to the specified joining techniques, adhesive bonding has been widely investigated and integrated in industrial applications such as aerospace and marine structures [1]. Adhesive bonding is an effective joining method that allows the efficient bonding of similar and dissimilar materials. Furthermore, adhesive joining resolves typical problems faced by riveting and bolting, where stress concentrations are induced due to the creation of holes. It also allows the bonding of galvanically problematic metals [2] and provides improved corrosion resistance [3]. Adhesive bonding allows the elimination of various machining and forming techniques and provides an appreciable fatigue resistance compared to riveted elements [4]. Adhesively bonded joints have been integrated in various applications and have seen multiple uses. Brittle adherends, on one hand, are typically adhesively bonded rather than mechanically fastened to prevent damage due to drilling [5]. Moreover, adhesive bonding has seen usage in the aerospace industry in various applications where epoxies are utilized to bond aluminum skins to the aircraft's body [6]. Adhesive bonding can also be used in integral fuel tanks since they can prevent fuel and pressure leakage [7].

Adhesive bonding has been used in multiple geometrical configurations such as single lap joints, double lap joints and scarf joints. Of all designs, single lap joints (SLJ)

have received major attention as they are considered the most common joint designs employed in industry, and allow simple determination of adhesive joint properties [3]. Adhesive models are typically analyzed through analytical solutions and numerical simulations using the finite element method (FEM). Analytical solutions have been researched extensively starting with the Volkersen analysis [8], and Goland and Reissner's [9] improved solution. Multiple theories were then developed to accurately model the stress distribution in adhesively bonded single lap joints. The mentioned analytical models, as well as other, cannot determine the strength of adhesively bonded joints without an uncertainty factor [10]. Consequently, numerical models have been a more popular route to study adhesively bonded single lap joints.

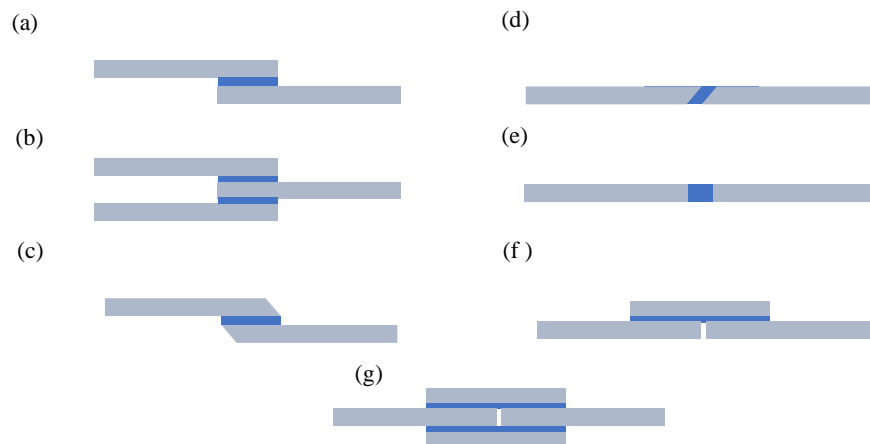


Figure 1. Various lap joint configurations : (a) single lap joint, (b) double lap joint, (c) tapered lap joint, (d) scarf joint, (e) butt joint, (f) single strap joint, (g) double strap joint.

1.1. Motivation and Research Questions

The impressive properties and weight reductions of composite materials have allowed their integration in multiple fields. Similarly, adhesive bonding has been the joining method of choice for various applications. This integration in multiple areas requires a comprehensive study to analyze the effect of various conditions on their

performance. The proposed study examines the impact of operating conditions such as temperature and loading rate on the performance of single lap joints bonded with MS polymer-based adhesive. Moreover, the effect of variable bondline thickness will also be analyzed. The impact of these variables is highly important as it provides users of such bonded systems with guidance regarding their usage in areas where they are exposed to elevated temperatures and are under variable loading rates. Moreover, economic benefits attributed to possible reduction in material usage can also be considered a result of the presented study. Another direct benefit of the proposed study is covering the gap in literature regarding the performance MS polymer or silyl modified polymer adhesives that have a significant industrial importance. Moreover, this research aims to analyze the performance of dissimilar single lap joints with adherends having dissimilar thicknesses. Finally, the applicability of the hyperelastic numerical model will be analyzed for the selected flexible adhesive. Consequently, the proposed study provides paramount information regarding impact of operating conditions (testing temperature and loading rate) and adhesive thickness on the performance of adhesively bonded single lap joints. The research questions and methodology followed to tackle them can be summarized as follows:

1) **Impact of testing conditions , temperature and loading rate, on the performance of CFRP-Steel single lap joints.**

The fabricated single lap joints will be tested in a universal testing machine (UTM) mounted with an environmental chamber that allows variation of testing temperature.

2) **Impact of adhesive thickness on the performance of CFRP-Steel single lap joints.**

In addition to the tensile testing of the fabricated joints, a mold design is presented in this study that allows simple variation of adhesive bondline thickness.

3) Impact of operating conditions and adhesive bondline thickness on dissimilar single lap joints.

All fabricated joints are composed of two different adherends with dissimilar thicknesses: carbon fiber reinforced polymer (CFRP) and steel.

4) Applicability of the hyperelastic model in modeling single lap joints bonded with the flexible MS polymer adhesive.

A hyperelastic numerical model will be established to extract the force - displacement curves and the stress distribution along the adhesive bondline. The obtained numerical results will be compared to the applicable analytical solutions and experimental results to ensure the accuracy of the hyperelastic model.

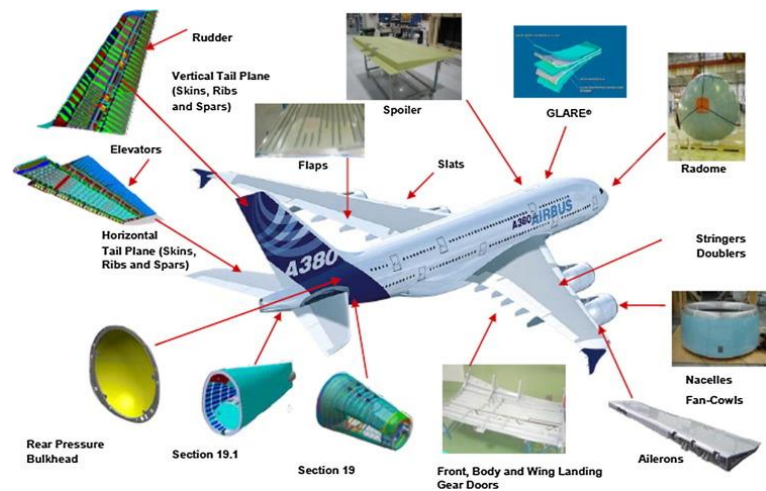


Figure 2. Adhesive bonding utilized in the Airbus A380. [11]

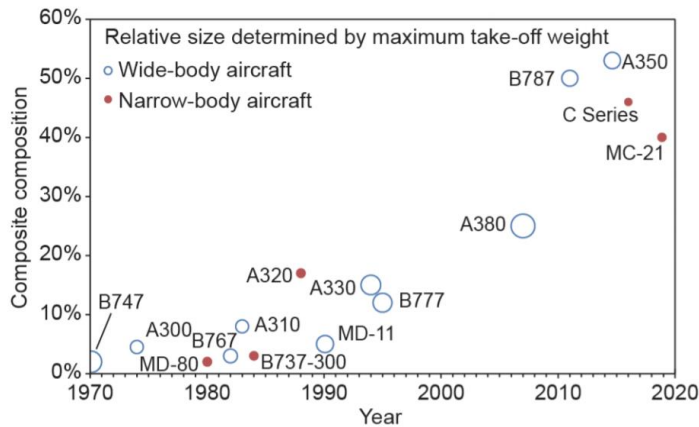


Figure 3. Composite usage in various commercial aircraft. [12]

1.2. Methodology

In this study a comprehensive experimental and numerical analysis is performed to test the effects of temperature, loading rate and adhesive thickness on the performance of adhesively bonded single lap joints. Dissimilar (CFRP – Steel) adhesively bonded single lap joints are tested under variable conditions and the experimental results are integrated in a numerical and analytical study. A statistical analysis was also performed to deduce the contribution and main effect of the selected variables on the lap joint shear strength. The experimental and numerical methodology can be summarized as follows:

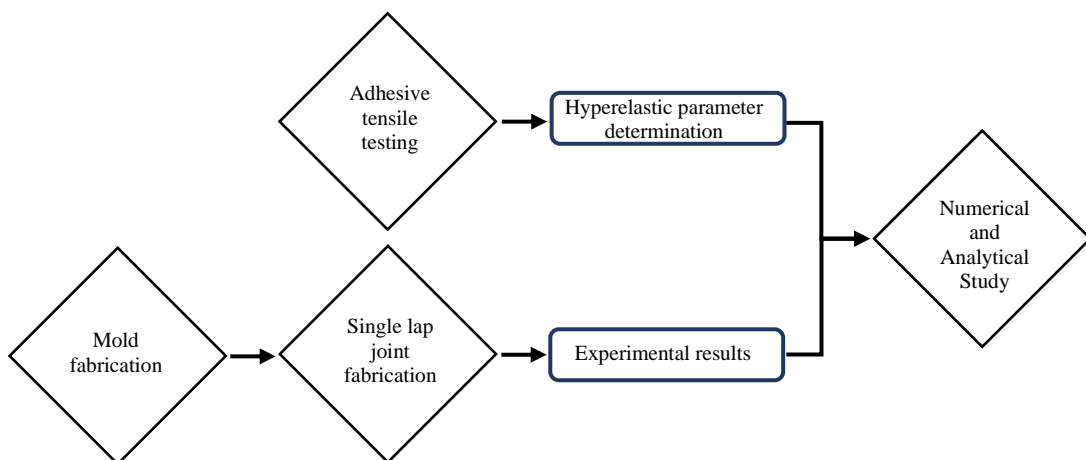


Figure 4. Proposed experimental and numerical study.

CHAPTER 2

LITERATURE REVIEW

2.1. Adhesion

Adhesion can be simply defined as the attraction between substances [3]. The materials being bonded are termed as adherends or substrates while the bonding substance is referred to as the adhesive. In an adhesive system, the achievement of an acceptable bond requires the following conditions to be satisfied: formation of a strong bond between substrate and adhesive, the adhesive must have sufficient strength to transfer load from one substrate to the other, and the adhesive must accommodate the difference in thermal expansion between itself and the bonded substrates [13]. There is no single mechanism by which adhesion occurs, but rather multiple different mechanisms are responsible for adhesion with the role of each depending on the bonding system [14]. The primary theories that describe the mechanism of adhesion are mechanical interlocking, adsorption, diffusion, and the electrostatic theory. A schematic of various theories of adhesion are shown in Figures 5, 6, 7 and 8 which are based on figures from [15].

2.1.1. Mechanical Interlocking

Mechanical interlocking is the penetration of adhesive material into the pores and irregularities on the surface of a rough substrate. This process allows the adhesive to penetrate through the pores of both adherends and thus bonding them together. Adhesives typically form tougher bonds to rough abraded surfaces rather than smooth surfaces; however, it is not always the case as decent adhesion can occur between smooth surfaces [14].

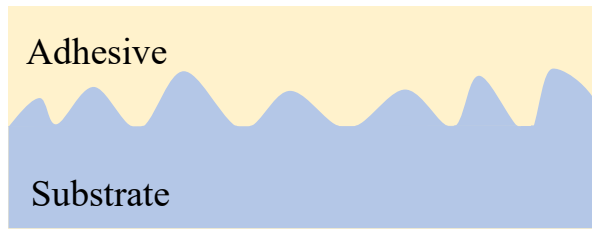


Figure 5. The mechanical interlocking mechanism.

2.1.2. Adsorption

The adsorption theory states that when close and intimate contact is attained at the interface between adhesive and substrate, adhesion will take place due to the pairwise interaction between involved atoms and molecules [16]. In fact, a bond develops from adsorption of adhesive molecules on the substrate and the attractive forces known as the van der Waals forces [17].

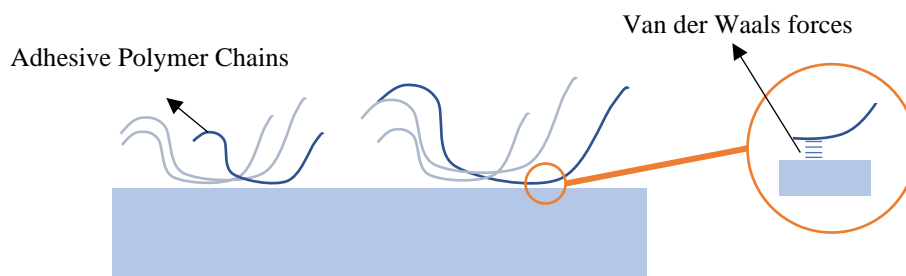


Figure 6. The adsorption theory showing the van der Waals attracting forces.

2.1.3. Diffusion

Diffusion theory states that adhesion occurs due to interdiffusion of molecules between the adhesive material and adherends. This theory is highly applicable when both adhesives and adherends are polymers with free to move long chain molecules [14].

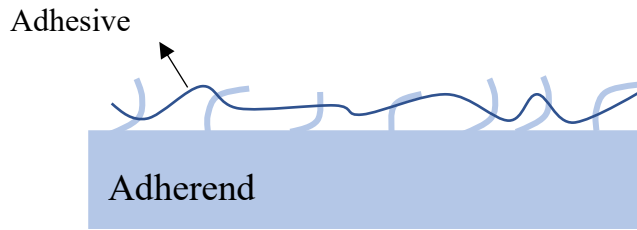


Figure 7. Interdiffusion of molecules between adhesive and adherend material.

2.1.4. *Electrostatic Theory*

The electrostatic theory considers that forces in the form of an electrical double layer are invoked at the adhesive adherend interface which results in adhesion [17]. The electrical double layer occurs at the interface where electron transfer between the adhesive and adherend takes place.

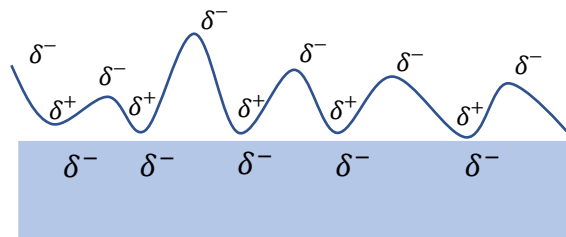


Figure 8. The electron transfer between adhesive and adherend at the interface.

2.2. Adhesive Types

Multiple adhesive types exist and are integrated into a variety of bonding and sealing applications. MS polymer adhesives have seen an increasing usage in numerous applications due to their promising properties. Moreover, epoxy based, urethane and acrylic adhesives have been researched extensively due to their integration in many commercial applications [18]. A general description regarding the composition, advantages and applications of various adhesive types will be provided.

2.2.1. MS Polymer Adhesives

MS polymer adhesives are hybrid adhesives that are typically referred to as silyl-modified polymers or simply modified silane polymers. MS polymers can be synthesized through three main routes: (1) introduction of the reactive group during polymerization known as in situ functionalization (ISF) or (2) post polymerization chemical modification of a preformed polymer (post-polymerization functionalization (PPF) or (3) metathesis of olefins [19]. The chemical structure of MS polymers is shown in Figure 9. These hybrid adhesives have multiple advantages including: good adhesion to various materials such as metals, ceramics, glass, and plastics; offer good UV and temperature resistance; excellent durability with limited surface treatment [19]. These characteristics allowed the integration of MS polymer adhesives and sealants in variety of applications especially in construction and automotive industry. A summary of the multiple applications of MS polymer adhesive and sealants is presented in Table 1.



Figure 9. MS polymer chemical structure having a polyether group in the polymeric backbone and two active dimethoxy silane groups. [20]

Table 1. Various applications of MS polymer adhesives and sealants. [19]

Application Area	Application
Construction	Glass bonding Insulation Container construction
Automotive	Glass bonding in all vehicle types and side panels of trucks
Medical	Novel drug delivery system

2.2.2. Epoxy Adhesives

Epoxyes are mainly compounds composed of one or more epoxide group . The most used epoxy resins are diglycidyl ethers of bisphenol A (BPA) that are obtained by the reaction of bisphenol A with epichlorohydrin (ECH). Epoxy resins gain their toughness, high temperature performance and rigidity from BPA. On the other hand, ether linkages offer chemical resistance, whereas the epoxy and hydroxyl groups provide the adhesive properties [21]. The general synthesis of epoxy resin is shown in Figure 10. Epoxyes are usually supplied as: one-part epoxyes and two-part epoxyes. Two-part epoxyes package the epoxy component and curing agent separately whereas one-part epoxyes have the epoxy and curing agent already mixed. Two part epoxyes mainly cure at room temperatures while one-part epoxyes require elevated temperatures to successfully cure and are usually stored at low temperatures [22]. Epoxyes have seen usage in many fields due to their good mechanical properties such as tensile strength, resilience, compression, flexion; ability to bond a variety of materials; decent resistance to high temperatures of

up to 190 °C; and excellent chemical resistance [23]. The various applications of epoxies are presented in Table 2.

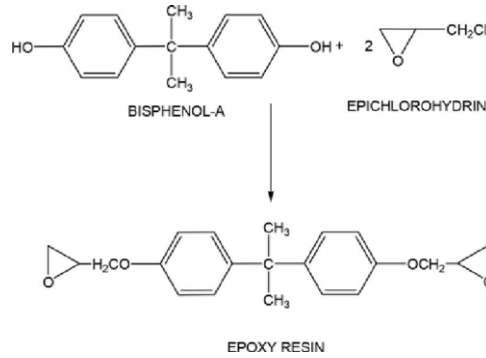


Figure 10. The general synthesis of epoxy resin.

Table 2. Various applications of epoxy adhesives. [22] [24] [25]

Application Area	Application
Industrial	Structural bonding
	Production of molds, castings, and fixtures
Construction	Concrete repairing
	Anchor bolt fixture
Automotive	Structural bonding
	Hemming adhesion
Aerospace	Metal, honeycomb, and composite bonding and repairing
Electronics	Electrically conductive adhesive
	Display assembly
	Image sensor assembly
	Underfills
Medical	Wound dressings
	Orthodontics

2.2.3. Polyurethane Adhesives

Polyurethanes are another type of adhesives that have been used in a variety of applications. Similar to epoxy adhesives, polyurethane also come in one part or two-part systems. These adhesives are produced by the addition polymerization of isocyanates with di and poly-functional hydroxy compounds which include hydroxy-terminated polyesters or polyethers. A typical polyurethane synthesis reaction is shown in Figure 11. Each of polyurethane's monomers and additives play a specific role where the isocyanate group permits reactivity and curing properties while the polyol maintains the elastomeric properties [26]. Polyurethane adhesives offer multiple benefits such as good flexibility at low temperatures, fatigue resistance, impact resistance, and are durable [27]. The mentioned properties have allowed polyurethanes to be integrated in multiple applications such as: bonding of structural plastics in automotive industry, wood bonding, structural sealants and adhesives for transportation industry and particle board fabrication [28]. Polyurethane has also been integrated as an electrically conductive adhesive in flexible electronics [29]. The various applications of the polyurethane adhesive are summarized in Table 3.

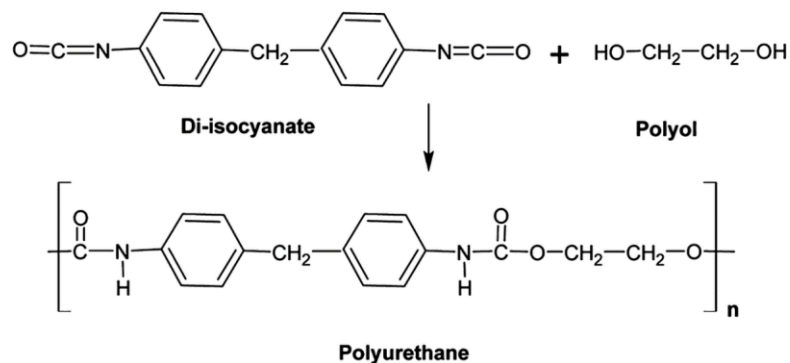


Figure 11. The general synthesis of polyurethane. [26]

Table 3. Various applications of polyurethane adhesives.

Application Area	Application
Transportation	Structural sealant and adhesive
Construction	Wood joining Particle board fabrication
Automotive	Structural bonding
Electronics	Electrically conductive adhesive

2.2.4. Acrylic Adhesives

Acrylic adhesives are a more recent type of adhesives compared to urethane and epoxy-based adhesives . Acrylic based adhesives are composed of a mixture of polymers and low molecular weight, unsaturated, free-radical polymerizable monomer with additional material depending on end use [18]. Acrylic adhesives are composed of two or more acrylic monomers such as acrylic acid and methyl methacrylate [13]. The chemical structure of both monomers is presented in Figure 12. Acrylic adhesives offer multiple advantages such as: rapid cure at room temperature and ability to adhere to unprepared metal surfaces and low surface energy substrates [18] , good shear strength and ability to bond various materials such as metals, plastics and composites [13]. Although acrylic adhesives are more recently developed compared to urethanes and epoxies, they have seen wide usage in various fields. The primary applications of acrylic adhesives are shown in Table 4.

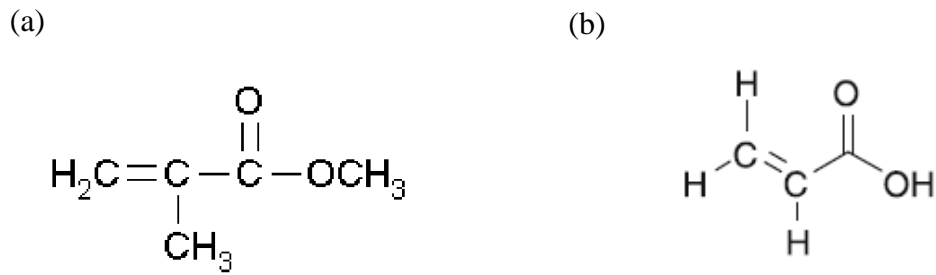


Figure 12. The chemical structure of two acrylic monomers: (a) methyl methacrylate [30] and (b) acrylic acid [18].

Table 4. Various applications of acrylic adhesives

Application Area	Application
Industrial	Cable splice enclosure bonding
Construction	Glass laminates
Automotive	Exterior roof repair Hem flanges bonding
Medical	Skin contact applications (bandages, tapes)

2.3. Hyperelasticity

As the current study is focused on the analysis of flexible adhesives, it is important to discuss hyper elasticity and its respective constitutive equations. Hyperelasticity is a nonlinear elastic model theory that is used to characterize the large strain response of various soft and flexible materials such as elastomers and rubbers [31]. A constitutive model that derives stress-strain relationship from a strain energy density function is then utilized to define such material. Multiple constitutive models exist to represent hyperelastic material which include: Neo-Hookean, Mooney-Rivlin and Ogden model. Each model offers advantages such as reduced complexity and ability to represent large

strains. Multiple FEM tools can be utilized to facilitate modeling of hyperelastic materials as they integrate a wide variety of constitutive models. ABAQUS software was selected for this study as it provides a built-in calibration tool to extract the hyperelastic parameters and provides a stability check for each model across the input strains. A thorough analysis of the utilized hyperelastic models as well as their respective equations is provided in the numerical modeling section.

2.4. Related Work

Adhesive bonding is a joining technique where an adhesive material sets between two uncoupled adherends [32]. These bonds are typically loaded in shear configurations where the force's line of action is parallel to the adhesive's cross sectional area [2]. Various combinations of adherends have been studied in literature with carbon fiber reinforced polymers (CFRP) adherends receiving particular interest. Hu et al. [33] tested experimentally the effects of cyclic temperature conditions on CFRP-Steel single lap joints and validated the results using numerical analysis. Goudarzi & Khedmati [1] analyzed GFRP-Al single lap joints and discussed the fracture response of this configuration experimentally and numerically. Furthermore, Stuparu et al. [34] performed an extensive numerical analysis employing the extended finite element method (XFEM) on CFRP-Al joints and conducted experimental tests for comparison. Two different configurations of adhesively bonded joints was analyzed by Barile et al. [35], the joggled and single lap joint specimen, where the damage modes in both variations was studied. Moreover, the issue of strip defects introduced to CFRP single lap joints was analyzed by de Moura et al. [36].

Furthermore, the effects of loading rate and temperature on the performance of single lap joints have also been widely researched. Banea et al. [37] analyzed the effect

of temperature on the strength of single lap joints having aluminum adherends bonded by epoxy adhesive. The authors were able to show that the bond strength increased at temperature below the adhesive's glass transition temperature (T_g) and decreased for temperatures above T_g . Moreover, Bellini et al. [38] studied the impact of operating temperature on aged CFRP-CFRP SLJ with epoxy adhesive, and were able to show that the shear strength of the bonded joints was significantly decreased for temperatures much higher than T_g . On the other hand, a decrease in shear strength of aluminum single lap joints bonded with silyl modified polymer adhesive was observed with the increase of temperature as shown by Na et al. [39]. The cross head testing velocity also impacts the bonded joint strength, where higher strengths for Epoxy/Ceramic Composites – Steel lap joints were observed for higher cross head velocities Mattos et al. [40]. This result was also reached by Wang et al. [41] where the strength of CFRP-Al SLJ was increased from 19.3 to 29.3 MPa upon increasing the loading rate from 2 mm/min to 12 m/s.

The mentioned references tackled the effect of testing factors on single lap joint performance. Geometrical parameters such as adhesive thickness, overlap length and width also have a direct correlation with the joint strength. A parametric study was performed by Wei et al. [42] where CFRP-Steel joints were investigated using different adhesives and overlap lengths. Seong et al. [43] conducted a thorough study where the effects of varying parameters such as overlap length, bonding pressure, adherend thickness and material type were studied for CFRP-Al joints. LFM da Silva & Campilho [44] resorted to literature and concluded that as the bond line increases, the joint strength decreases for metal adherends. However, for composite adherends the impact of using thinner adhesive bond lines is reduced due to possible delamination of composite adherends. Although the authors mention that experimental results show optimum

performance for thin bond lines, analytical models used to tackle SLJ problems predict opposite information and this issue remains controversial [44]. On the other hand, Neto et al. [45] has performed a parametric study on single lap joints with composite adherends and were able to show that for ductile adhesives, the strength of the SLJ increased with the increase in overlap length. This conclusion was also applicable for brittle adhesive but up to a certain limit, where a plateau was reached. The effect of adhesive thickness was studied by Lucas F M da Silva et al. [46] and Kahraman et al. [47], and it was shown that single lap joint increased with decreased adhesive bondline thickness. Finally, Pisharody et al. [48] studied the impact of adhesive distribution on the strength of bonded joints.

On the other hand, variables such as surface treatment and surface roughness can also play a role in the performance of single lap joints. The study performed by Boutar et al. [49] on Al – Al single lap joints has shown that the lap shear strength has been improved upon decreasing the surface roughness. An optimum performance was observed for lap joints being abraded using fine abrasive paper of grade p1000 compared to the coarser grades p50, p180 and the non-abraded counterparts. Moreover, Diharjo et al. [50] studied the impact of various surface treatment techniques on the shear strength of CFRP-Al single lap joints. Treatment using acetone resulted in improved single lap joint shear strength compared to other treatment methods such as caustic etch, tucker's reagent, and chromate sulfur acid treatment.

Considering numerical modeling, hyperelastic modeling of flexible adhesives was incorporated in multiple studies tackling single lap joints. Hoang-Ngoc & Paroissien [51] utilized Mooney-Rivlin constitutive equation to model the behavior of the adhesive in bonded and hybrid (bolted/bonded) single lap joints. Moreover, Moreira & Nunes [52]

studied the simple and pure shear states on hyperelastic material under large deformation and used the Ogden model to represent the adhesive.

A summary of various results obtained from literature is provided in Table 5, where the mentioned single lap joint adherend and adhesive material, adhesive thickness, bonded area, surface preparation and testing conditions are provided.

Table 5. Results obtained from literature for single lap joints tested under different testing conditions and composed of different material combinations.

Adherends	Adhesive Commercial Name	Adhesive Chemistry	Adhesive Thickness (mm)	Bonded Area (mm ²)	Average Shear Strength (MPa)	Surface Preparation	Testing Conditions	Reference
CFRP – DC04 Steel	7779	Polyurethane Structural Adhesive	1	1000	~ 11*	Abrasive Paper - Acetone	- Loading Rate: 2 mm/min	[42]
CFRP – Cr. D Q235 Steel	Araldite® AV138	Epoxy Structural Adhesive	0.2	312.50	18.72*	Abrasive Paper - Acetone	- Loading Rate: 2mm /min - Temperature: Room Temperature	[33]
GFRP-Al	Araldite® 2015	Epoxy Structural Adhesive	0.3	625	8.33	Abrasive Paper - Acetone	- Loading Rate: 1 mm/min	[1]
CFRP-CFRP	-	-	8.5	658.58	10.66	-	- Loading Rate: 13 mm/min	[35]
CFRP-CFRP	Fiber Glast 1101	Epoxy Structural Adhesive	0.2	645.16	~12.40	Abrasive Paper- Iso-propyl alcohol	- Loading Rate: 1.2 mm/min - Temperature: Room Temperature	[48]
Steel-Steel (ASTM 36)	-	Epoxy/ceramic composite adhesive	0.4 (with spew fillets)	312.50	6.89	Grit Blasting – Surface Spraying Silanisation	- Loading Rate: 12 mm/min	[40]
Aluminum Copper Alloy -Aluminum Copper Alloy	-	Polyurethane adhesive	1	312.50	4.56	Abrasive Paper- Acetone	- Loading Rate: 1.3 mm/min - Temperature: Room Temperature	[53]

*Based on maximum failure force

CHAPTER 3

ANALYTICAL MODELS

Analytical models are important tools to study the stress distribution of adhesively bonded joints. Adhesive models are typically analyzed through numerical simulations using the finite element method (FEM). However, multiple analytical solutions have been developed to analyze stress distribution along the adhesive bondline. Analytical models include classical theories such as the Volkersen [8] and Goland and Reissner [9] which were expanded to more general solutions discussed in [54] and [55]. However, an increase in solution complexity is observed as models become more general. Such complication makes numerical methods a more favorable route for obtaining stress distributions in general cases such as dissimilar and asymmetric adherends.

In the proposed study, the analytical solution obtained from the classical analysis, particularly Volkersen equation, will be compared to those obtained from numerical simulations. The Volkersen equation was selected due to its incorporation of adherends with different elastic moduli and dissimilar thicknesses. Consequently, the Volkersen equation will be expanded upon and derived in this study. It is important to note that classical analysis include certain limitations such as: (1) not accounting for adhesives stresses through the thickness of the adhesive and (2) ignoring stress free condition at the ends of the overlap which results in peak shear stress at overlap ends which violates the stress- free condition [56].

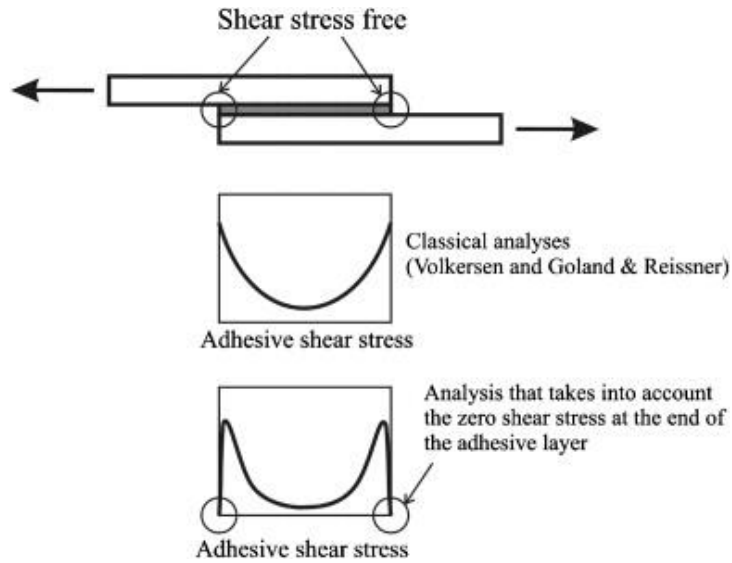


Figure 13. Difference in shear stress distribution predicted by classical analysis and analysis that consider zero shear stress at overlap ends. [57]

3.1. Volkersen Model

This approach considers the adhesive and substrates as linearly elastic, Hookean solids. The adhesive is also assumed to undergo only shear deformation. Moreover, plane stress condition is considered and out of plane stresses are neglected for the adhesive and adherends [5]. Volkersen’s analysis shows that the shear strain decreases progressively along overlap length and reaches maximum values at the ends of the overlap [3]. Although this analysis provides significant information regarding stress distribution in single lap joints; however, it fails to include peel stresses and adherend’s bending that play an important role in fracture of single lap joints. The SLJ configuration and governing equation for the shear stress distribution along bonded joints are presented in Figure 14 and Equation (1) respectively.

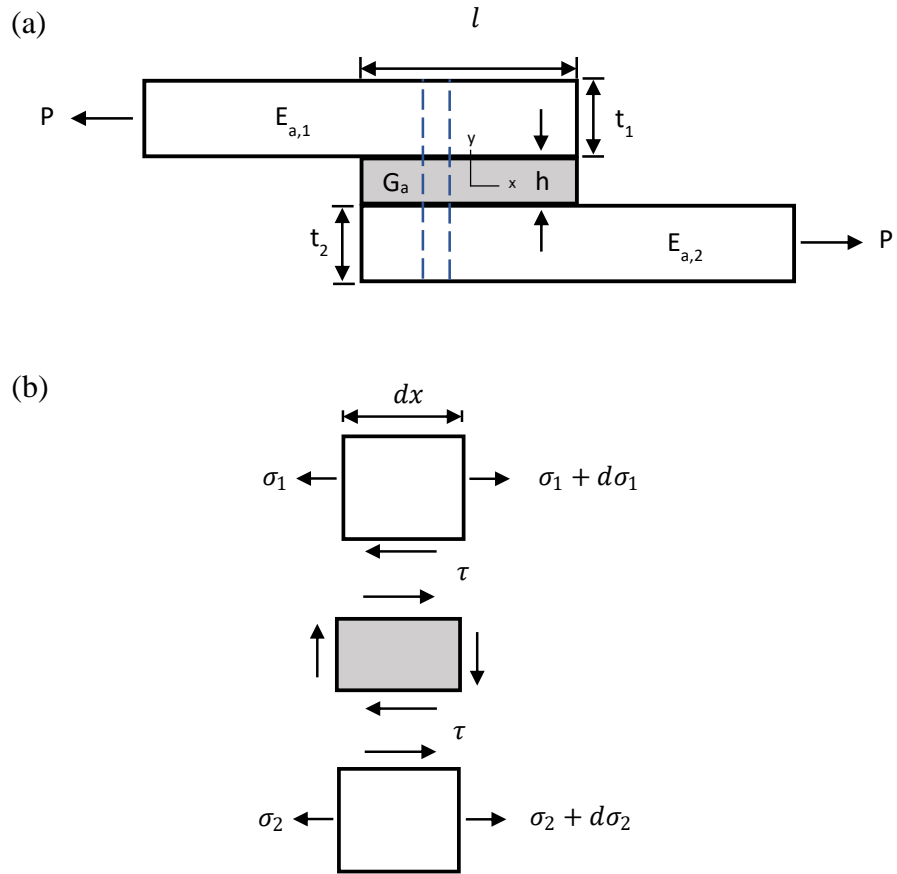


Figure 14. Single lap joint configuration to derive the Volkersen model. (a) Parameters of the Volkersen model (b) Elemental diagram.

Based on the elemental diagram and summarizing David A. Dillard [58] derivation, we have the following equilibrium equations:

$$\frac{d\sigma_1}{dx} = \frac{1}{t_1} \tau \quad \frac{d\sigma_2}{dx} = -\frac{1}{t_2} \tau$$

The kinematic equations can be expressed as follows:

$$\frac{d\delta}{dx} = \varepsilon_1 - \varepsilon_2 \quad \gamma_s = \frac{\delta}{h}$$

Constitutive relationships:

$$\varepsilon_1 = \frac{\sigma_1}{E_{a,1}} \quad \varepsilon_2 = \frac{\sigma_2}{E_{a,2}} \quad \gamma_s = \frac{\tau}{G_a}$$

Combining the above equations, we obtain a second order differential equation:

$$\frac{d^2\tau}{dx^2} - \omega^2\tau = 0$$

$$\text{with } \omega = \sqrt{\frac{G_a}{h} \left(\frac{E_{a,1}t_1 + E_{a,2}t_2}{E_{a,1}t_1 E_{a,2}t_2} \right)}$$

The solution of the presented differential equation is of the form:

$$\tau(x) = A \cosh \omega x + B \sinh \omega x$$

The complete solution can be obtained by applying the boundary conditions.

Consequently, by combining the constitutive and kinematic equations we have:

$$\frac{d\tau}{dx} = \frac{G_a}{h} (\varepsilon_1 - \varepsilon_2)$$

At $x = -\frac{l}{2}$ and at $x = \frac{l}{2}$ we have zero strains ε_1 and ε_2 respectively as they are free ends. Therefore, the boundary conditions can be deduced as follows:

$$\left. \frac{d\tau}{dx} \right|_{x=-\frac{l}{2}} = -\frac{G_a P}{h E_{a,2} t_2} \quad \left. \frac{d\tau}{dx} \right|_{x=\frac{l}{2}} = \frac{G_a P}{h E_{a,1} t_1}$$

Substituting the boundary conditions, we can obtain the final solution:

$$\tau(x) = \frac{P\omega}{2 \sinh\left(\frac{\omega l}{2}\right)} \cosh \omega x + \frac{P\omega}{2 \cosh\left(\frac{\omega l}{2}\right)} \left(\frac{E_{a,2}t_2 - E_{a,1}t_1}{E_{a,1}t_1 + E_{a,2}t_2} \right) \sinh \omega x \quad (1)$$

$$\text{with } \omega = \sqrt{\frac{G_a}{h} \left(\frac{E_{a,1}t_1 + E_{a,2}t_2}{E_{a,1}t_1 E_{a,2}t_2} \right)}$$

3.2. Goland and Reissner Model

Goland and Reissner [9] then incorporated the effect of the edge moment due to eccentric loading, which was not included in Volkersen's analysis [3]. The eccentric loading also results in a transverse force applied to the joint end. Goland and Reissner's inclusion of the bending moment is highly important as it leads to a nonlinear geometric problem where the large deflections of the adherends must be considered [57]. Goland and Reissner's solution provides a similar shear stress distribution compared to the Volkersen solution; however, it predicts a higher shear stress at overlap ends [57]. The SLJ configuration and governing equation based on [59] are presented in Figure 15 and Equation (2) respectively.

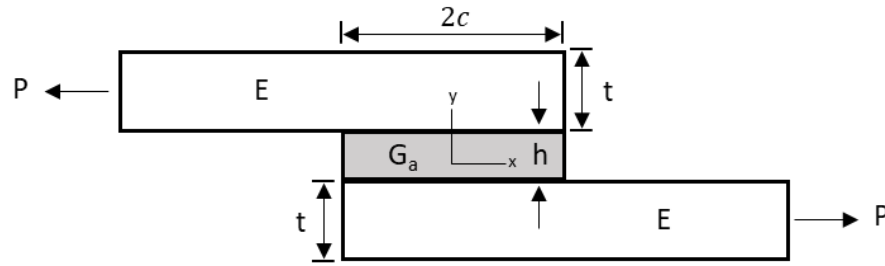


Figure 15. The parameters and SLJ configuration of Goland and Reissner model.

$$\tau(x) = -\frac{1}{8} \frac{P}{c} \left[\frac{\beta c}{t} (1 + 3k) \frac{\cosh \frac{\beta c x}{t}}{\sinh \frac{\beta c}{t}} + 3(1 - k) \right] \quad (2)$$

$$\text{with } k = \frac{\cosh \gamma}{\cosh \gamma + 2\sqrt{2} \sinh \gamma}, \quad \gamma = \sqrt{\frac{3(1-\nu^2)}{2}} \frac{c}{t} \sqrt{\frac{P}{tE}} \quad \text{and} \quad \beta = \sqrt{8} \frac{G_a}{E} \frac{t}{h}$$

On the other hand, while the mentioned analytical techniques, as well as others, fail to predict the strength of adhesive bonded joints without an uncertainty factor, finite element methods can successfully predict adhesive joint strength by incorporating nonlinear mechanics and properties [10]. Therefore, finite element techniques can

accurately predict adhesive bond strength but the results are highly sensitive to mesh refinements due to the presence of singularities at joint ends [60]. Consequently, a numerical model should be established to compare the numerical results to the analytical solutions.

CHAPTER 4

EXPERIMENTAL VARIABLES

For this study a flexible MS polymer-based adhesive is selected. Literature studies have focused extensively on rigid epoxy-based adhesives as shown in Table 5 with minimal work done on flexible MS polymer-based adhesives. Flexible adhesives tend to have minimum stress peaks compared to rigid and stiff adhesives that have large stress peaks. These adhesives tend to have a more uniform stress distribution with less difference between average and maximum stress [61]. A ductile adhesive is capable in redistributing the load and utilize the less stress overlap areas, whereas brittle adhesives tend to concentrate the load at the ends of overlap resulting in low average shear stress [62]. Consequently, this study aims to provide a parametric analysis where single lap joints, fabricated with the selected MS polymer adhesive, are tested under variable operating conditions (temperature and loading rate) and adhesive bondline thickness. The mentioned variables were selected due to their direct correlation with single lap joint performance. The primary impact of these parameters on the single lap joint performance is summarized in the following sections.

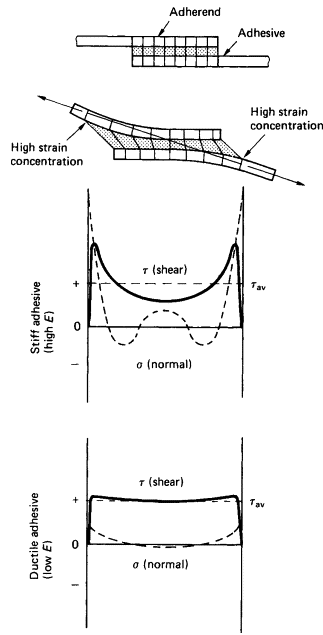


Figure 16. Stress distribution along bondline for stiff and ductile adhesives. [63]

4.1. Temperature

Considering adhesively bonded joints, temperature variation has a direct impact on the adhesive material properties. Temperature variation typically results in direct effects on adhesive properties. Low temperatures result in increased adhesive brittleness while higher temperatures result in enhanced ductility at the expense of adhesive's strength and more creep liability [64]. In fact, Banea & da Silva [65] characterized the lap joint shear strength as a function of temperature. Referring to Figure 17, although an increase in temperature results in a decrease in the adhesive's bulk strength; however, an increase in ductility is observed. Consequently, the largest lap shear strength is observed at the temperature at which the optimum compromise is achieved between bulk strength and ductility. Moreover, it is important to note that upon approaching the glass transition temperature and exceeding it, the sharp drop and increase in adhesive's strength and ductility respectively, results in significant decrease in lap shear strength. This is due to the fact that the T_g of the adhesive has been surpassed and thus the adhesive tends to

soften and transition toward the rubbery region. This transition significantly impacts the adhesives elastic modulus and strength, resulting in a large decrease in the single lap joint strength.

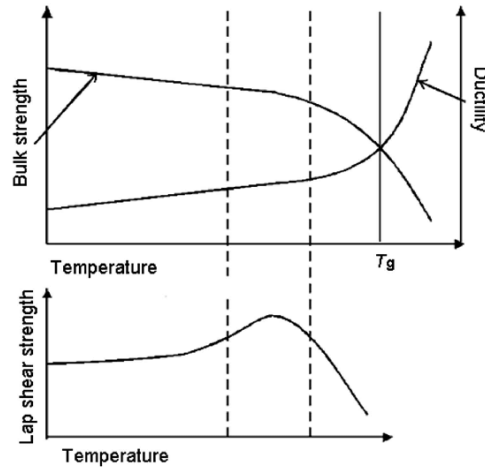


Figure 17. Lap-shear strength as a function of adhesive's ductility and strength. [65]

4.2. Loading Rate

Another important variable that is tested in the proposed study, is the variation of loading rate on the SLJ's performance. In general, an increase in material properties such as ultimate strength, yield stress and modulus are observed with increasing strain rates. This phenomenon is referred to as the strain rate effect. For example, in polymers, an increasing strain rate results in decreased molecular mobility of polymer chains by making polymer chains stiffer [66]. This in turn results in an increased strength. In fact, increasing the strain rate tends to increase the modulus, yield and flow stress of polymer materials [67]. Moreover, A strain rate sensitivity factor, m , can be calculated to quantify the strain rate effect on material properties [68]. The equation to calculate the strain rate sensitivity is shown below, where σ_A and σ_B correspond to flow stresses at strain rates $\dot{\epsilon}_A$ and $\dot{\epsilon}_B$.

$$m = \frac{d \ln \sigma}{d \ln \dot{\epsilon}} = \frac{(\ln \sigma_A - \ln \sigma_B)}{(\ln \dot{\epsilon}_A - \ln \dot{\epsilon}_B)}$$

A larger value of m signifies a larger strain rate sensitivity. A study performed by Liu et al. [68] has shown a larger m factor for the epoxy polymer adhesive compared to the CFRP and aluminum adherends. Moreover, Zhang et al. [69] has shown a larger m factor for the epoxy adhesive compared to steel and aluminum adherends. The increased strain rate sensitivity of the adhesive can be attributed to its viscoelastic nature [70].

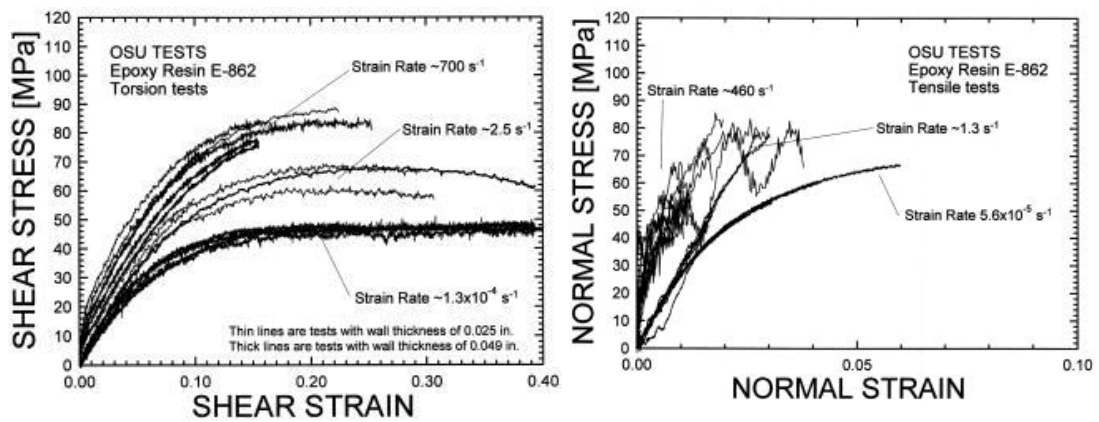


Figure 18. Shear and normal stress improvement with increased strain rate for a selected epoxy resin. [71]

4.3. Adhesive Thickness

Adhesive thickness is a critical parameter that has been widely investigated in literature. While experimental studies show that single lap joint strength decreases with the increase in bondline thickness; however, analytical models such the Voleksen and Goland and Reissner predict opposite results. R D Adams & Peppiatt [72] state that the decrease in joint strength with increased adhesive thickness is due to the increase in defects and micro cracks in thick bondlines. Furthermore, Grant et al. [60] attributes the reduction in lap joint strength with thick bondlines to the increase in bending moments due to the increased loading offset. Moreover, while thick bondlines can alter the cure properties inducing internal stress and affecting short and long term performance, thin

bondlines can result in adhesive stravation and debonding [73]. Therefore, bondline thickness is a contreversial issue that requires extensive testing to ensure the ideal thickness for optimal performance.

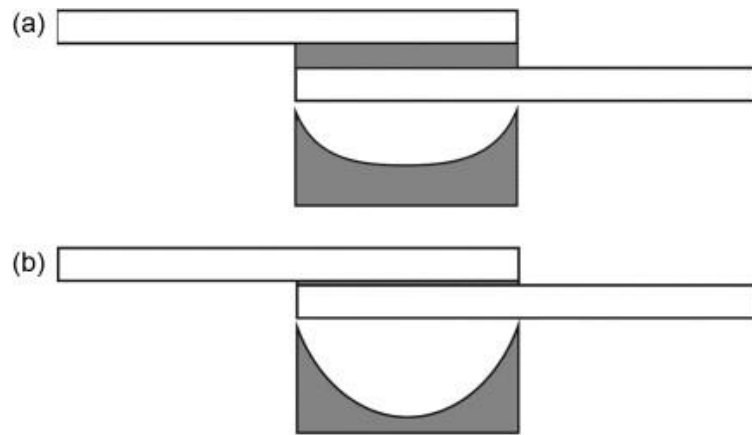


Figure 19. Stress distribution in (a) thick bondline and (b) thin bondline single lap joint.

[44]

CHAPTER 5

EXPERIMENTAL TESTING

5.1. Material Characterization

Prior to the fabrication and testing of single lap joints, the mechanical properties of the adherend and adhesive material should be determined. These properties are determined either from manufacturer's data or through tensile tests. Consequently, the material characterization process for various material can be summarized as follows:

5.1.1. Adhesive Material

The stress strain response of the flexible adhesive under study is of significant importance, as it is a prerequisite for the extraction of the hyperelastic parameters. Consequently, tensile tests of bulk adhesive samples were performed. The flexible adhesive material used in this study is the MS polymer based AMS55 (Produced by *Akfix*). The selected adhesive is characterized by excellent elasticity and adhesion to porous and non-porous substrates. Moreover, it offers significant heat resistance for temperatures between -40°C and 90°C.

The material is placed in a mold machined to ASTM D638 dimensions, Figure 20 (a), with an average thickness of 3.5 mm. The samples were cured according to the manufacturer's data which recommends an approximate curing rate of 24 hours/ 3.5mm. Consequently, the bulk samples were left to cure for approximately 48 hours to ensure full cure. A fully cured sample is presented in Figure 20 (b). The samples are then tested using the H100KS tensile machine at a constant loading rate of 50 mm/min and a temperature of 25°C. Three samples were tested and a representative curve, MSP-1, was

chosen to be imported to ABAQUS for hyperelastic parameter extraction. The results for the tensile tests of bulk adhesive samples are shown in Figure 21.

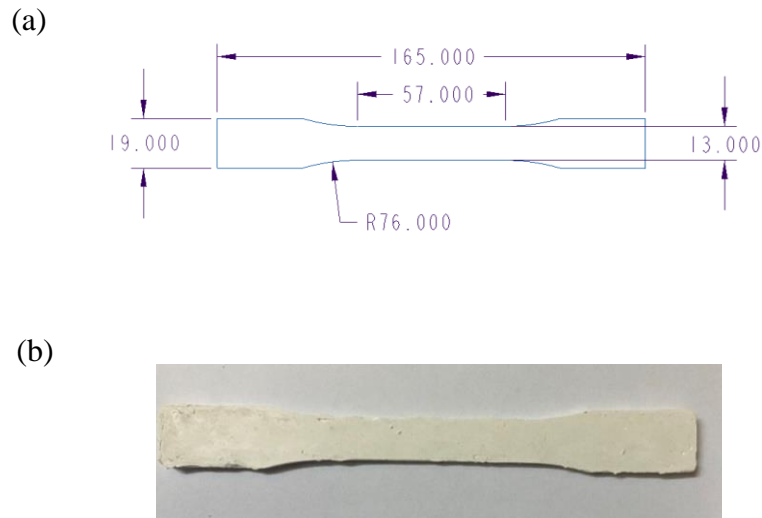


Figure 20. (a) ASTM D638 dimensions (b) Fully cured bulk MS polymer sample.

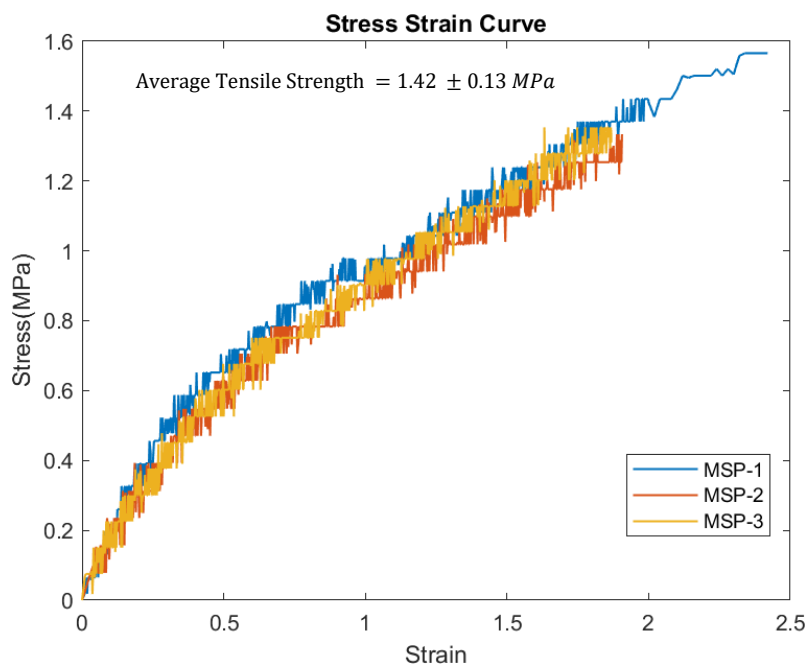


Figure 21. MS polymer: Three stress-strain response curves coplotted (Loading rate = 50 mm/min; Testing temperature = 25°C).



Figure 22. The Hounsfield H100KS universal tensile testing machine mounted with an environmental chamber and laser extensometer.

Table 6. AMS 55 material properties.

	AMS 55
ρ (kg/m^3)	1.49×10^3
Hyperelastic parameters	Determined in the Numerical Modeling section.

5.1.2. Adherend Material

Two adherends materials were used in this study, carbon fiber reinforced polymer (CFRP) and steel. The composed CFRP laminates were produced from XC130 carbon fiber prepreg supplied by *easycomposites*. The formed composite laminate had a thickness of 3.3 mm with unidirectional fibers oriented at 0° . Typical steel substrates were also selected as the second adherend with properties listed on [74]. The mechanical properties of discussed materials are presented in Table 7 and Table 8 with only the

longitudinal young's modulus and in plane Poisson's ratio were extracted for the CFRP material.

Table 7. CFRP adherend material properties.

	CFRP
E_{11} (GPa)	135
ν_{12} [75]	0.25

Table 8. Steel adherend material properties.

	Steel
ρ (kg/m^3)	7.80×10^3
E (GPa)	200
ν	0.25

CHAPTER 6

SINGLE LAP JOINT FABRICATION AND TESTING

Single lap joints composed of CFRP and metal adherends were fabricated using specially designed molds. Moreover, prior to bonding appropriate surface treatment techniques were implemented to ensure strong adhesion to adherend's surfaces. The single lap joint dimensions and fabrication process can be summarized as follows:

6.1. Dimensions

Single lap joints composed of CFRP and metal adherends were cut and machined to the dimensions shown in Figure 23 and Table 9. All adherends were cut to a width of 25.4 mm and bonded using the MS polymer-based adhesive. Apart from the adherend's thicknesses and considering the bondline thickness of 0.76 mm, the adherend's and adhesive's dimensions are all based on the ASTM D5868 standard. Furthermore, two additional bondline thicknesses (1 mm and 1.2 mm) were selected to characterize the impact of increasing adhesive's thickness on lap joint strength.

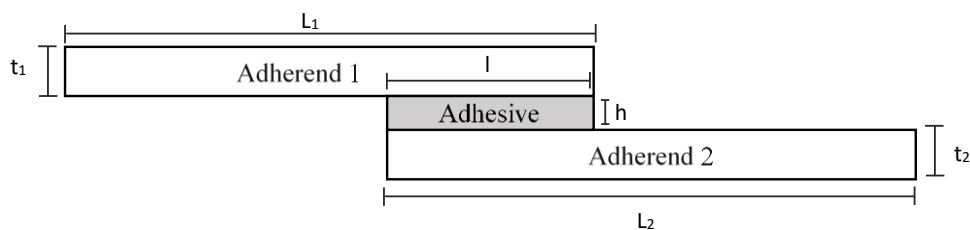


Figure 23. Single lap joint configuration with letter codes representing geometrical dimensions.

Table 9. Dimensions of the fabricated SLJ joints.

L_1 (mm)	t_1 (mm)	L_2 (mm)	t_2 (mm)	l (mm)	h (mm)
101.6	3.3	101.6	2.5	25.4	(0.76, 1.00, 1.20)

6.2. Surface Treatment

Prior to applying the adhesive material, proper surface treatment procedure must be applied to the adherend surfaces to ensure appropriate adhesive bonding [76]. In fact, surface treatment is paramount for achieving initial bond strength and joint durability [77]. Typically, a mechanical or chemical form of treatment is performed before applying the adhesive to the adherend's surface. These pretreatment methods effectively eliminate contaminant such as grease and dust and result in chemical or physical modification of the adherend's surface to allow appropriate bonding between the adherend and adhesive [78]. In this study, the sandblasting technique was utilized to treat the steel adherend's surface prior to applying the adhesive. Sandblasting is a surface treatment method that promotes optimal surface roughness which plays a significant role in the bonding process [79]. In this method, abrasive particles are blasted to the adherend's surface to ensure appropriate surface roughness. The sandblasted samples are presented in Figure 24. On the other hand, the CFRP adherends were degreased and cleaned using an ethanol solution. The CFRP adherends were also smoothed using a fine abrasive paper to ensure proper surface roughness along the overlap area.



Figure 24. Sandblasted steel samples.

6.2. Mold Preparation

Ensuring proper bondline thickness and uniform distribution of the adhesive along the overlap area is a necessary step for accurate testing of the adhesive's performance. Consequently, a specially designed mold was fabricated to bond the SLJ adherend's. The mold has a machined step that has a total thickness equal to the sum of the bondline and steel sample thicknesses. Multiple holes were drilled and threaded across the mold to insert screws and washers to fix the adherend's in place. The mold was modeled using Creo Parametric software and was machined using the CNC milling machine. The dimensions and views of the obtained mold are shown in Figure 25 and Figure 26 respectively. Similarly, a second mold with a step size of 3.5 mm was fabricated to bond the single lap joints with a 1mm adhesive thickness. This step size was further milled to 3.7 mm to allow the production of single lap joints with 1.2 mm bondline thickness.

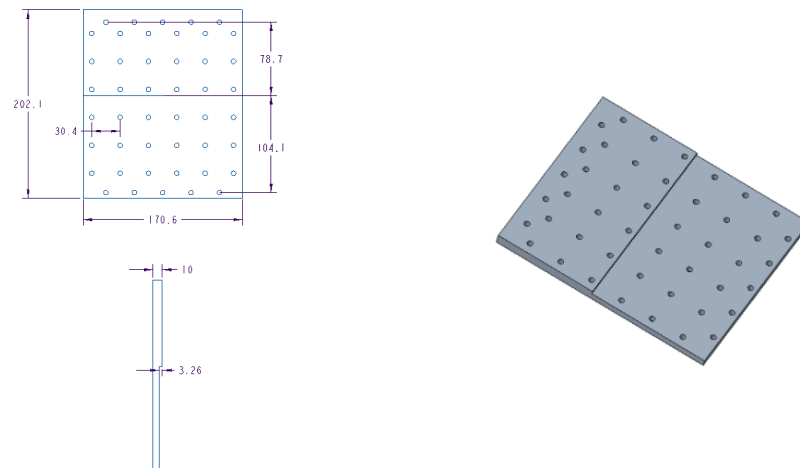


Figure 25. Dimensions and CAD model of the fabricated mold with a 3.26 mm step size.

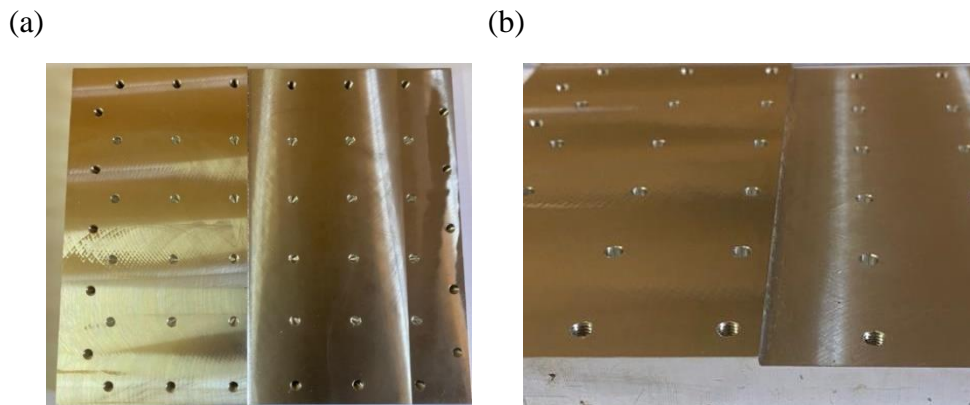


Figure 26. Top (a) and side (b) views of the machined mold.

6.4. Single Lap Joint Bonding

After the surface preparation of the SLJ adherends, the CFRP and steel samples are placed on the fabricated mold as shown in Figure 27. The adherends are held in place by screws and washers. Screws across the overlap area were not fully tightened to allow a uniform adhesive distribution. Weights are placed along this area to ensure appropriate clamping pressure. After curing according to the provided curing rate, excessive adhesive

is removed from the final SLJ specimen to prevent adhesive fillets from strengthening the joint.

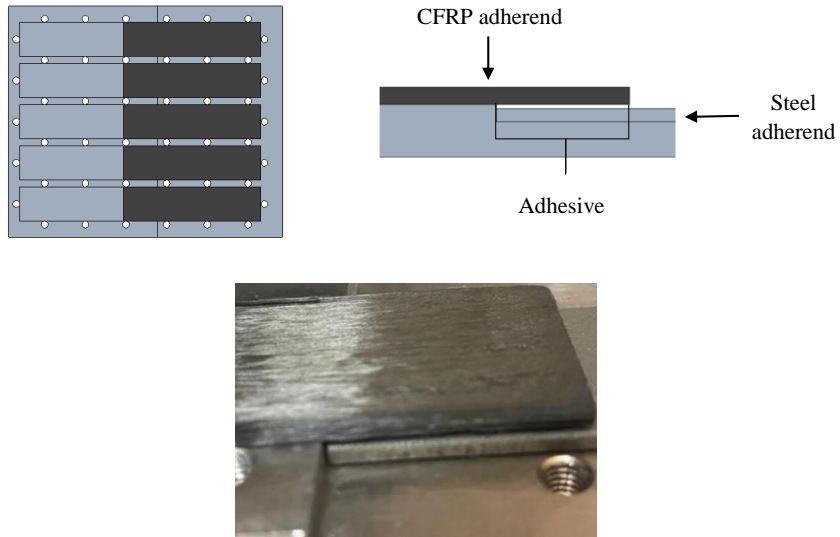


Figure 27. Placement of SLJ adherends and adhesive material on the fabricated mold.

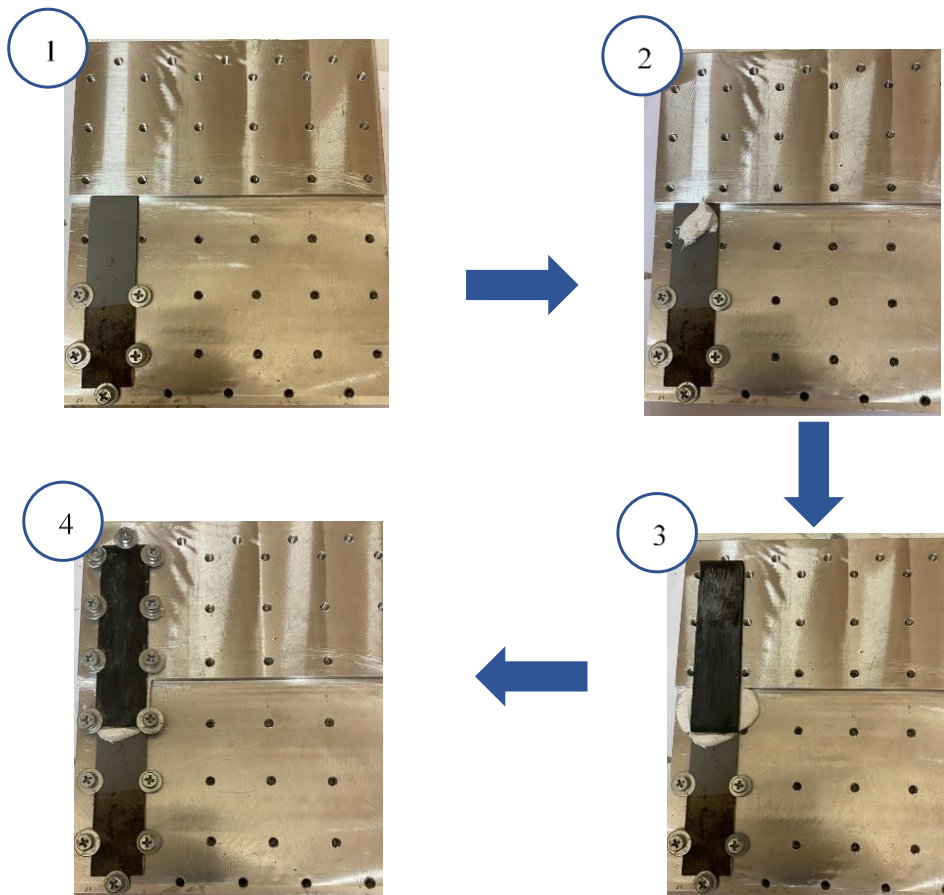


Figure 28. Bonding process of one single lap joint sample.

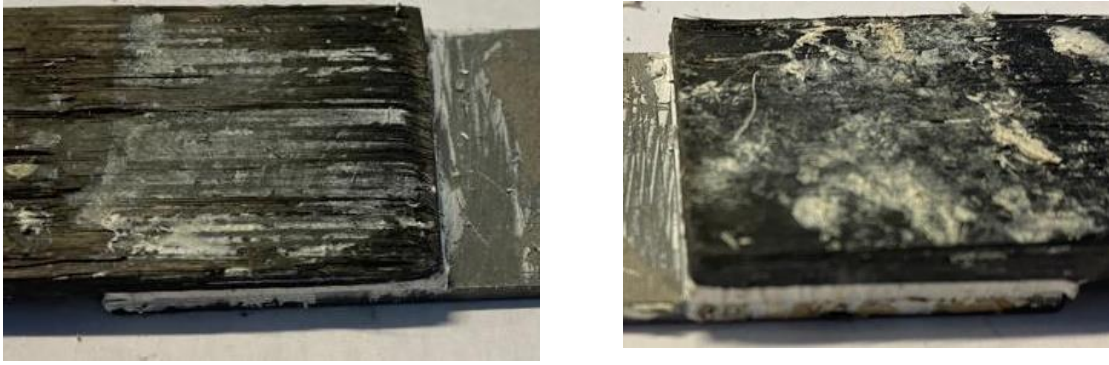


Figure 29. Uniform adhesive bondline thickness along the overlap length.



Figure 30. Various fabricated single lap joints.

6.5. Testing

The fabricated joints are loaded in tension using the Hounsfield H100KS universal testing machine. Testing was performed under variable conditions to study their impact on the lap joints strength. The joints were tested at loading rates of 1 mm /min, 10 mm/min, and 250 mm/min. Moreover, the bonded joints were subjected to different testing temperatures (25 °C, 40°C, 55°C and 100 °C). An environmental chamber, Figure

31, is incorporated to the tensile testing machine to allow testing at elevated temperatures. A laser extensometer was also utilized to obtain the deformation of the bonded region. Moreover, all samples were gripped at a distance of 25.4 mm from the adherends' ends and thus establishing a gripping area of $25.4 \times 25.4 \text{ mm}^2$. Samples with different adhesive bondline thickness were all tested at 25°C and a loading rate of 10 mm/min. On the other hand, single lap joints with 0.76 mm bondline thickness were tested under variable testing temperatures and loading rates. For each combination of loading rate and testing temperature, three different samples were fabricated and tested to ensure statistical significance.

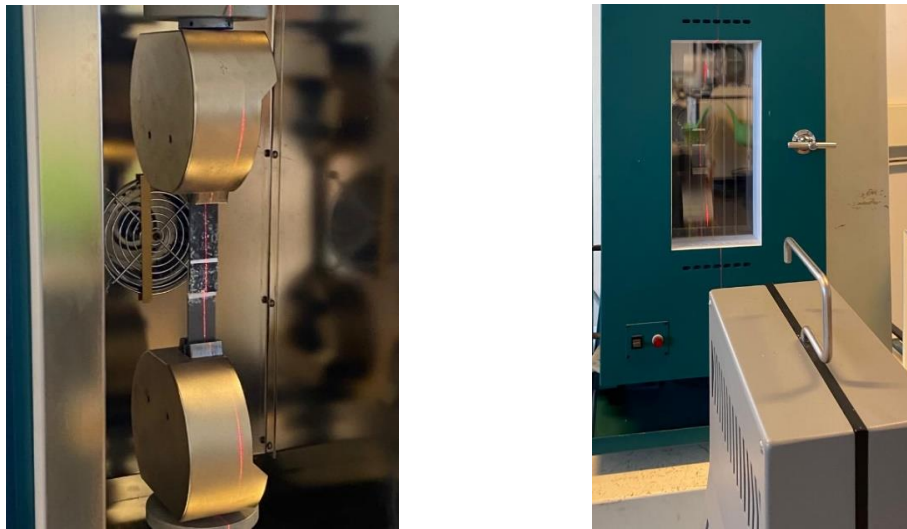


Figure 31. Tensile testing of a SLJ specimen placed in the environmental chamber.

CHAPTER 7

EXPERIMENTAL RESULTS

In total 42 single lap joint specimen were fabricated and tested. Error charts composed of the mean and standard error are plotted and statistical analysis techniques were utilized to understand the effect of each variable. The obtained results are summarized in the following sections.

7.1. Impact of Testing Temperature and Loading Rate

As shown in Figure 32, the average shear strength increases progressively with the increase in applied loading rate at various testing temperatures. This behavior can be explained by the strain rate effect that resulted in a substantial improvement in the adhesive's mechanical properties coupled with the adhesive's heat resistance of up to 90°C according to manufacturer's data. On the other hand, the single lap joints' strength generally decreased with increase in temperature compared to the mean values obtained at room temperature. However, upon increasing the testing temperature, an appreciable increase in adhesive's ductility is induced. Thus, increasing the adhesive's strain rate dependency and resulting in improvement in average shear stress particularly at the 55°C testing temperature. Additionally, it is important to note the deterioration in shear strength at an elevated temperature of 100 °C which surpasses the adhesive's heat resistance range. At this temperature a substantial decrease in adhesive's strength is expected which results in poor lap joint performance.

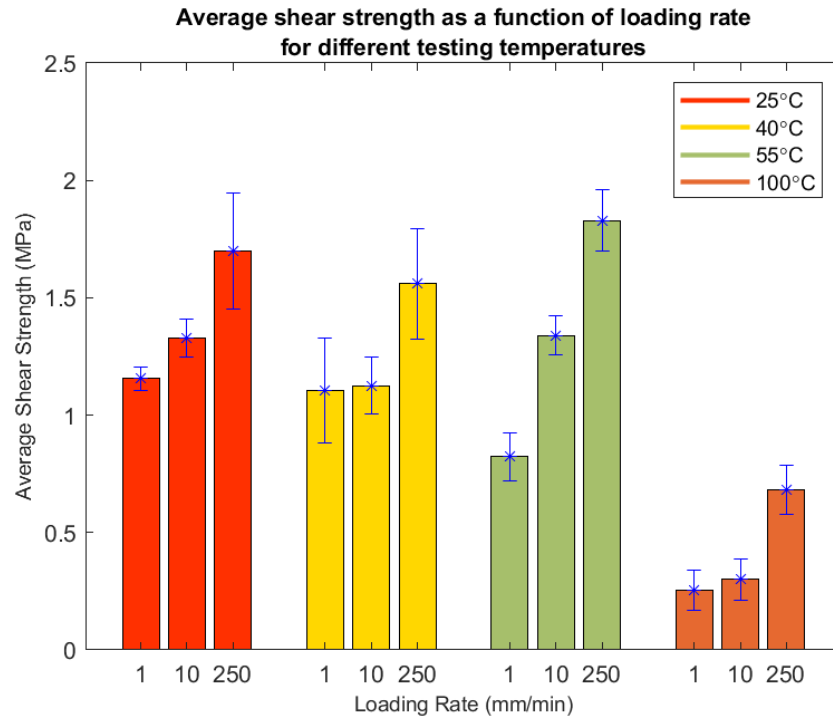


Figure 32. Effect of operating conditions on the average shear strength of the adhesively bonded single lap joints.

As observed, both the testing temperature and loading rate tend to affect and contribute to the lap shear strength. To quantify this effect, a statistical analysis must be performed to deduce the main effect of each of these factors. Consequently, an analysis of variance (ANOVA) study is established to extract the main effect of each of the experimental variables.

7.1.1. ANOVA Study

Analysis of variance (ANOVA) is a statistical method that allows the determination and quantification of the effect of different experimental factors on the outcome of an experiment [80]. Such analysis is optimally suited for experimental designs that involve repeated measures on same subjects [81]. Consequently, an ANOVA study is performed using STATA SE (14.1 , StataCorp LLC , College Station , TX) software to

determine the contribution of each of the operating conditions on the SLJ performance. Therefore, the loading rate and temperature were set as the independent variable, while the dependent variable is the SLJ's shear strength. The significance level, or α , chosen for this study is 0.05 . Thus, if $\text{Prob}>F$, or p-value, is less than the selected α , the null hypothesis, which states that no correlation between the independent and dependent variable exists, should be rejected. On the other hand, if the p-value is less than 0.05, a correlation does exist. The obtained ANOVA results are presented in Table 10.

Table 10. ANOVA analysis performed on the tested samples.

Source	Partial SS	df	MS	F	Prob>F
Loading Rate	2.319372	2	1.159686	18.48	5.881e-06
Temperature	5.754519	3	1.918173	30.57	2.960e-09
Residual	1.882539	30	0.062751		
Total	9.956431	35	0.284469		

As observed both p values for the loading rate ($\text{Prob}>F=5.881e-06$) and temperature ($\text{Prob}>F=2.960e-09$) are much less than the significance level. Consequently, we can deduce that their effect on the shear strength is significant.

To quantify the contribution of each of those variables, we can divide the partial sum of squares for each factor by the total sum of squares. Thus, the approximate contribution of each variable is as follows:

- % Contribution for loading rate: 23.3%
- % Contribution for temperature: 57.8%

Therefore, although both factors contributed to the lap joints' shear strength, testing temperature had a much more significant contribution than the loading rate.

7.2. Impact of Adhesive Thickness

As observed in Figure 33, upon increasing the adhesive bond line thickness, the average shear strength decreased progressively. The decrease observed was highly linear with a calculated R squared value of approximately $R^2 = 0.9866$. This result agrees with Lucas F M da Silva et al. [46] findings, who in the contrary, utilized highly ductile adhesive with 44% strain to failure value. Consequently, this declining trend extends to the studied adhesive that has a strain to failure that exceeds 240% as shown in Figure 21. As previously mentioned, this decrease in average shear strength can be attributed to the increase in defects in thick adhesive bondline and the increase of bending moment due to increased loading offset. Furthermore, by considering the shear strength as 50% of the tensile strength, which conforms with common engineering practice [82], the lap joint shear strength tends to decrease progressively towards the bulk shear strength.

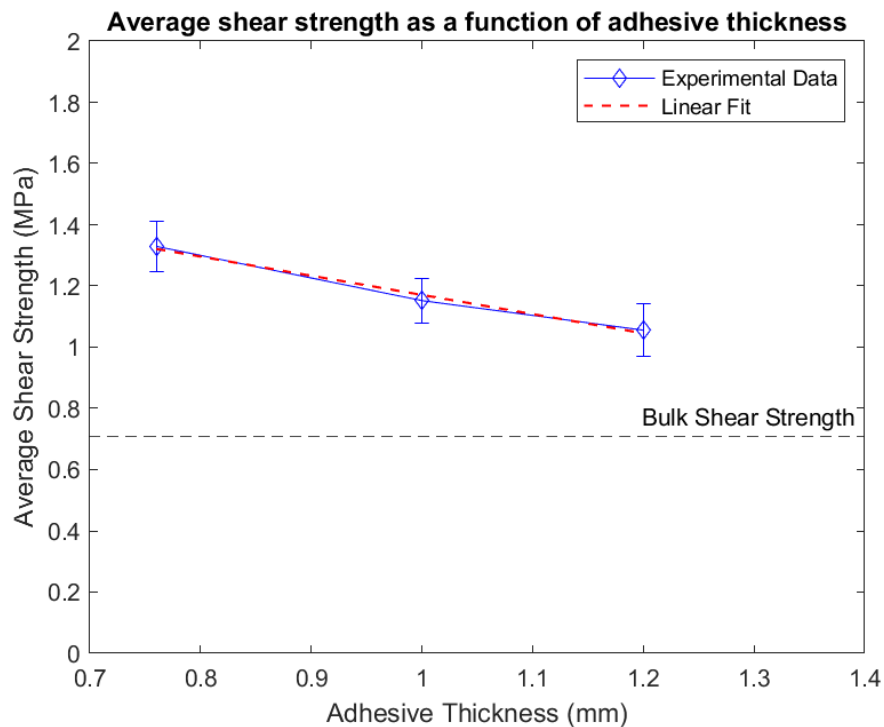


Figure 33. Average shear strength as a function of adhesive thickness with standard error bars.

7.3. Failure Modes

Another important inference that can be deduced from the presented study is the failure mode of the tested single lap joints. The type of failure can vary according to the experimental conditions and quality of the bond. Therefore, it is important to extract the surface morphology of the tested samples after failure. Six different modes of failure can be considered for CFRP adhesively bonded joints and are presented in Figure 34. Furthermore, a mixed mode failure is possible where a combination of different failure modes occurs.

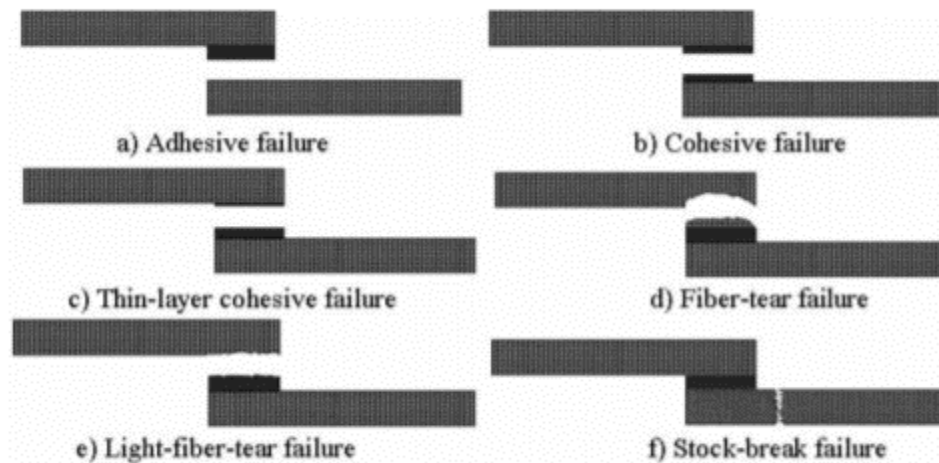


Figure 34. Various failure modes of FRP adhesive bonded joints. [27]

- **Adhesive Failure:** This type of failure occurs directly on the interface between the adherends. The adhesive material is observed on one of the adherend's surface. Although manufacturing issues can cause such failure; however, adhesive failure can occur on interfaces between dissimilar adherend materials subjected to overstress loads [83].

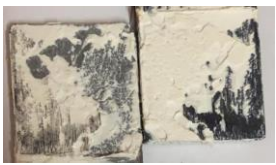
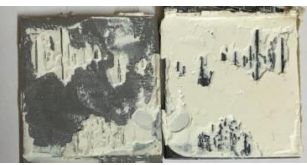







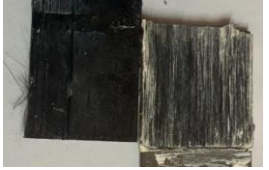
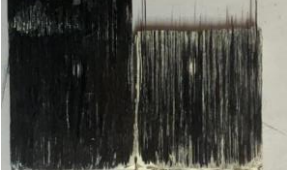

- **Cohesive Failure:** Cohesive failure occurs when a layer of adhesive material remains bonded to both adherend surfaces. This type of failure signifies that the bond exhibits high strength performance and failure occurs due to shear or a combination of shear and peel stresses [84].
- **Thin Layer Cohesive Failure:** This failure mode is similar to cohesive failure; however, it occurs very close to an adhesive-adherend interface [85]. A thick layer of adhesive is observed on one adherend surface while a thinner layer is present on the other adherend.
- **Fiber Tear Failure:** Fiber tear failure occurs upon the appearance of reinforcing fibers on both surfaces after adhesive bond failure. This type of failure is common in adhesively bonded joints having continuous fiber reinforced composite [86].
- **Light Fiber Tear Failure:** This type of failure is characterized by a thin layer of FRP resin matrix appearing on the adhesives, with few or no glass fibers transferred from adherend to adhesive [85].
- **Stock Break Failure:** This failure mode occurs outside the bonded region . Stock break failure is usually observed in composites with frail fibers [86].

7.3.1. Tested Samples Failure Modes

Majority of the tested samples failed in a mixed mode (cohesive - adhesive) with larger areas encompassing adhesive failure at the loading rate of 250 mm/min at temperatures below 100°C. On the other hand, at 100°C, although multiple samples exhibited extensive softening of the CFRP adherend at the loading rates of 1 and 10 mm/min, light fiber tear failure was apparent at the mentioned loading rates. However,

increasing the loading rate to 250 mm/min resulted in a mixed mode cohesive – adhesive failure. Table 11 presents the obtained surface morphology for the tested joints.


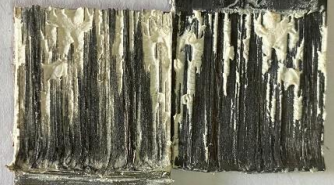

Table 11. Surface morphology of the tested joints after failure.

<div style="display: flex; flex-direction: column; align-items: center;"> <div style="display: flex; flex-direction: row;"> <div style="writing-mode: vertical-rl; transform: rotate(180deg);">Loading Rate (mm/min)</div> <div style="writing-mode: vertical-rl; transform: rotate(180deg);">Temperature (°C)</div> </div> </div>	1	10	250
25			
40			
55			
100			

The mixed mode (cohesive - adhesive) failure was also the prevalent failure mode upon increasing adhesive thickness. However, a thinner adhesive layer was observed on the CFRP adherend for the joints having a 1mm bondline thickness. Moreover, light fiber tear was also apparent for one of the tested samples. On the contrary, mixed mode (cohesive - adhesive) failure was prevalent for the joints bonded with a 1.2 mm adhesive

thickness. Table 12 presents the obtained surface morphology for the tested joints with different bondline thicknesses.

Table 12. Surface morphology of the tested joints with different adhesive bondline thickness.

Adhesive Thickness (mm)		
0.76	1	1.2
		

CHAPTER 8

NUMERICAL MODELING

To model the hyperelastic behavior of the flexible adhesive understudy, a numerical analysis was performed using the FEM software ABAQUS. For hyperelastic materials, ABAQUS relates the stresses to strains using the strain energy potential (U). ABAQUS integrates multiple strain energy potentials such as: polynomial model, reduced polynomial model, Ogden model, Marlow model, Arruda-Boyce and van der Waals model. Two cases of the available models are selected to model the behavior of the hyperelastic material understudy: The Neo-Hookean model, which is a special case of the reduced polynomial model, which in turn is a particular case of the polynomial model, and the Mooney-Rivlin model which is a special case of the polynomial model. Consequently, the polynomial and reduced polynomial formulation of the strain energy potential, Equation (3) and Equation (4) respectively, will be represented:

$$U = \sum_{i+j=1}^N C_{ij} (\bar{I}_1 - 3)^i (\bar{I}_2 - 3)^j + \sum_{i=1}^N \frac{1}{D_i} (J_{el} - 1)^{2i} \quad (3)$$

$$U = \sum_{i=1}^N C_{i0} (\bar{I}_1 - 3)^i + \sum_{i=1}^N \frac{1}{D_i} (J_{el} - 1)^{2i} \quad (4)$$

With the deviatoric strains, \bar{I}_i , being defined as:

$$\bar{I}_1 = \bar{\lambda}_1^2 + \bar{\lambda}_2^2 + \bar{\lambda}_3^2 \quad (5)$$

$$\bar{I}_2 = \bar{\lambda}_1^{(-2)} + \bar{\lambda}_2^{(-2)} + \bar{\lambda}_3^{(-2)} \quad (6)$$

With the deviatoric stretches $\bar{\lambda}_i$ being formulated as follows:

$$\bar{\lambda}_i = J^{-\frac{1}{3}} \lambda_i$$

However, with the assumption of incompressibility, the right terms of Equation (3) and Equation (4) disappear. Equation (3) and Equation (4) can be written as follows:

$$U = \sum_{i+j=1}^N C_{ij} (\bar{I}_1 - 3)^i (\bar{I}_2 - 3)^j \quad (7)$$

$$U = \sum_{i=1}^N C_{i0} (\bar{I}_1 - 3)^i \quad (8)$$

Moreover, the invariants should also be reformulated due to the incompressibility assumption where the total volume ratio, J , is set to unity. Thus, Equation (5) and Equation (6) can be written as follows:

$$\bar{I}_1 = \lambda_1^2 + \lambda_2^2 + \lambda_3^2 \quad (9)$$

$$\bar{I}_2 = \lambda_1^{-2} + \lambda_2^{-2} + \lambda_3^{-2} \quad (10)$$

Considering the case of uniaxial loading, with λ_1 being the stretch ratio along the loading direction, the stretch ratios can be defined as follows:

$$\lambda_1 = \lambda = \frac{L}{L_0} ; \quad \lambda_2 = \lambda_3 = \frac{1}{\sqrt{\lambda}}$$

Thus, the strain invariants, Equation (9) and Equation (10), can be rewritten in terms of the stretch ratios as follows:

$$\bar{I}_1 = \lambda^2 + 2\lambda^{-1}$$

$$\bar{I}_2 = 2\lambda + \frac{1}{\lambda^2}$$

As previously mentioned, the Neo-Hookean and Mooney-Rivlin models are special cases of the polynomial form of the strain energy potential where when only one parameter is retained from Equation (8), we obtain the Neo-Hookean model, and when two terms are retained from Equation (7), we obtain the Mooney-Rivlin model. An overview of both models is presented below:

1. Neo-Hookean:

The Neo-Hookean model is a simple hyperelastic constitutive model that can predict stress strain behavior of materials [87]. This model is a special case of the reduced

polynomial model and requires only one material parameter C_{10} . The Neo-Hookean model is as follows:

$$U = C_{10}(\bar{I}_1 - 3) \quad (11)$$

Although this model allows simple prediction of the hyperelastic behavior of the material; however, it is known that it fails to predict this phenomenon at large strains. Therefore, models that incorporate additional parameters can be used such as the Mooney-Rivlin model.

2. Mooney-Rivlin:

The Mooney-Rivlin hyperelastic model is one of the most used models that presents good convergence for a relatively large range of deformation [88]. The Mooney-Rivlin model has a strain energy function of the form shown in Equation (12):

$$U = C_{10}(\bar{I}_1 - 3) + C_{01}(\bar{I}_2 - 3) \quad (12)$$

Therefore, to obtain the required parameters for both presented models, uniaxial tensile data should be incorporated to fit Equation (11) and Equation (12). This process can be performed by ABAQUS software that calibrates material parameters from the input stress - strain curve through the least squares fit. Moreover, a stability check across the input strain is performed to ensure applicability of the selected models.

Consequently, numerical analysis of the bonded joints was performed to analyze the stress distribution along the adhesive bondline and compare the results, particularly shear stress distribution, to the Volkersen analytical solution. A 2D hyperelastic numerical model was established to study the stress distribution along the adhesive bondline. A particular case of operating condition was selected for the various adhesive thicknesses (Testing Temperature = 25 °C , Loading Rate = 10 mm/min). The numerical procedure followed can be summarized as follows:

- Hyperelastic parameter determination:** The hyperelastic parameters should be first determined to replicate the adhesive's flexibility and behavior under the experimental load. These parameters are evaluated directly through ABAQUS after inputting the uniaxial tensile test data. As only the uniaxial extension case is considered, ABAQUS relates the nominal stress to the stretch ratio according to the following equation:

$$\sigma_{nominal} = 2(1 - \lambda^{-3}) \left(\lambda \frac{\partial U}{\partial I_1} + \frac{\partial U}{\partial I_2} \right)$$

Both models , Neo-Hookean and Mooney- Rivlin models, were stable for all input strains and the following parameters were obtained:

Table 13. Hyperelastic parameters obtained after the fitting process.

Model	C_{10} (MPa)	C_{01} (MPa)
Mooney-Rivlin	0.177	0.191
Neo-Hookean	0.269	

- Model dimensions and properties:** The SLJ is modeled according to the dimensions in Figure 23 and Table 9 with material properties mentioned in Table 7, Table 8, and Table 13. The CFRP and steel adherend are modeled as isotropic elastic materials and the adhesive is modeled using the obtained hyperelastic parameters.

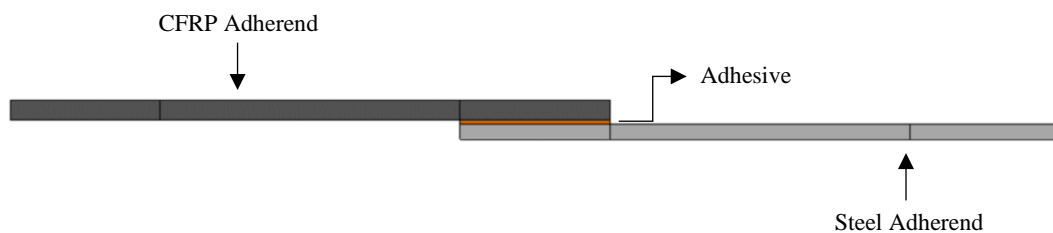


Figure 35. Modelled SLJ specimen.

- Boundary Conditions:** The boundary conditions represent the constraints and forces applied on the single lap joint specimen. The lap joint was fixed on one end using the encastre constraint and a force, based on the experimental results, is applied to a reference point coupled to all nodes constituting the gripping area. The reference point was also constrained in all directions except the direction of the applied force.

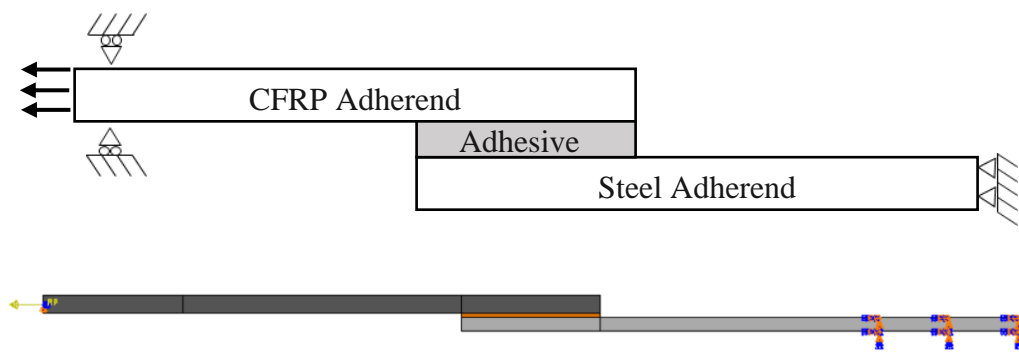


Figure 36. The applied boundary conditions on the modeled SLJ specimen.

- Mesh:** A fine mesh is established particularly near the overlap area where a higher mesh density was used to achieve more precise results. A four-node, two-dimensional plane stress element with reduced integration and hourglass control (CPS4R) was selected for the SLJ components.

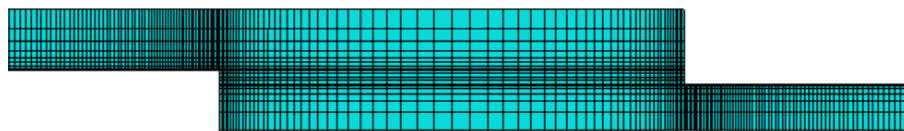


Figure 37. Meshing of the SLJ model with a higher mesh density in the overlap region.

8.1. Numerical Results

The simulation was then performed for all bondline thicknesses, and the numerical results were exported and compared to the experimental data. The stress distributions and force-displacement curves were plotted to study the behavior of the adhesive bond under prespecified loads.

8.1.1. Stress Distribution

The stress distributions were extracted along the centerline shown in Figure 38. The shear, peel and von Mises stresses were all extracted and plotted. To compare the shear stress distribution to the applicable analytical solution (Volkersen), the shear modulus (G_a) of the flexible adhesive should be determined. For small strains, this modulus depends only on the first order polynomial coefficients (C_{01} and C_{10}) through the following equation [89]:

$$G_a = 2(C_{01} + C_{10})$$

Therefore, the shear moduli for the Neo-Hookean and Mooney-Rivlin models are respectively:

$$G_{a,NH} = 0.538 \text{ MPa}$$

$$G_{a,MR} = 0.736 \text{ MPa}$$

Moreover, shear stress values were normalized by the average shear stress, $\tau_{average}$, calculated according to the following formula:

$$\tau_{average} = \frac{P}{l}$$

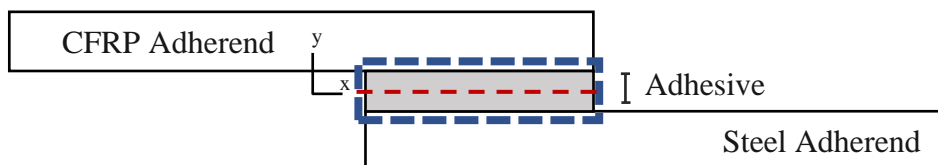
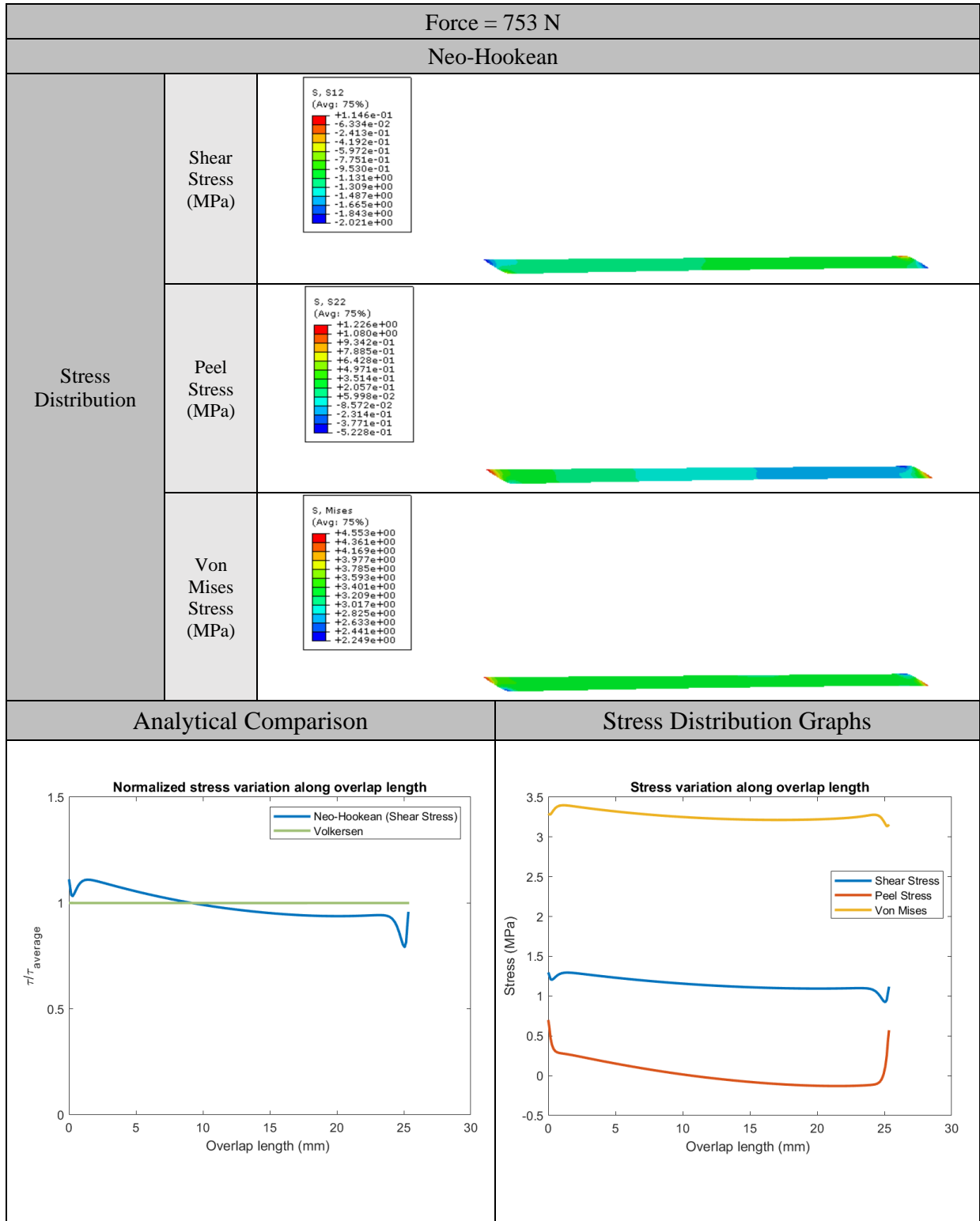
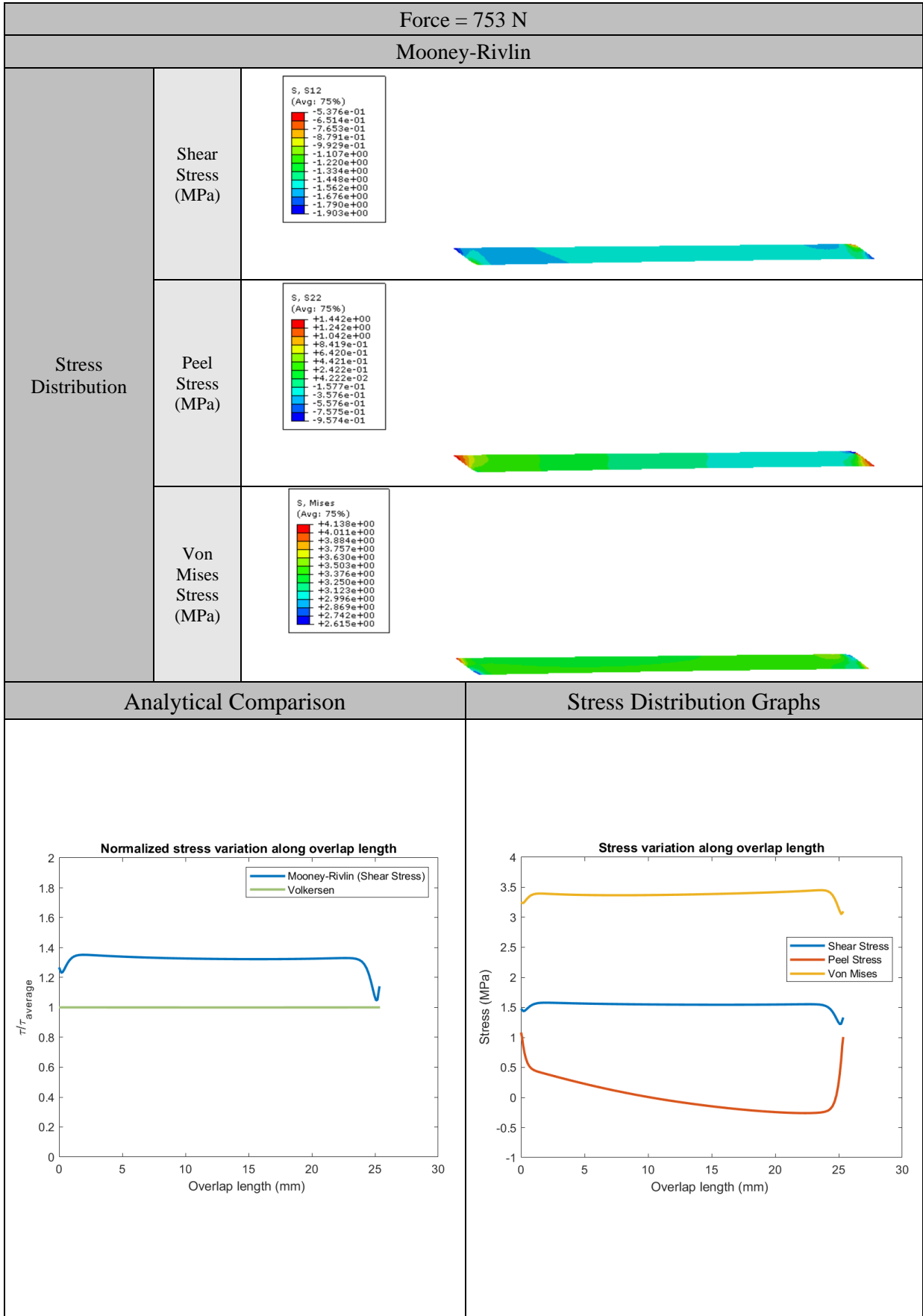


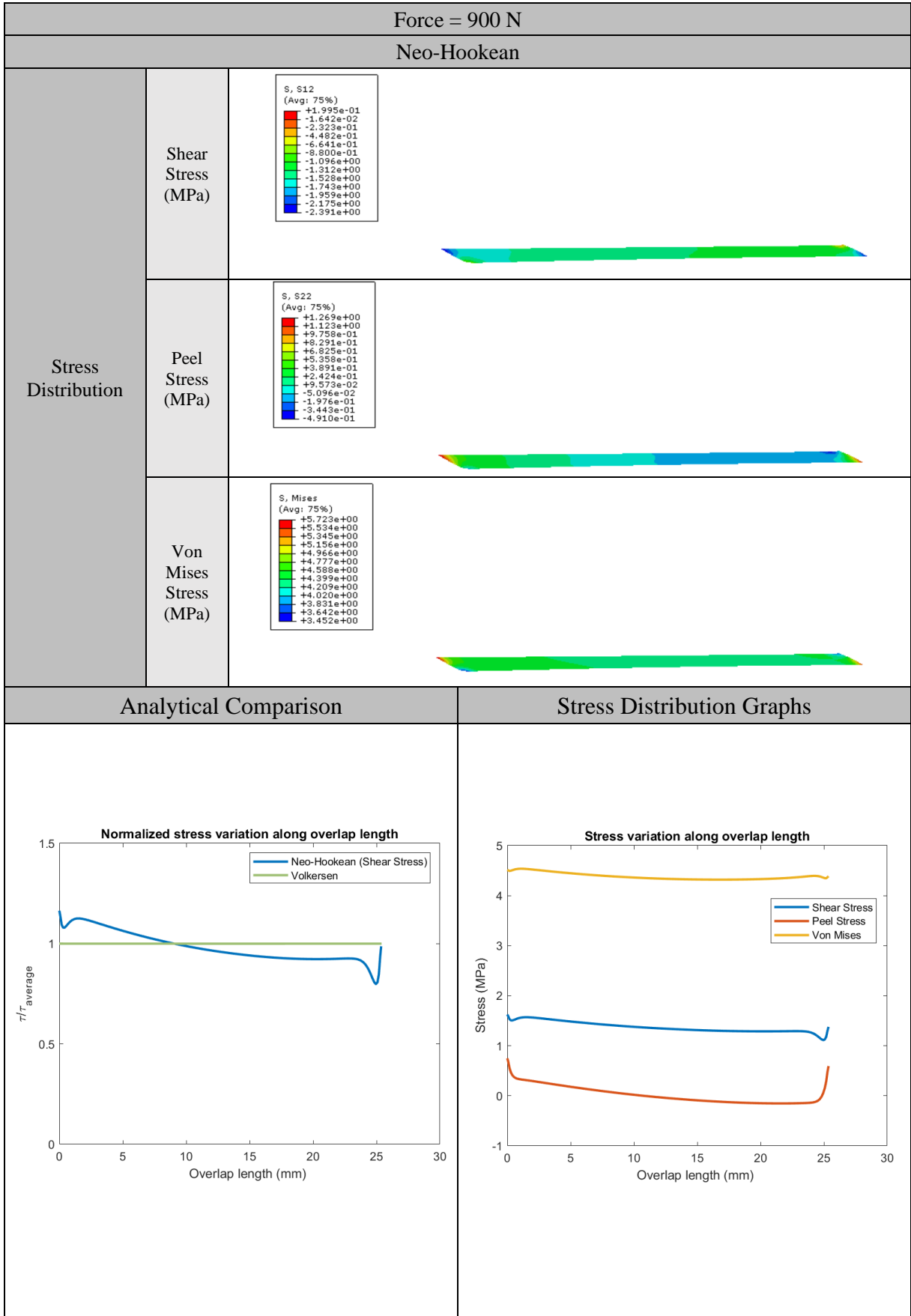
Figure 38. Centerline (red) selected to extract the stress distributions

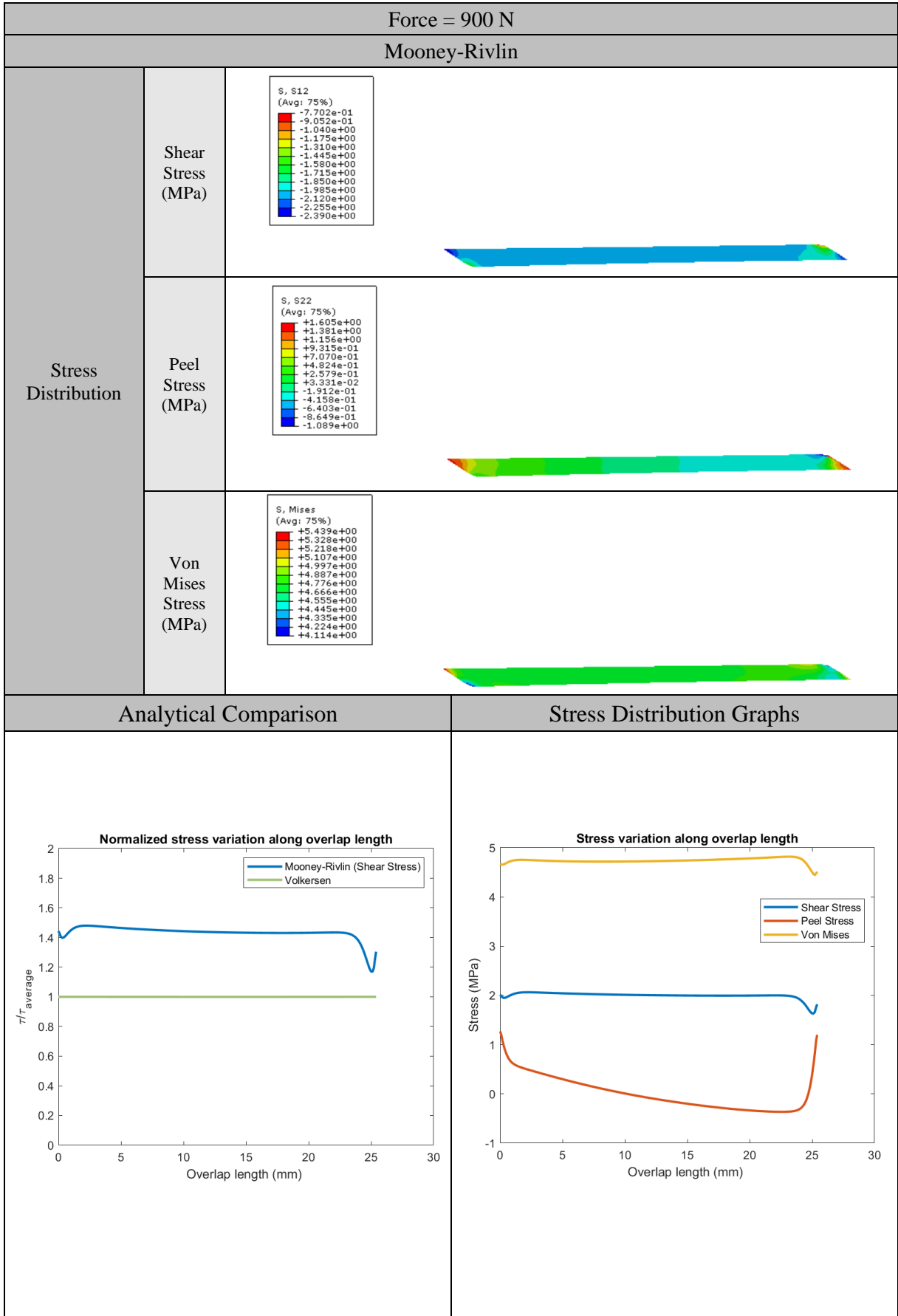
- For adhesive thickness = 0.76 mm:

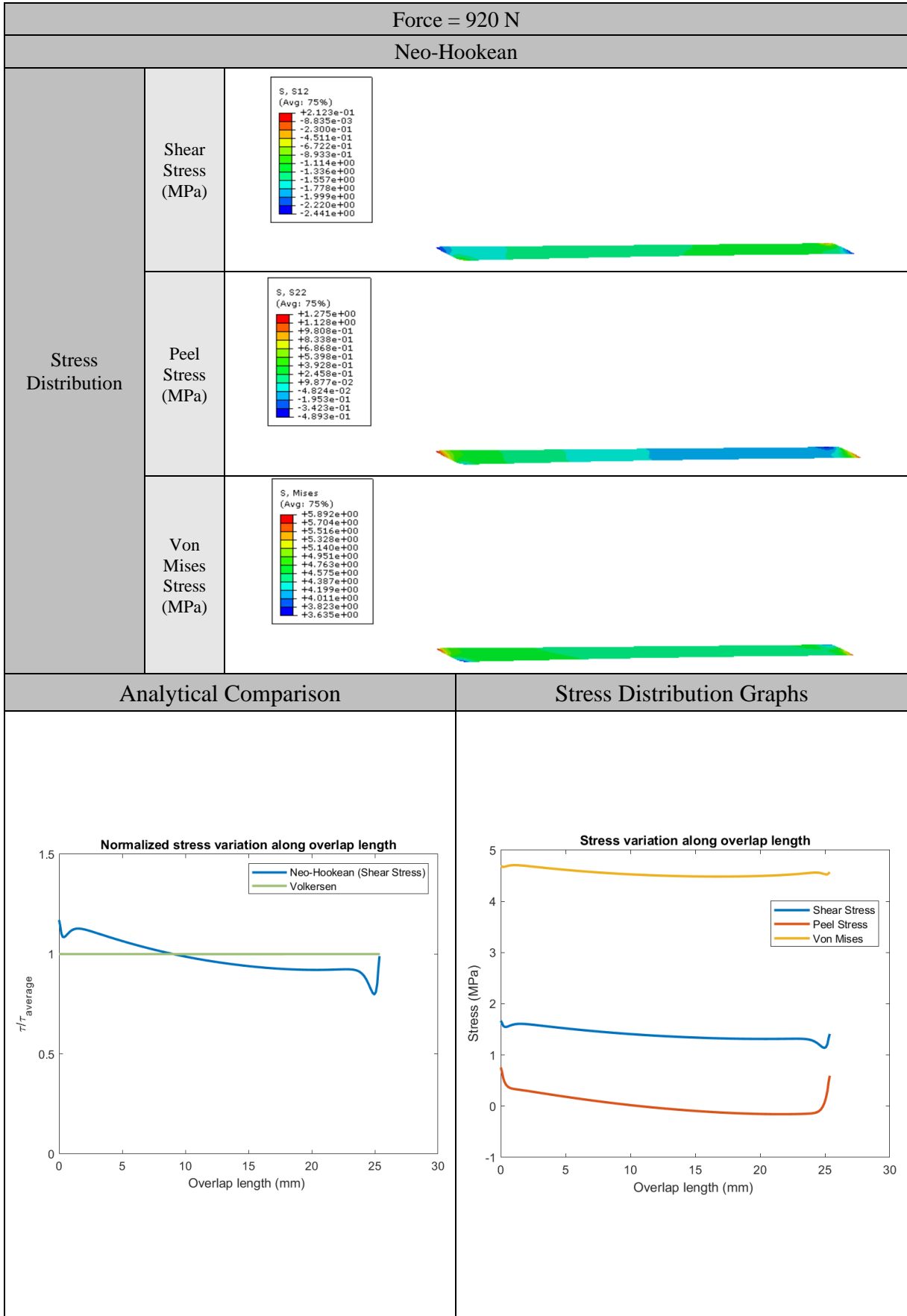
Table 14. Numerical results (Neo-Hookean and Mooney-Rivlin models) obtained for 0.76mm adhesive bondline thickness, where the maximum experimental force is applied for the selected joints.

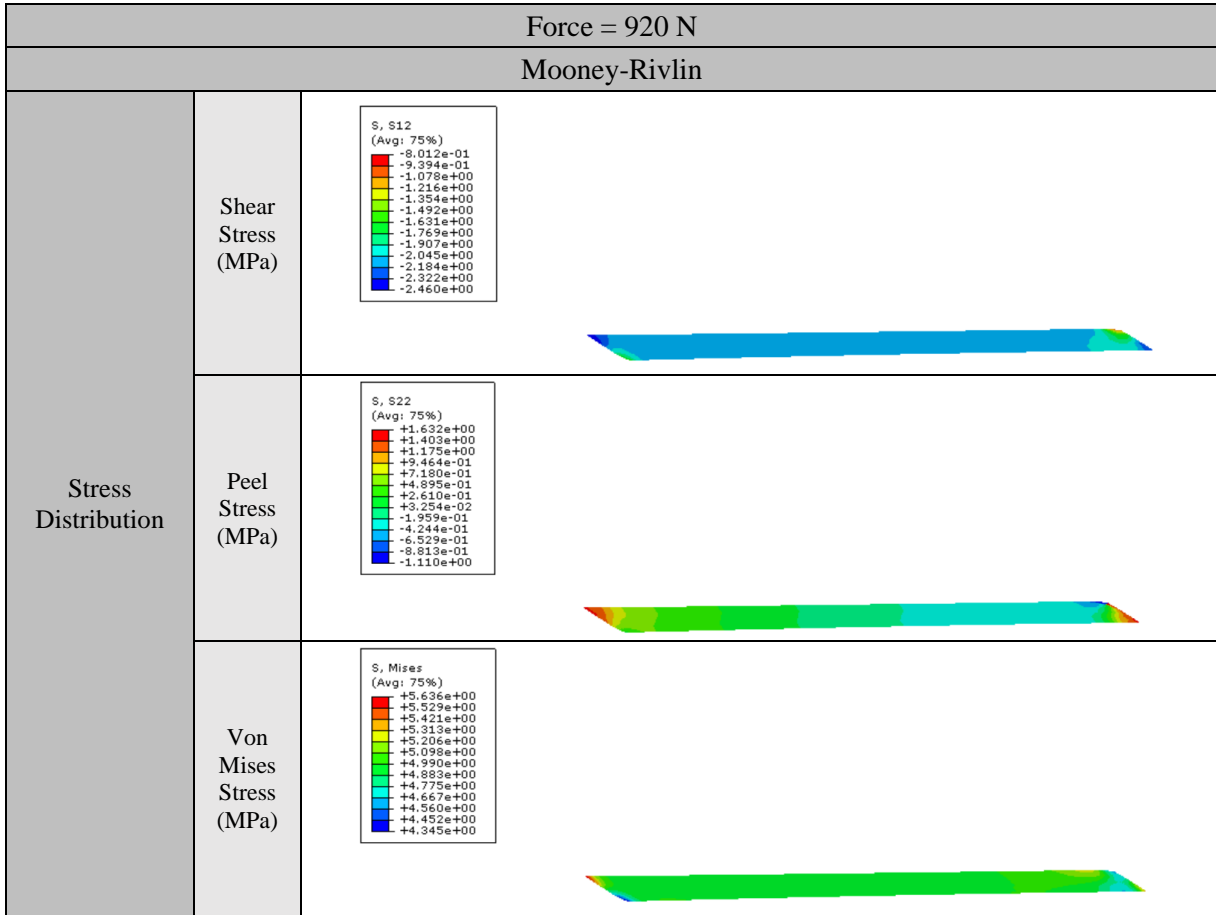




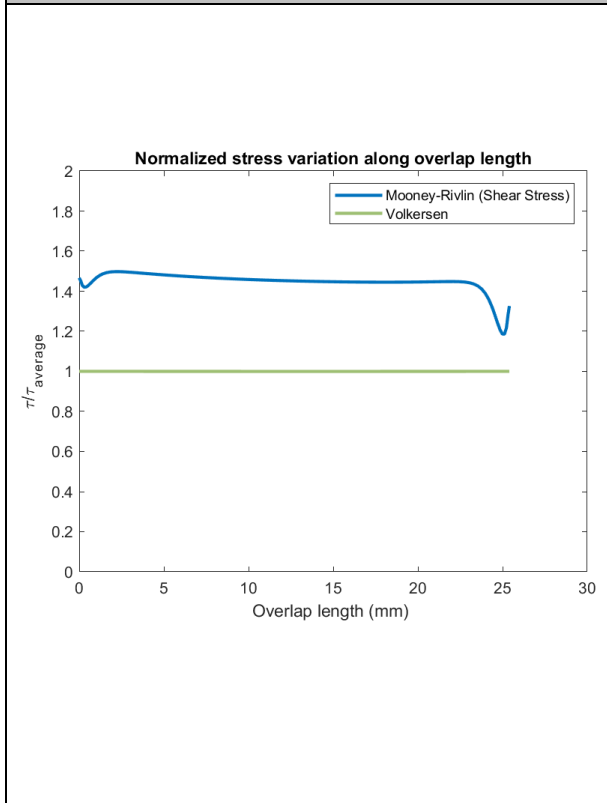




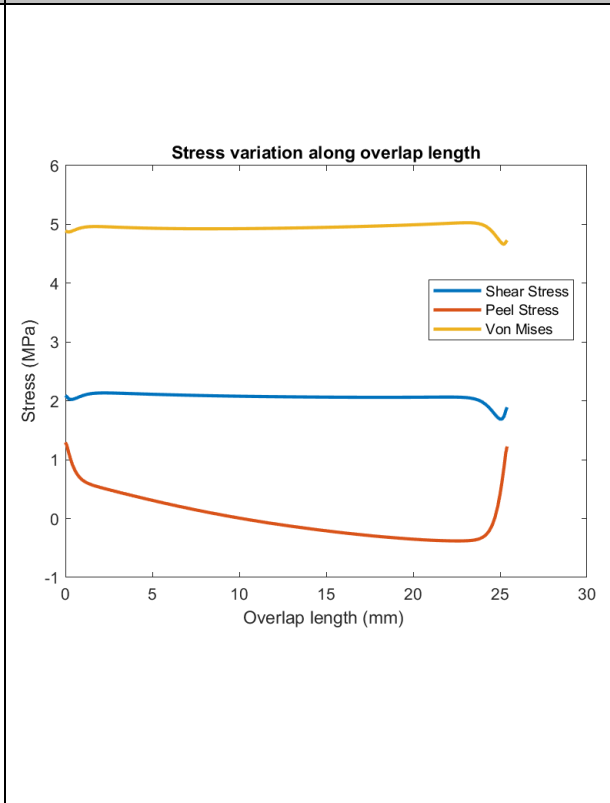




Analytical Comparison

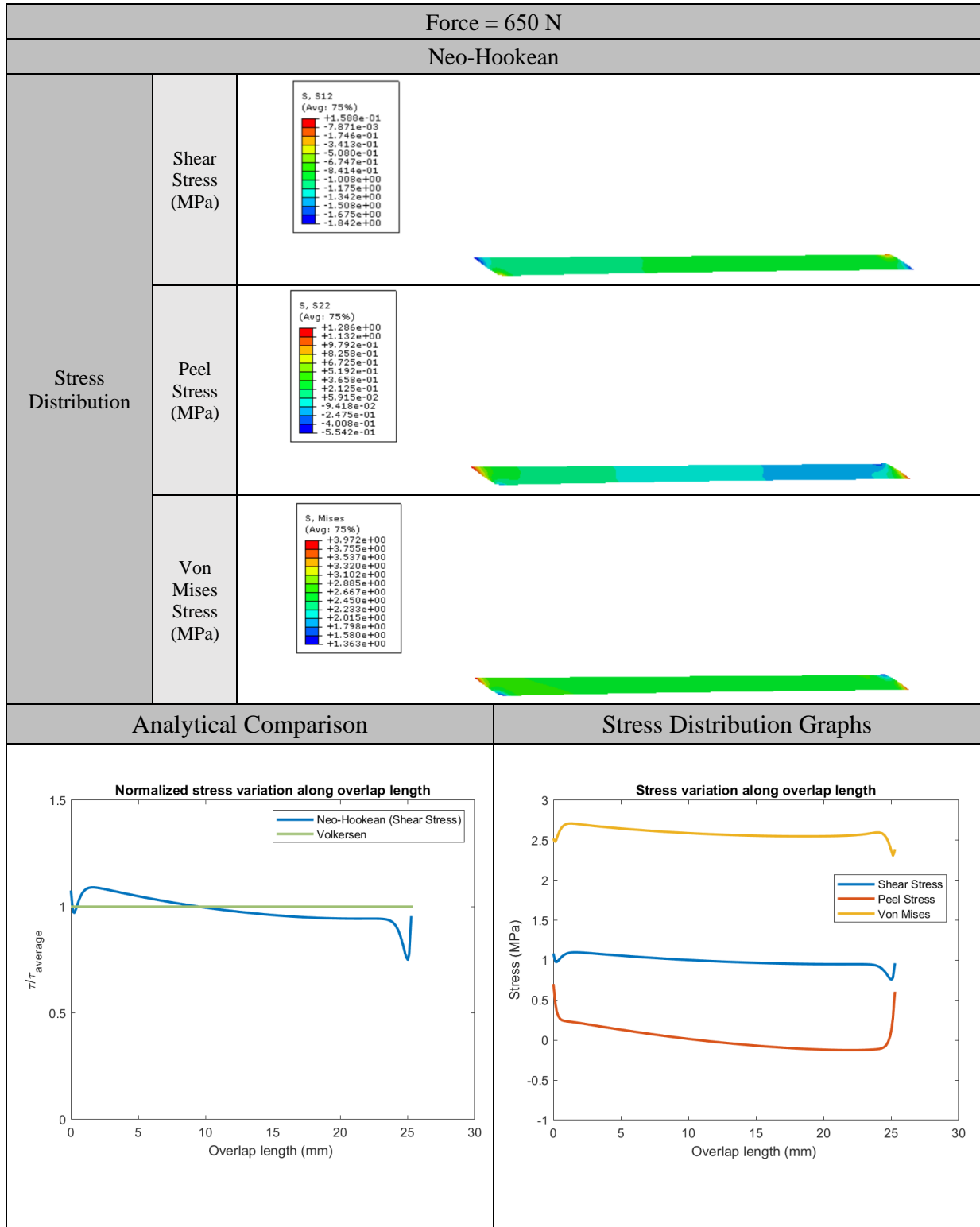


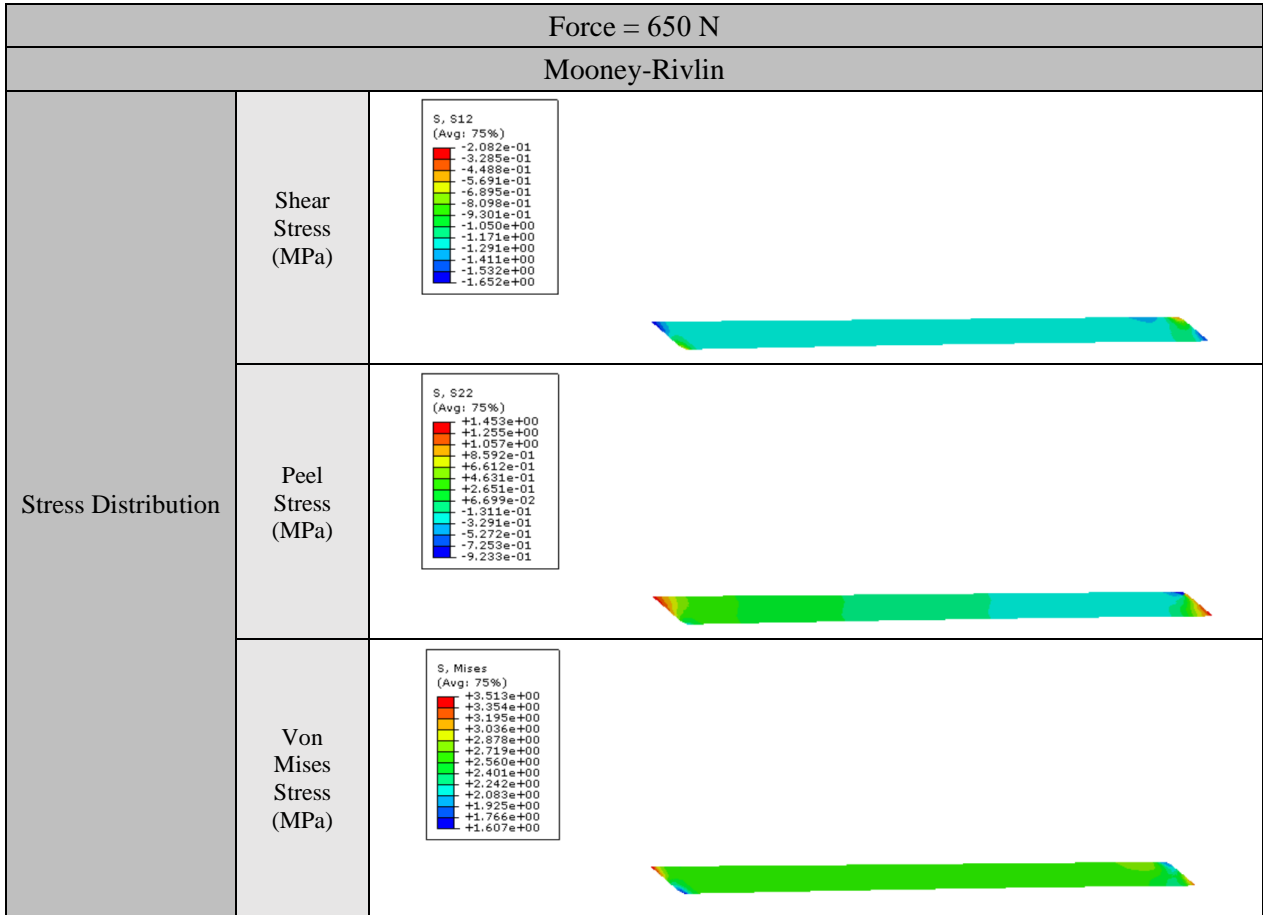
Stress Distribution Graphs



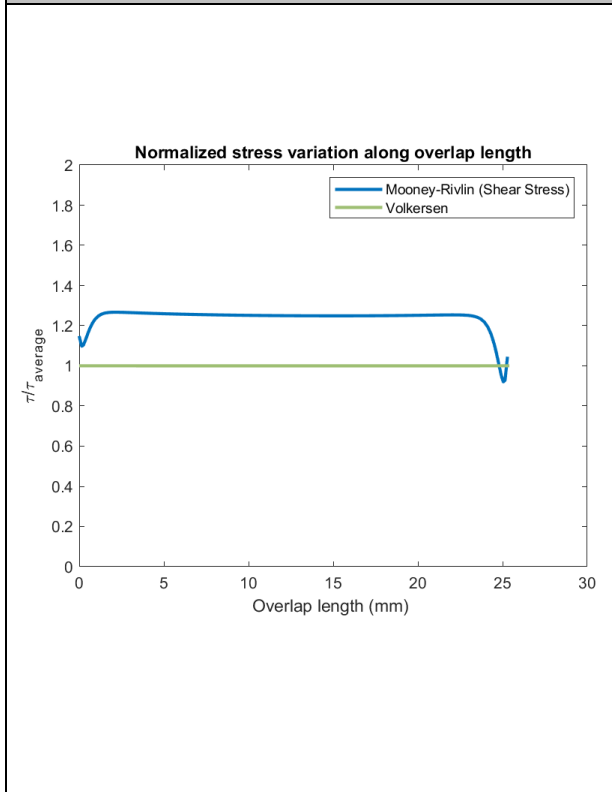
- For adhesive thickness = 1 mm:

Table 15. Numerical results (Neo-Hookean and Mooney-Rivlin models) obtained for 1mm adhesive bondline thickness, where the maximum experimental force is applied for the selected joints.

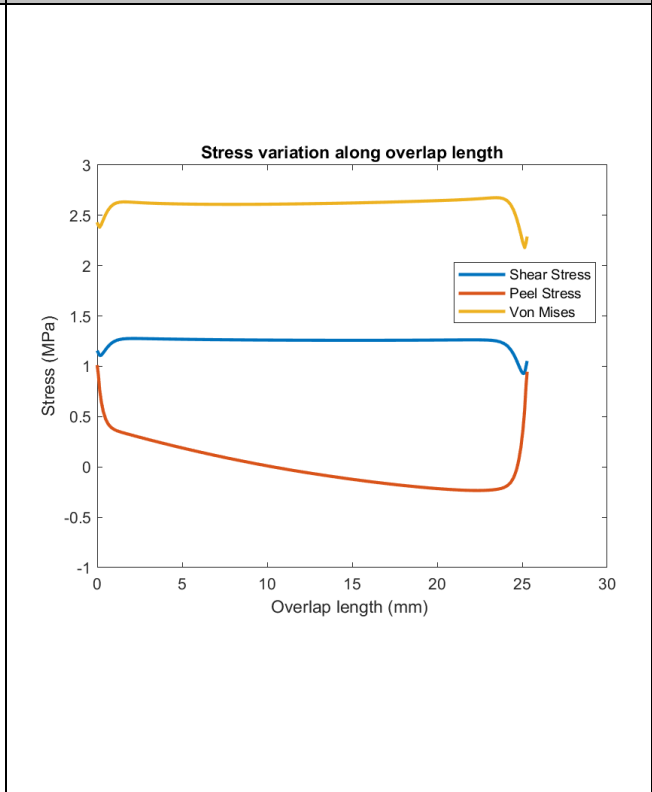




Analytical Comparison

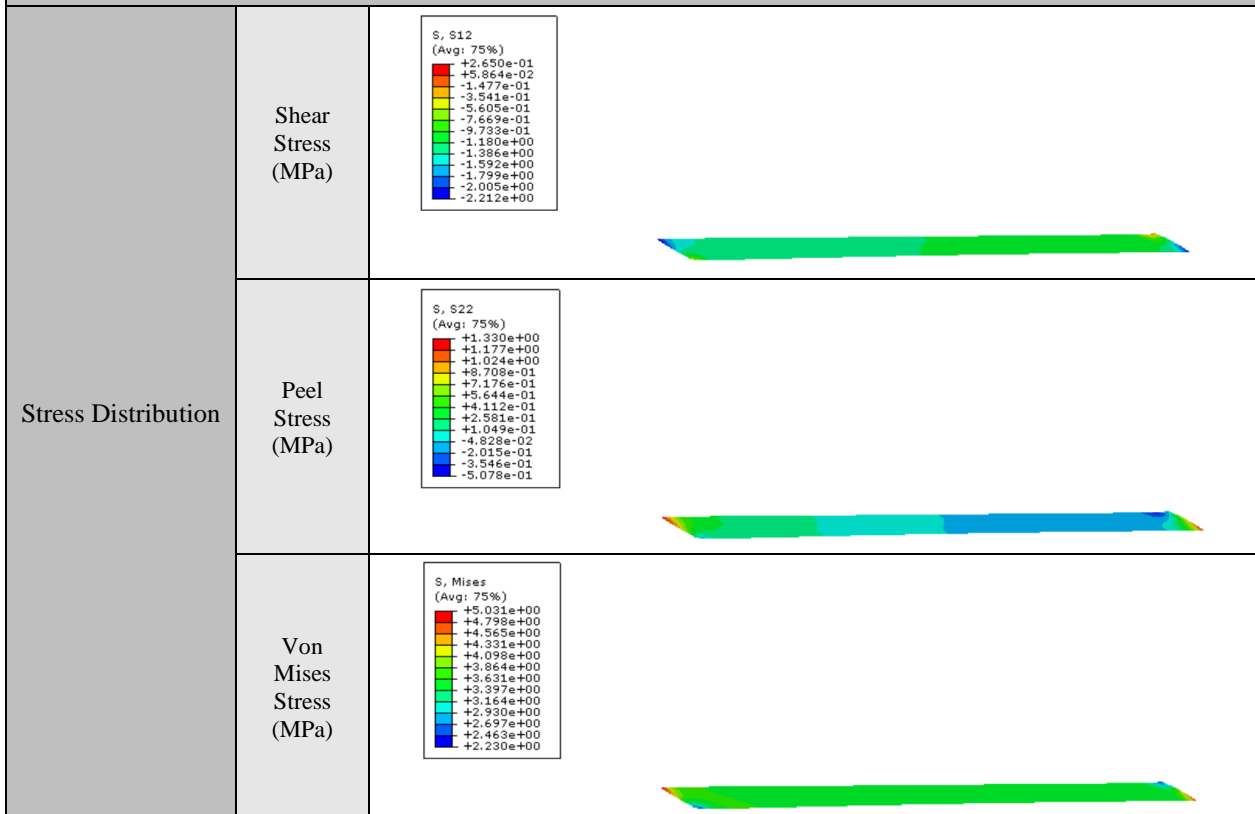


Stress Distribution Graphs

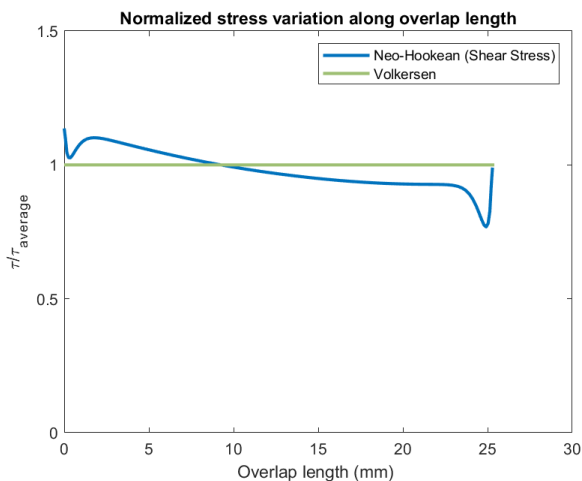


Force = 787 N

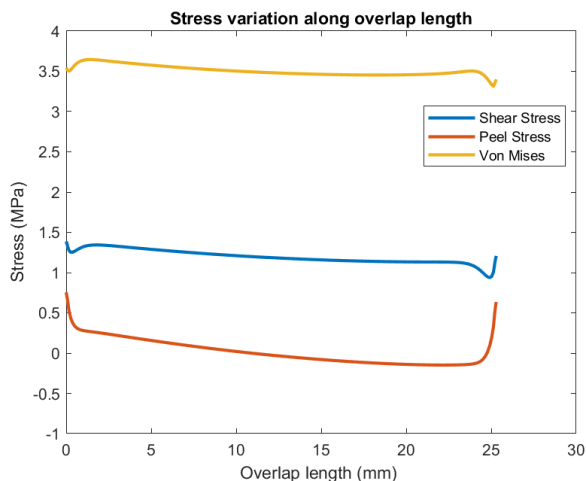
Neo-Hookean

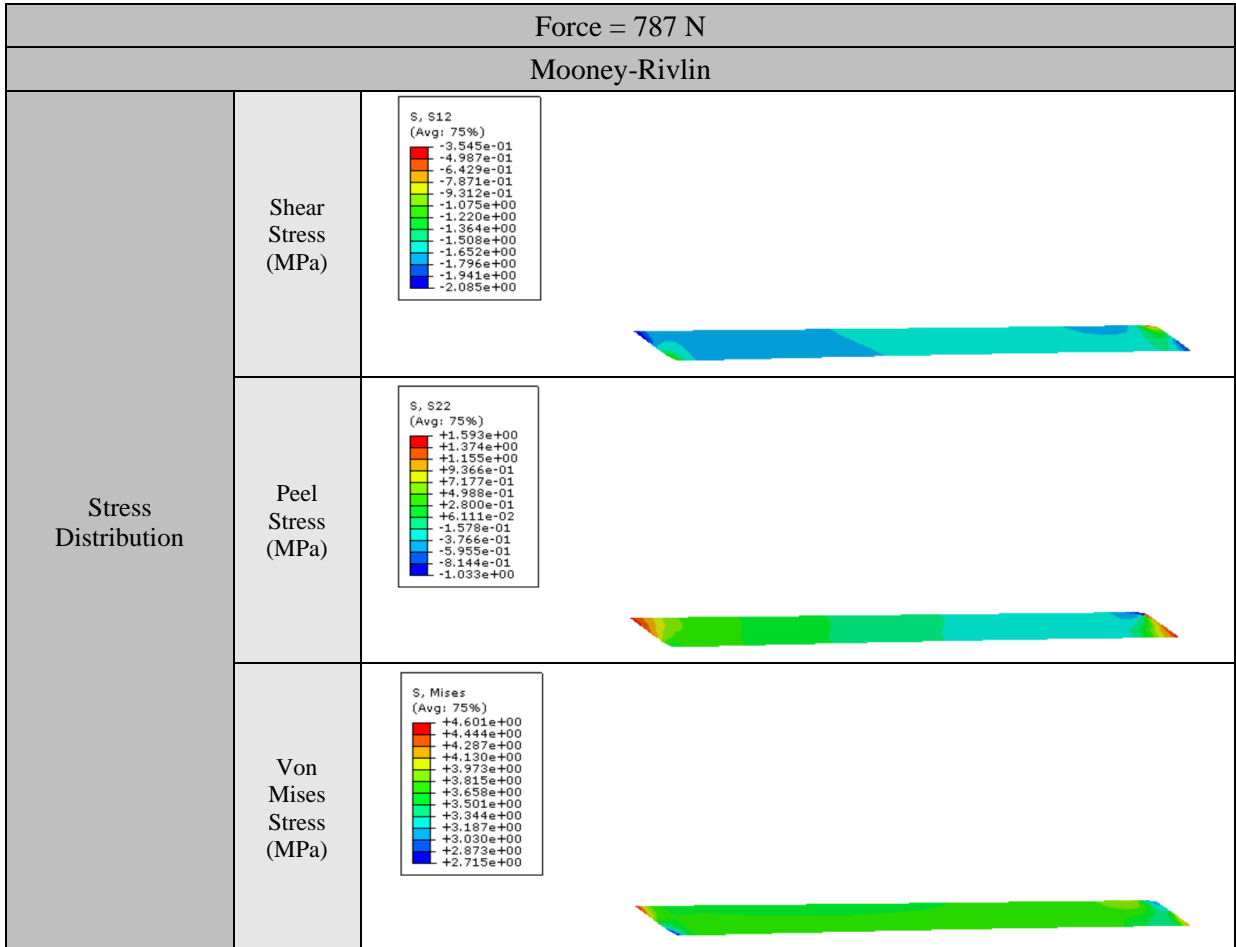


Analytical Comparison

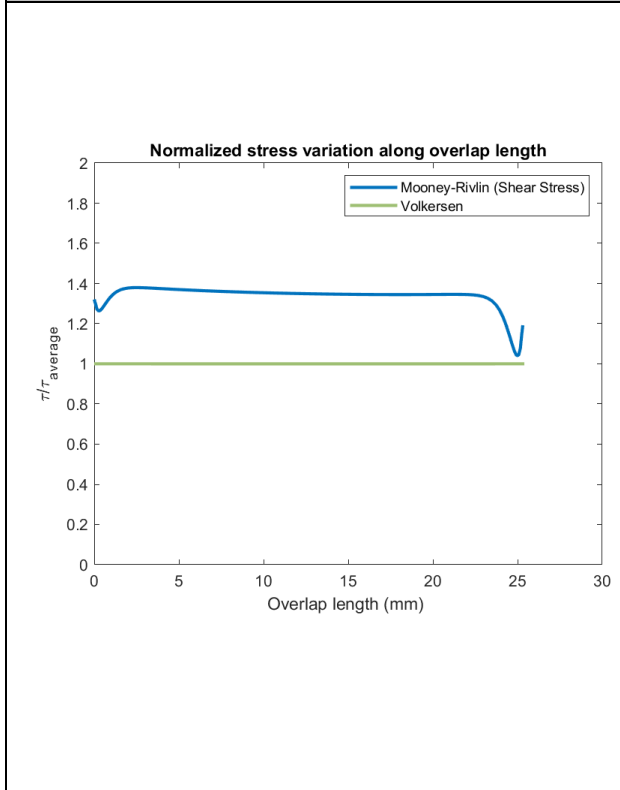


Stress Distribution Graphs

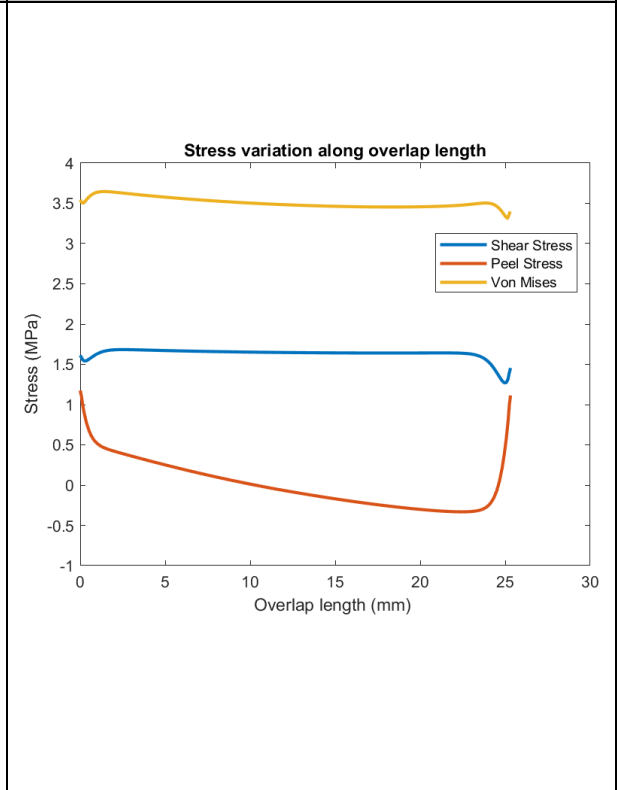


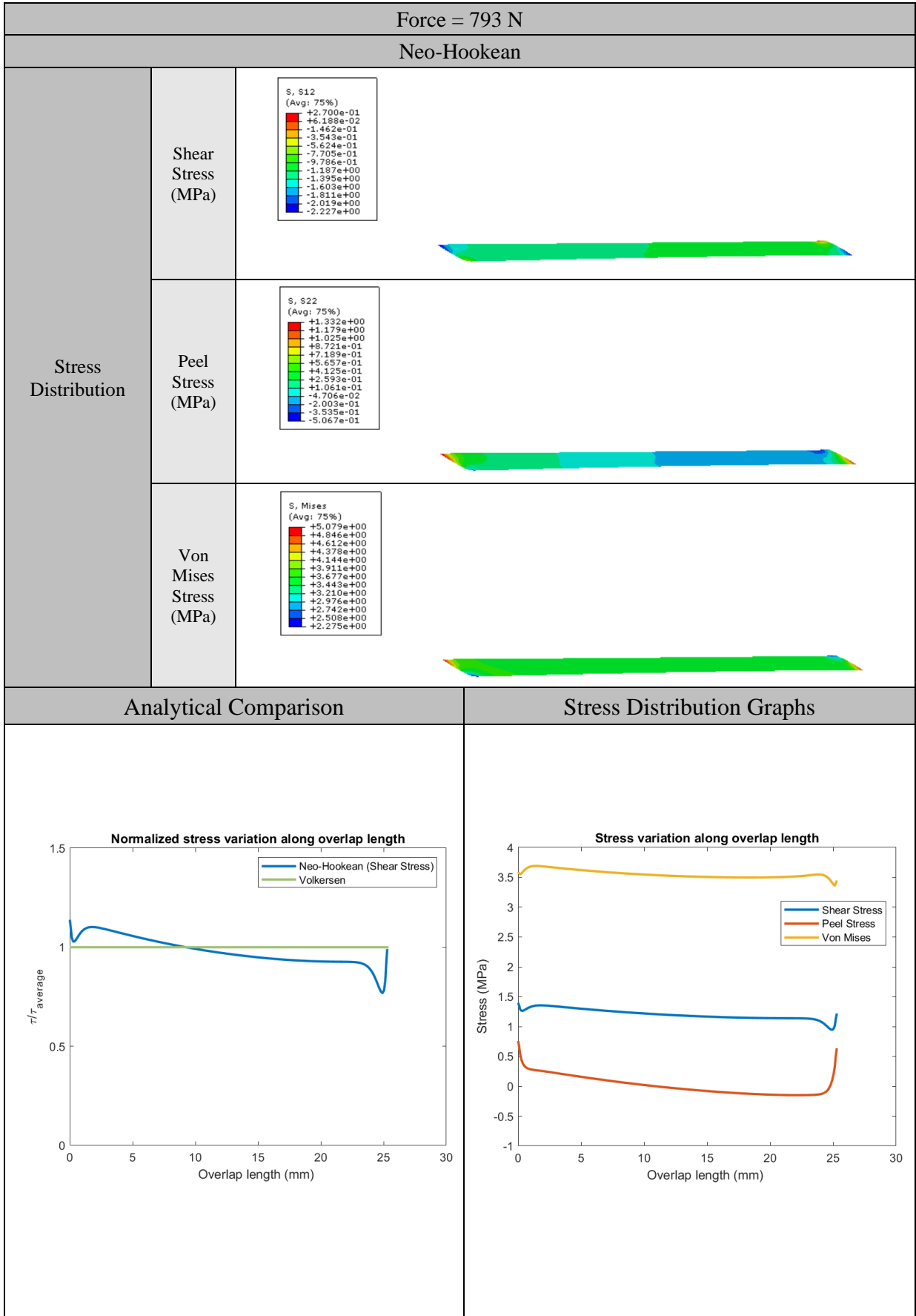


Analytical Comparison



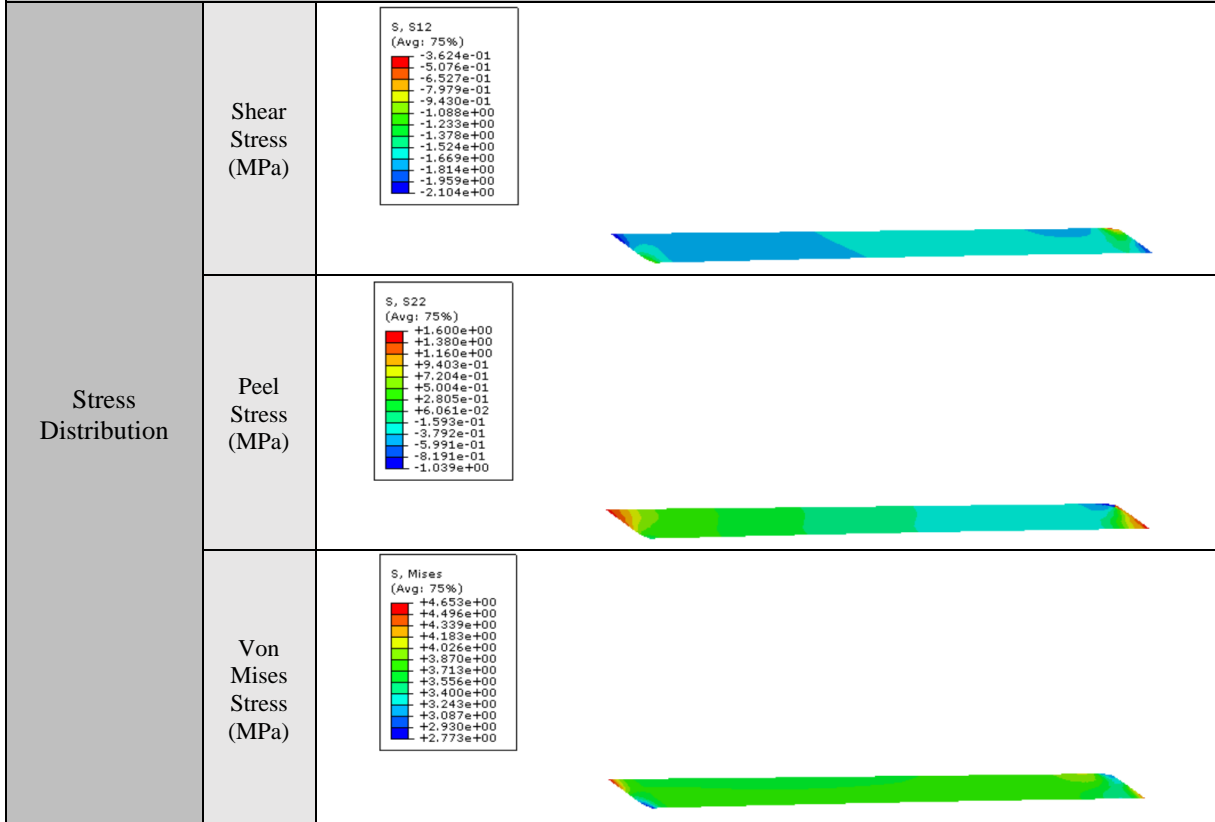
Stress Distribution Graphs



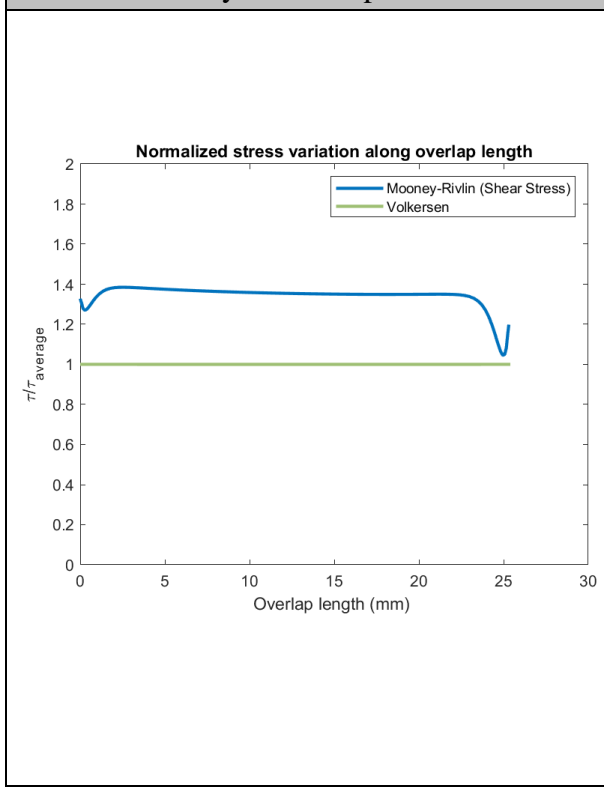


Force = 793 N

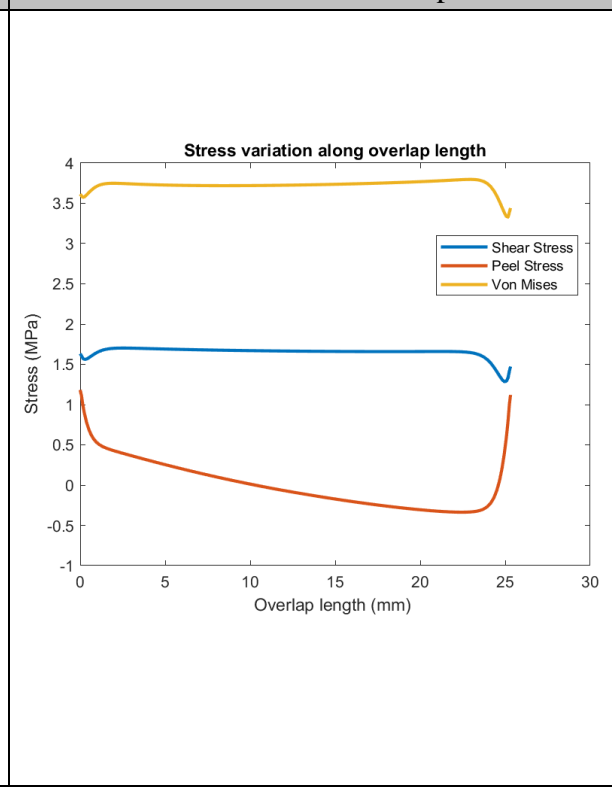
Mooney-Rivlin



Analytical Comparison

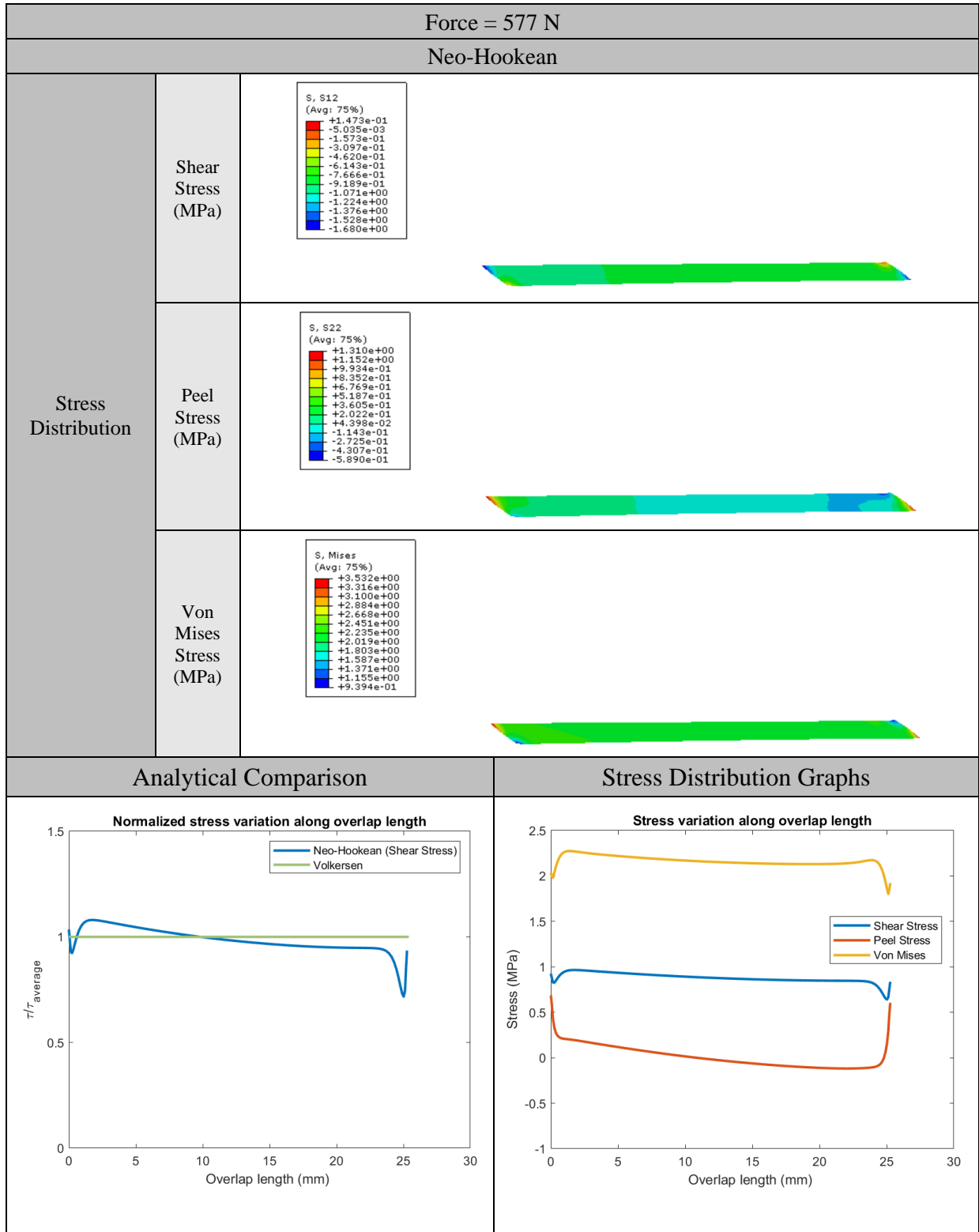


Stress Distribution Graphs



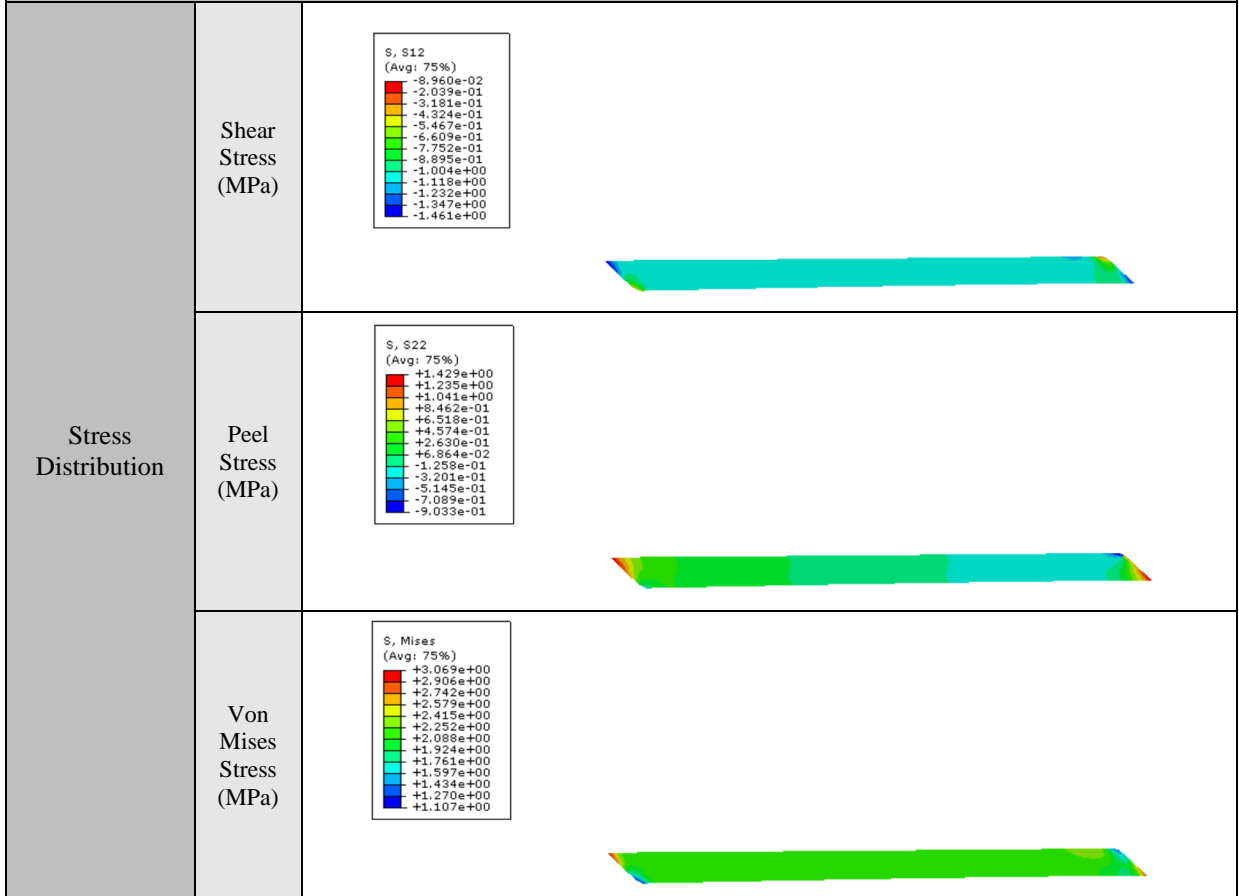
- For adhesive thickness = 1.2 mm:

Table 16. Numerical results (Neo-Hookean and Mooney-Rivlin models) obtained for 1.2mm adhesive bondline thickness, where the maximum experimental force is applied for the selected joints.



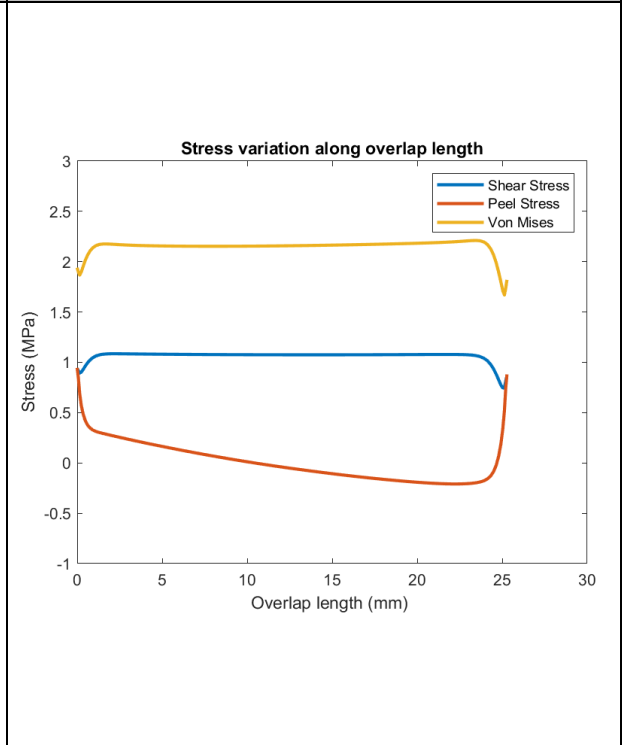
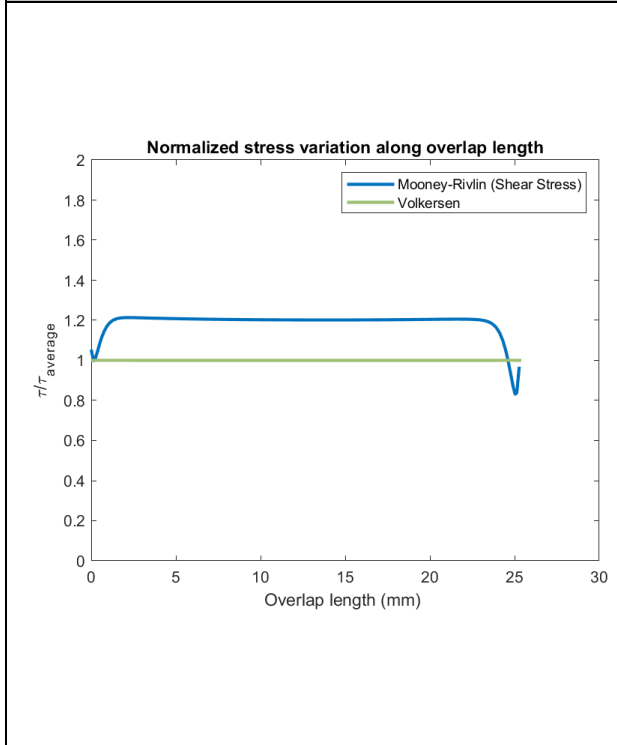
Force = 577 N

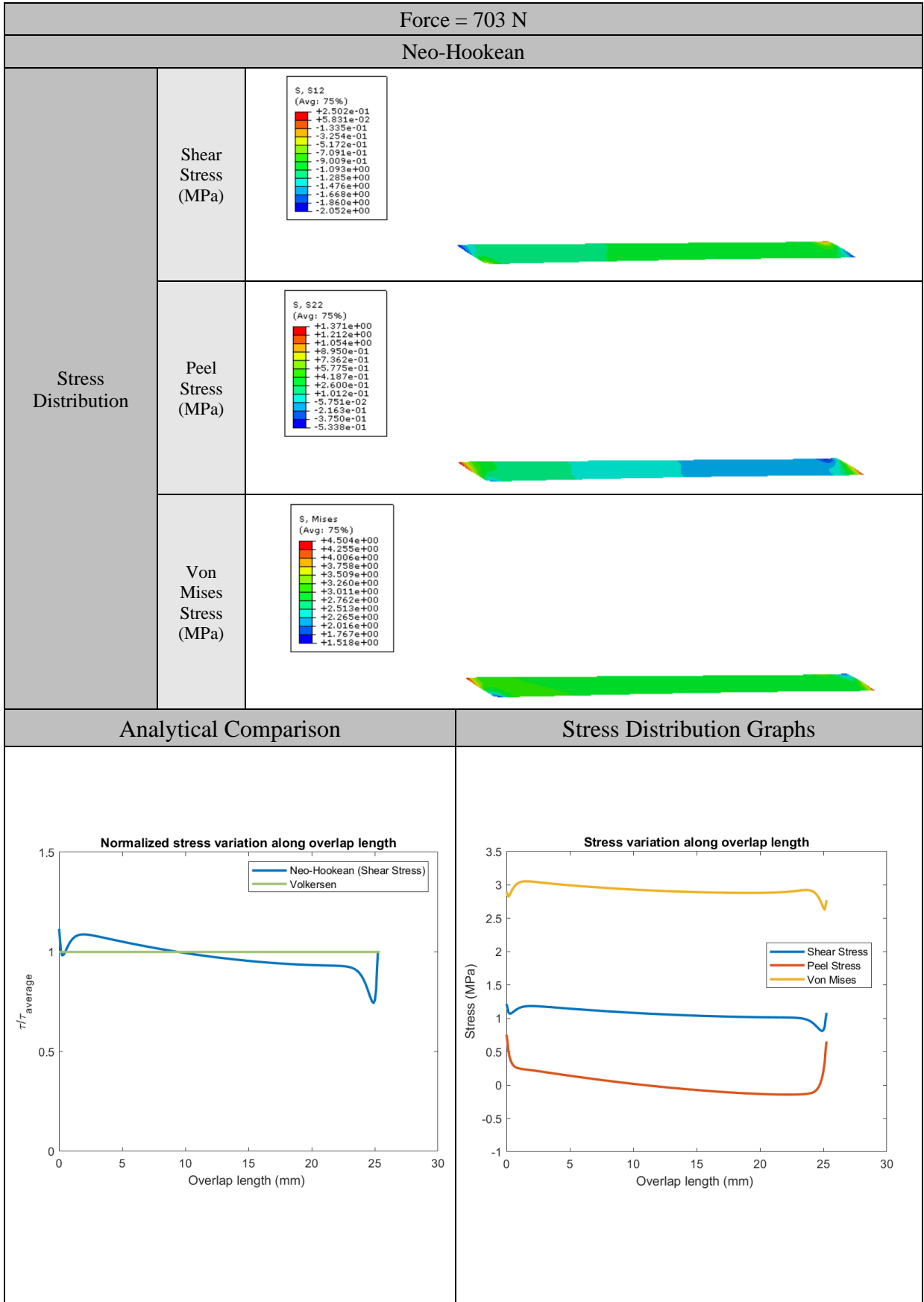
Mooney-Rivlin



Analytical Comparison

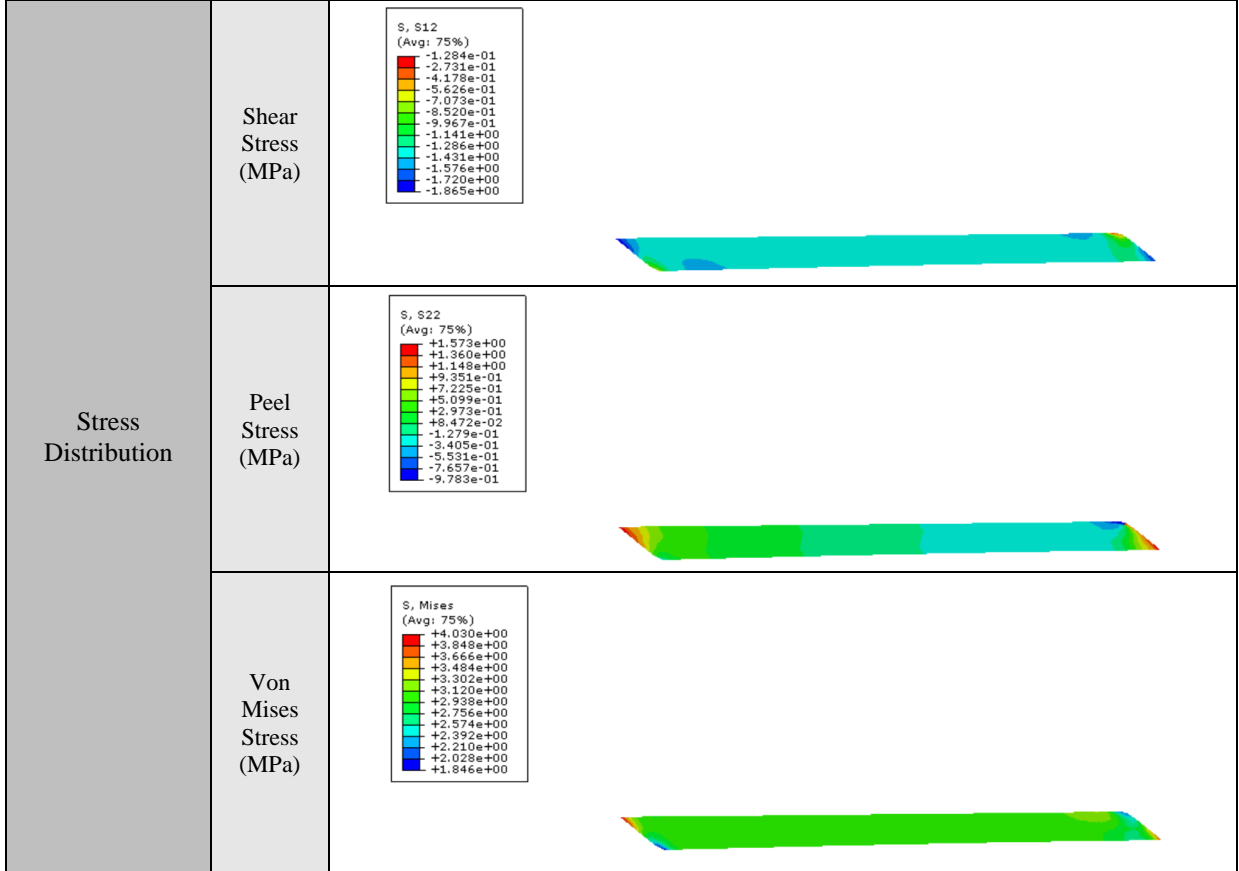
Stress Distribution Graphs





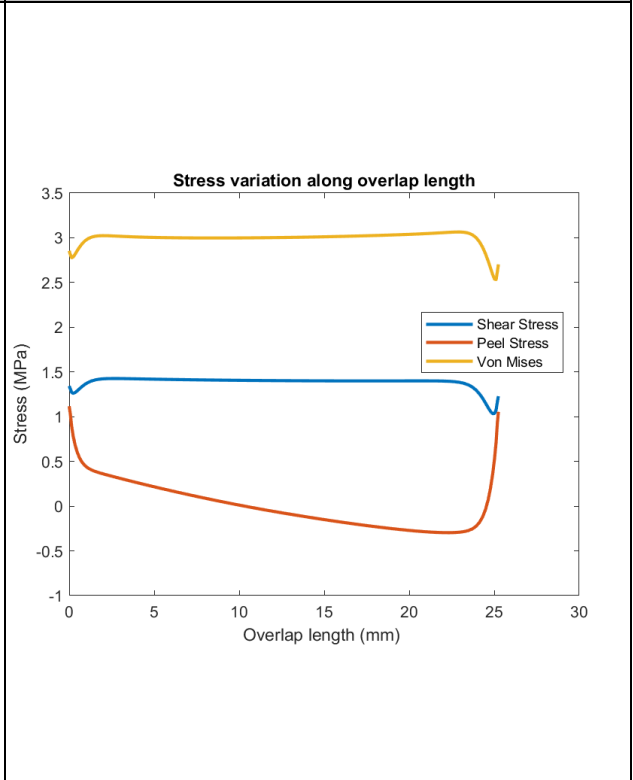
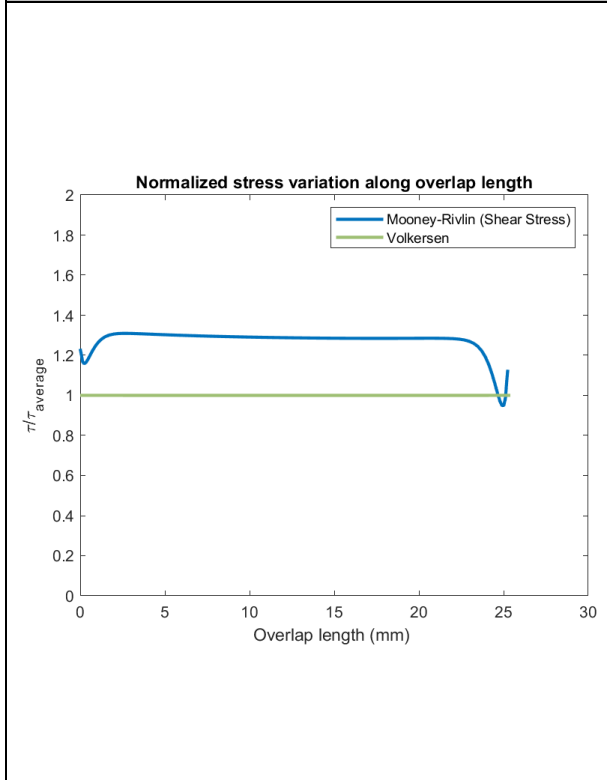
Force = 703 N

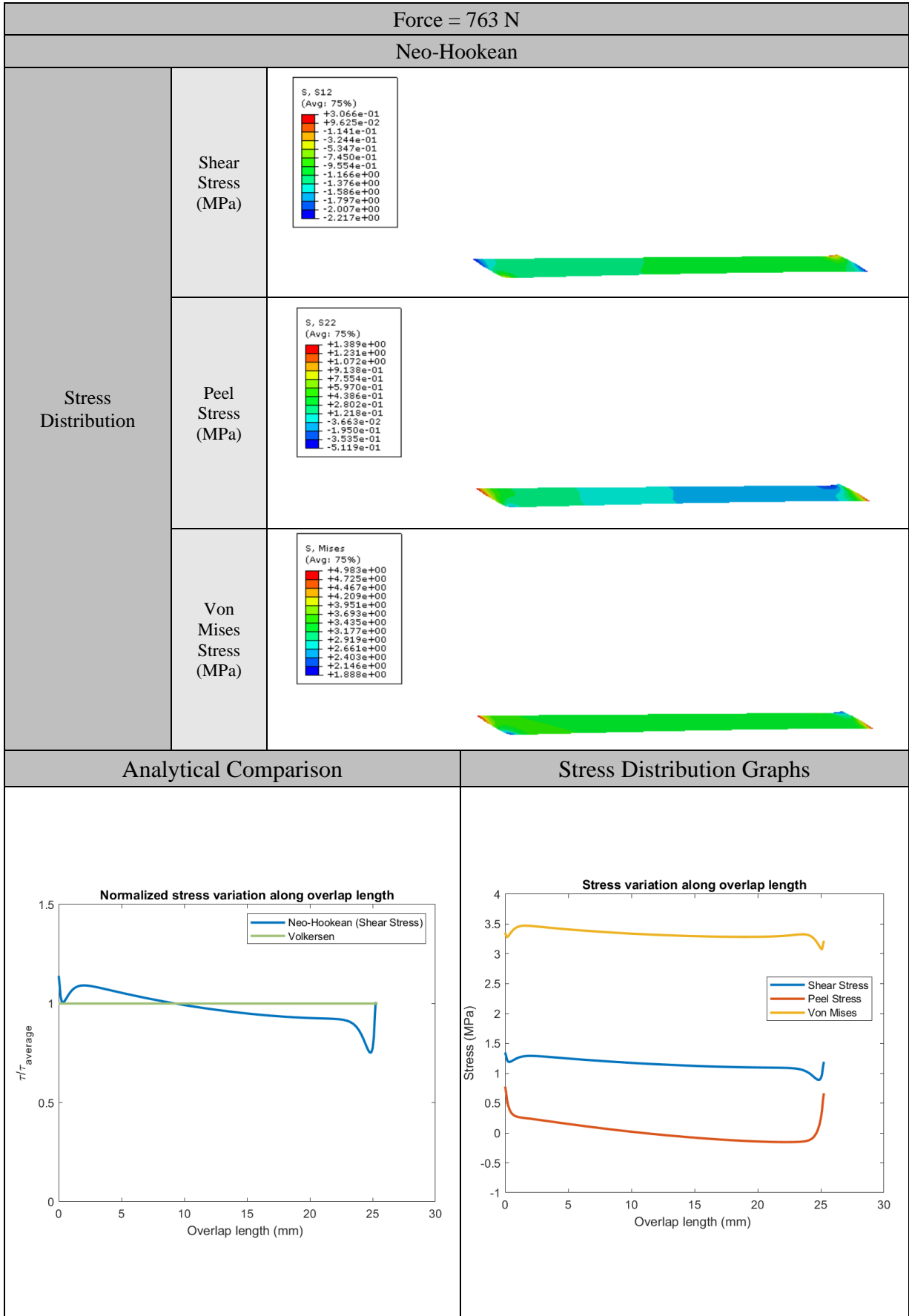
Mooney-Rivlin



Analytical Comparison

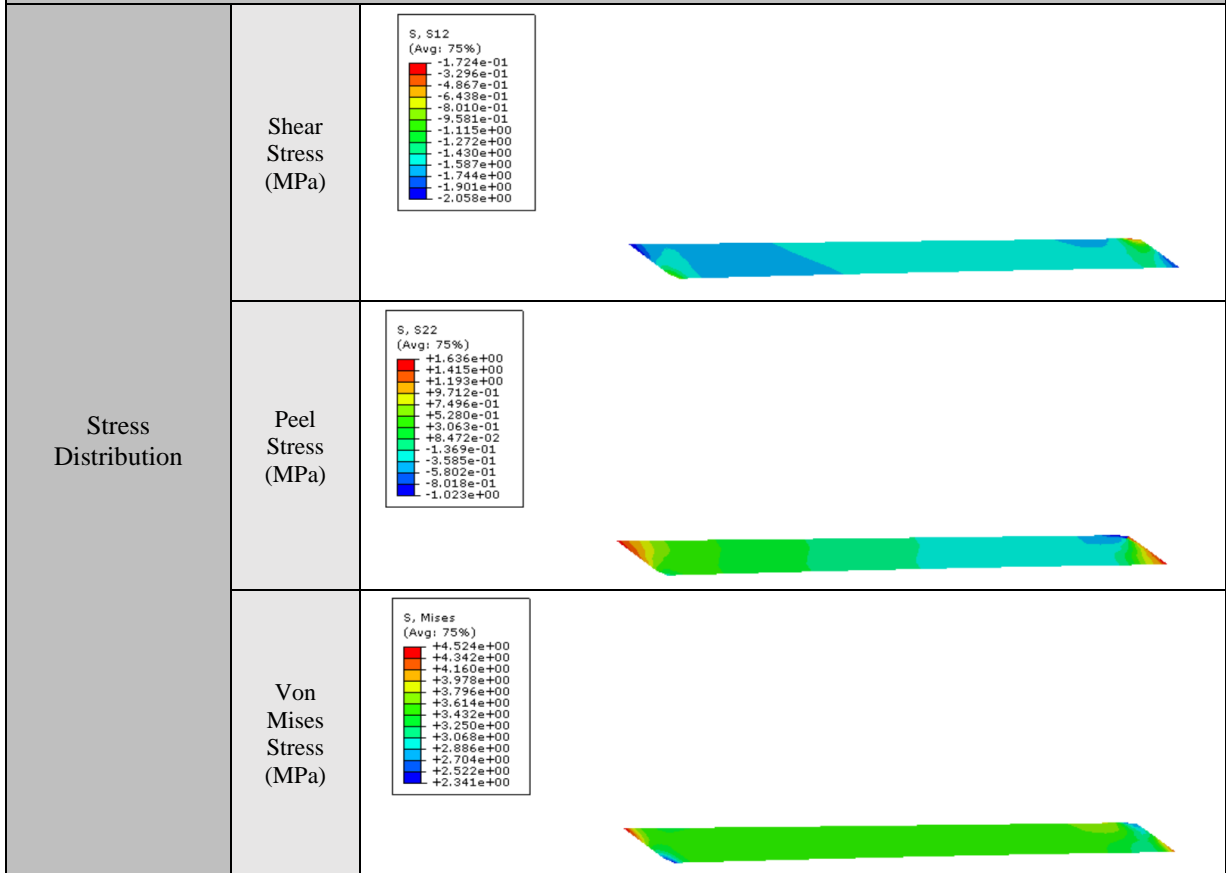
Stress Distribution Graphs



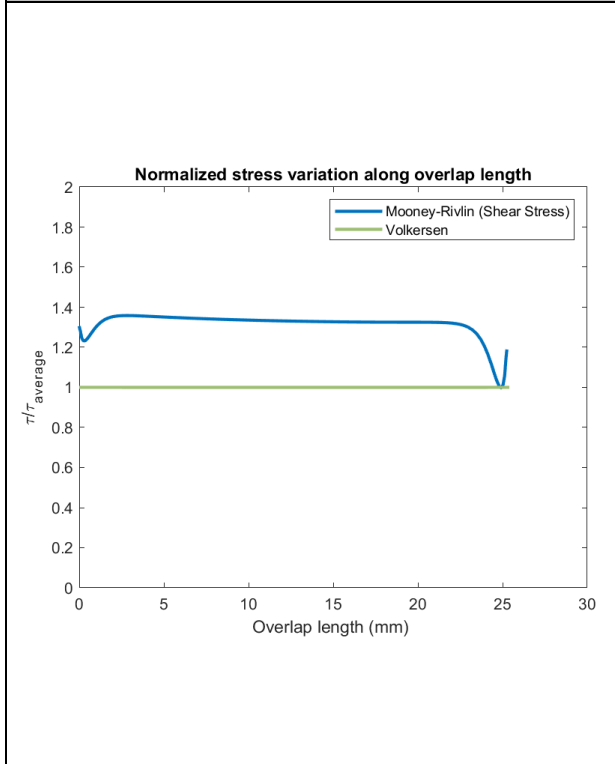


Force = 763 N

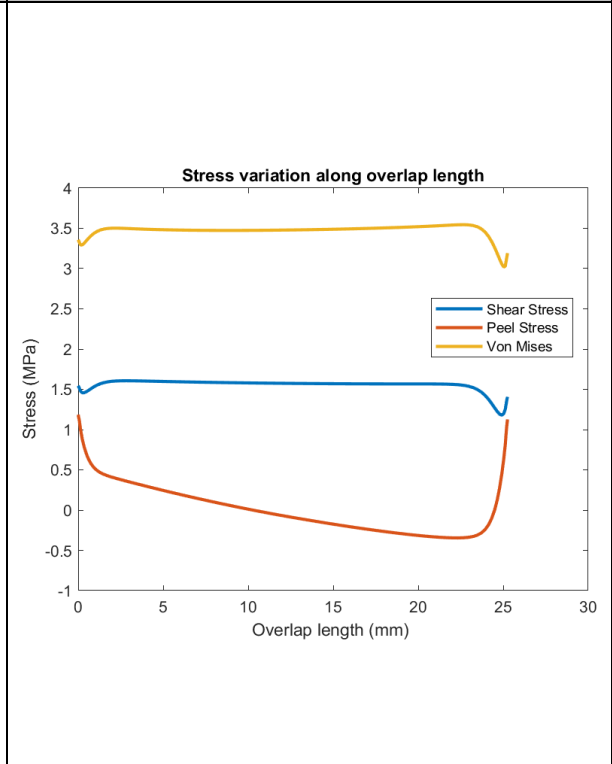
Mooney-Rivlin



Analytical Comparison



Stress Distribution Graphs



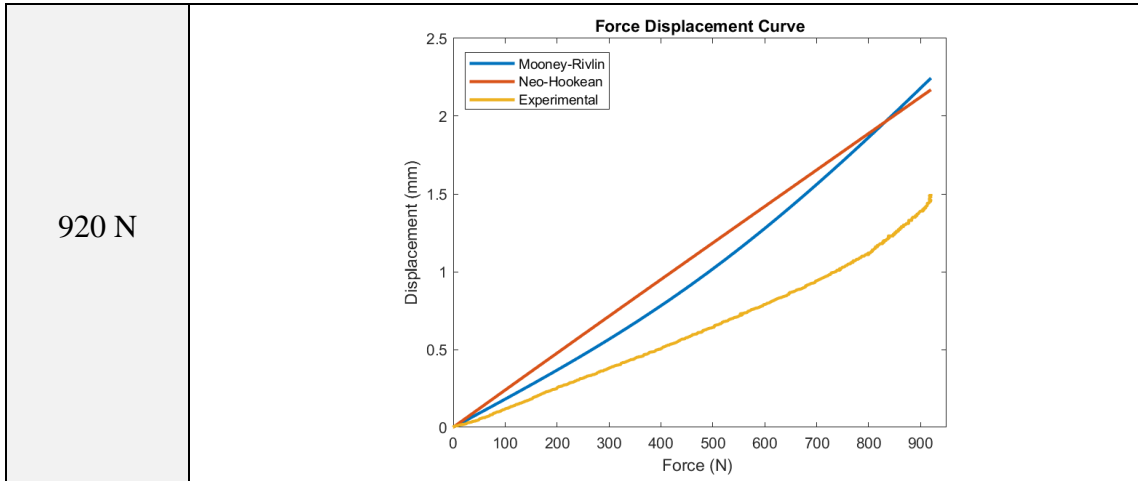
8.1.2. Force-Displacement Curves

In addition to the stress distribution plots, the force-displacement curves are plotted to compare the numerical simulation results to the obtained experimental data. The force- displacement curves are plotted for the three tested samples having different adhesive thicknesses at the previously selected operating conditions (Testing Temperature = 25°C, Loading Rate = 10 mm/min). The maximum force obtained for each tested sample is incorporated as a load and the respective displacement is extracted. The numerical results are then coplotted with the obtained experimental results.

- **For adhesive thickness = 0.76 mm:**

Table 17. Numerical force-displacement curves coplotted with the experimental results for the selected joints having a 0.76mm adhesive bondline thickness.

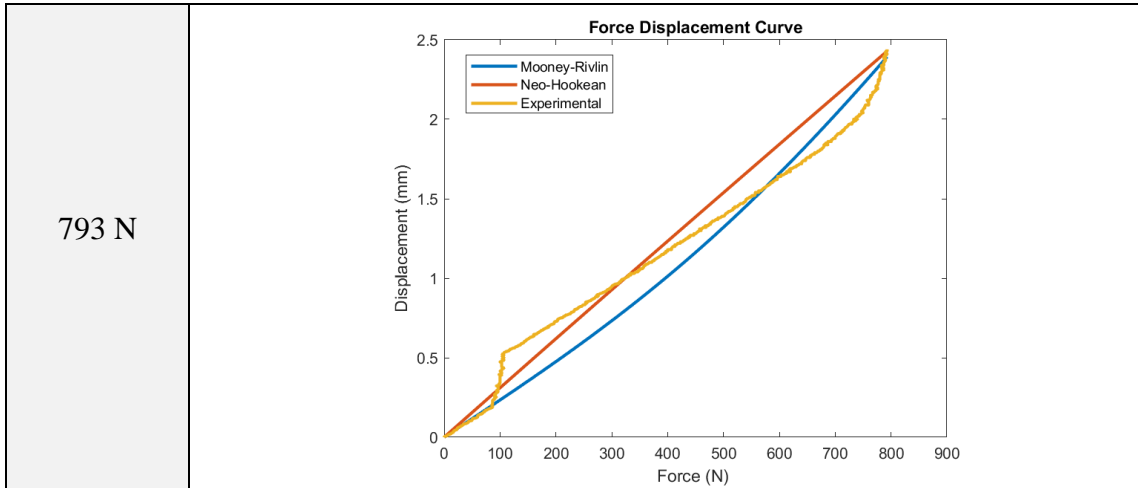
Force	Results
753 N	
900 N	



- **For adhesive thickness = 1 mm:**

Table 18. Numerical force-displacement curves coplotted with the experimental results for the selected joints having a 1mm adhesive bondline thickness.

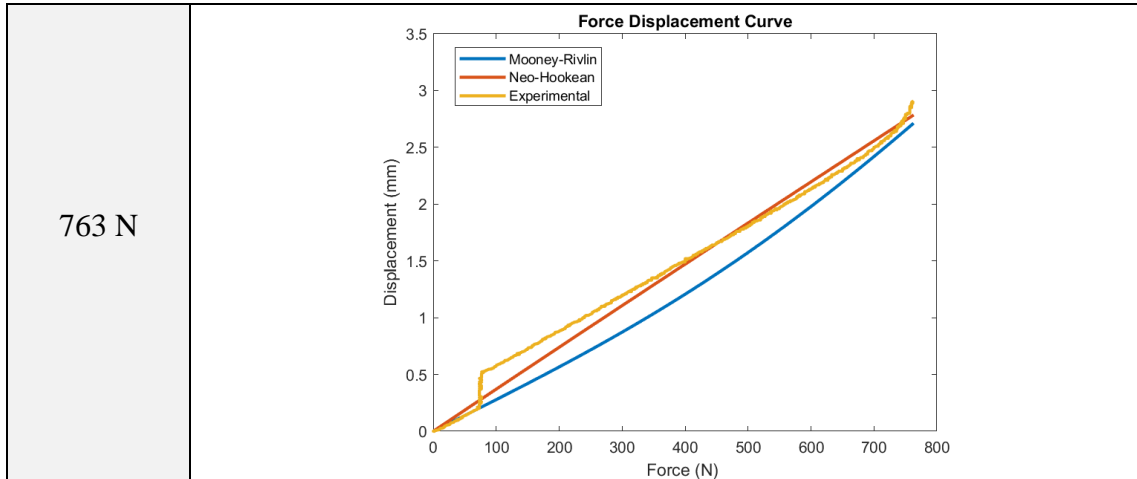
Force	Results
650 N	
787 N	



- For adhesive thickness = 1.2 mm:

Table 19. Numerical force-displacement curves coplotted with the experimental results for the selected joints having a 1.2mm adhesive bondline thickness.

Force	Results
577 N	
703 N	



8.2. Numerical Results Discussion

Although both models provided close results to the analytical solution, the Mooney-Rivlin model tends to slightly overestimate the shear stress distribution while the Neo-Hookean model provided an accurate shear stress distribution compared to the Volkersen analytical solution. Moreover, the asymmetry of the obtained stress distributions is a result of implementing the dissimilar adherends having different young's moduli. On the other hand, both models provided an accurate reproduction of the experimental force-displacement curves. The Mooney-Rivlin model was also capable in precisely replicating the nonlinear adhesive behavior in the experimental force-displacement graphs. Consequently, both models produced an accurate representation of the adhesive behavior under the specified load with minimal input data.

CHAPTER 9

CONCLUSION

In the presented study, various conclusions can be extracted regarding the performance of the MS polymer flexible adhesive under variable testing conditions and adhesive bondline thickness. Moreover, the hyperelastic numerical model provided accurate results compared to the Volkersen analytical solution. The significant inferences that can be deduced from this study can be summarized as follows:

1. Shear strength of single lap joints bonded with MS polymer adhesive generally decreased with temperature. However, upon increasing the testing temperature within the adhesive's heat resistance range, the strain rate effect was more evident and resulted in enhanced single lap joint strength.
2. Higher loading rates resulted in increased shear strength of single lap joints bonded with the flexible MS polymer adhesive.
3. ANOVA analysis signified that testing temperature has a larger contribution to the single lap joint shear strength compared to loading rate.
4. Increasing the adhesive bondline thickness resulted in a linear decrease in the lap shear strength.
5. The hyperelastic numerical model provided impressive accuracy in replicating the experimental force-displacement results. Moreover, the hyperelastic model was capable in accurately predicting the shear stress distribution along the adhesive bondline compared to the Volkersen solution.

APPENDIX

Table 20. Experimental testing summary for single lap joints tested under variable testing temperature and loading rate.

Specimen Number	Testing Temperature (°C)	Loading Rate (mm/min)	Failure Load (N)	Shear Strength (MPa)	Average Shear Strength (MPa)	Standard Error
1	25	1	786	1.22	1.16	0.051
2			680	1.05		
3			770	1.19		
4		10	753	1.17	1.33	0.082
5			920	1.43		
6			900	1.40		
7		250	827	1.28	1.70	0.248
8			1380	2.14		
9			1080	1.67		
10	40	1	540	0.84	1.11	0.224
11			1000	1.55		
12			600	0.93		
13		10	877	1.36	1.13	0.121
14			617	0.96		
15			686	1.06		
16		250	926	1.44	1.56	0.235
17			1300	2.02		
18			793	1.23		
19	55	1	437	0.68	0.82	0.102
20			500	0.78		
21			658	1.02		
22		10	947	1.47	1.34	0.083
23			880	1.36		
24			763	1.18		
25		250	1320	2.05	1.83	0.130
26			1030	1.60		
27			1190	1.84		
28	100	1	117	0.18	0.25	0.085
29			273	0.42		
30			100	0.16		
31		10	307	0.48	0.30	0.087
32			133	0.21		
33			143	0.22		
34		250	563	0.87	0.68	0.106
35			430	0.67		
36			327	0.51		

Table 21. Experimental testing summary for single lap joints fabricated with different bondline thicknesses.

Specimen Name	Adhesive Thickness (mm)	Failure Load (N)	Shear Strength (MPa)	Average Shear Strength (MPa)	Standard Error
1-A	1	793	1.23	1.15	0.072
1-B		650	1.01		
1-C		787	1.22		
1.2-A	1.2	703	1.09	1.06	0.085
1.2-B		577	0.89		
1.2-C		763	1.18		

REFERENCES

- [1] R. H. Goudarzi and M. R. Khedmati, "An experimental and numerical investigation of adhesive bond strength in Al-GFRP single lap and double butt lap joints due to applied longitudinal loads," *Ships Offshore Struct.*, vol. 15, no. 4, pp. 403–416, 2020, doi: 10.1080/17445302.2019.1659879.
- [2] A. V Pocius, "Adhesion and Adhesives Technology," A. V. B. T.-A. and A. T. (Third E. Pocius, Ed. Hanser, 2012, pp. I–XVI.
- [3] A. J. Kinloch, "Adhesion and adhesives: science and technology." Chapman and Hall: New York, 1987.
- [4] G. Jeevi, S. K. Nayak, and M. Abdul Kader, "Review on adhesive joints and their application in hybrid composite structures," *J. Adhes. Sci. Technol.*, vol. 33, no. 14, pp. 1497–1520, Jul. 2019, doi: 10.1080/01694243.2018.1543528.
- [5] D. A. DILLARD, "Chapter 1 - Fundamentals of stress transfer in bonded systems," D. A. Dillard, A. V Pocius, and M. B. T.-A. S. and E. Chaudhury, Eds. Amsterdam: Elsevier Science B.V., 2002, pp. 1–44.
- [6] E. Sancaktar, *Handbook of Adhesion Technology*. 2017.
- [7] K. D. PATE, "Chapter 25 - Applications of adhesives in aerospace," D. A. Dillard, A. V Pocius, and M. B. T.-A. S. and E. Chaudhury, Eds. Amsterdam: Elsevier Science B.V., 2002, pp. 1129–1192.
- [8] O. Volkersen, "Die Nietkraftverteilung in zugbeanspruchten Nietverbindungen mit konstanten Laschenquerschnitten," *Luftfahrtforschung*, vol. 15, pp. 41–47, 1938.
- [9] E. Reissner and M. Goland, "The stress in cemented joints," *J. Appl. Mech*, vol. 66, pp. A17–A27, 1944.
- [10] R. D. Adams, "Strength Predictions for Lap Joints, Especially with Composite Adherends. A Review," *J. Adhes.*, vol. 30, no. 1–4, pp. 219–242, Jan. 1989, doi: 10.1080/00218468908048207.
- [11] D. N. Markatos, K. I. Tserpes, E. Rau, S. Markus, B. Ehrhart, and S. Pantelakis, "The effects of manufacturing-induced and in-service related bonding quality reduction on the mode-I fracture toughness of composite bonded joints for aeronautical use," *Compos. Part B Eng.*, vol. 45, no. 1, pp. 556–564, 2013, doi: <https://doi.org/10.1016/j.compositesb.2012.05.052>.
- [12] R. S. Pierce and B. G. Falzon, "Simulating Resin Infusion through Textile Reinforcement Materials for the Manufacture of Complex Composite Structures," *Engineering*, vol. 3, no. 5, pp. 596–607, 2017, doi: <https://doi.org/10.1016/J.ENG.2017.04.006>.
- [13] R. A. Pethrick, "9 - Composite to metal bonding in aerospace and other applications," in *Woodhead Publishing Series in Welding and Other Joining Technologies*, M. C. B. T.-W. and J. of A. M. Chaturvedi, Ed. Woodhead Publishing, 2012, pp. 288–319.
- [14] S. B. T.-A. T. H. (Second E. Ebnesajjad, Ed., "Chapter 1 - Introduction and Adhesion Theories," Norwich, NY: William Andrew Publishing, 2009, pp. 1–19.
- [15] H. M. Clearfield, D. K. McNamara, and G. D. Davis, "Adherend Surface Preparation for Structural Adhesive Bonding," in *Adhesive Bonding*, 1991.
- [16] M. Ohring, "Chapter 12 - Mechanical Properties of Thin Films," M. B. T.-M. S. of T. F. (Second E. Ohring, Ed. San Diego: Academic Press, 2002, pp. 711–781.

- [17] E. M. Petrie, “8 - Adhesive bonding of textiles: principles, types of adhesive and methods of use,” in *Woodhead Publishing Series in Textiles*, I. Jones and G. K. B. T.-J. T. Stylios, Eds. Woodhead Publishing, 2013, pp. 225–274.
- [18] K. J. Abbey and D. J. Zalucha, “The Chemistry of Structural Adhesives: Epoxy, Urethane, and Acrylic Adhesives BT - Handbook of Industrial Chemistry and Biotechnology,” J. A. Kent, Ed. Boston, MA: Springer US, 2012, pp. 549–572.
- [19] S. M. Guillaume, “Advances in the synthesis of silyl-modified polymers (SMPs),” *Polym. Chem.*, vol. 9, no. 15, pp. 1911–1926, 2018, doi: 10.1039/C8PY00265G.
- [20] B. R. Burchardt and P. W. Merz, “Chapter 6 - Elastic Bonding and Sealing in Industry,” in *Adhesives and Sealants*, vol. 2, P. B. T.-H. of A. and S. Cognard, Ed. Elsevier Science Ltd, 2006, pp. 355–xlii.
- [21] S. R. Taylor, “Coatings for Corrosion Protection: Organic,” K. H. J. Buschow, R. W. Cahn, M. C. Flemings, B. Ilshner, E. J. Kramer, S. Mahajan, and P. B. T.-E. of M. S. and T. Veyssi re, Eds. Oxford: Elsevier, 2001, pp. 1274–1279.
- [22] C. Chen, B. Li, M. Kanari, and D. Lu, “Epoxy Adhesives,” 2019.
- [23] H. Abdellaoui, M. Raji, R. Bouhfid, and A. el kacem Qaiss, “2 - Investigation of the deformation behavior of epoxy-based composite materials,” in *Woodhead Publishing Series in Composites Science and Engineering*, M. Jawaid, M. Thariq, and N. B. T.-F. A. in B. Saba Fibre-Reinforced Composites and Hybrid Composites, Eds. Woodhead Publishing, 2019, pp. 29–49.
- [24] F.-L. Jin, X. Li, and S.-J. Park, “Synthesis and application of epoxy resins: A review,” *J. Ind. Eng. Chem.*, vol. 29, pp. 1–11, 2015, doi: <https://doi.org/10.1016/j.jiec.2015.03.026>.
- [25] Y. Zaokari, A. Persaud, and A. Ibrahim, “Biomaterials for Adhesion in Orthopedic Applications: A Review,” *Eng. Regen.*, vol. 1, pp. 51–63, 2020, doi: <https://doi.org/10.1016/j.engreg.2020.07.002>.
- [26] M. M. Rahman, M. M. Rabbani, and J. K. Saha, “Polyurethane and Its Derivatives BT - Functional Polymers,” M. A. Jafar Mazumder, H. Sheardown, and A. Al-Ahmed, Eds. Cham: Springer International Publishing, 2018, pp. 1–16.
- [27] M. D. Banea and L. F. M. da Silva, “Adhesively bonded joints in composite materials: An overview,” *Proc. Inst. Mech. Eng. Part L J. Mater. Des. Appl.*, vol. 223, no. 1, pp. 1–18, Jan. 2009, doi: 10.1243/14644207JMDA219.
- [28] B. H. Edwards, “Polyurethane Structural Adhesives BT - Structural Adhesives: Chemistry and Technology,” S. R. Hartshorn, Ed. Boston, MA: Springer US, 1986, pp. 181–215.
- [29] Z. Li *et al.*, “Highly Conductive, Flexible, Polyurethane-Based Adhesives for Flexible and Printed Electronics,” *Adv. Funct. Mater.*, vol. 23, no. 11, pp. 1459–1465, Mar. 2013, doi: <https://doi.org/10.1002/adfm.201202249>.
- [30] B. Liesenfeld, “Superparamagnetic folate-immobilized dye labeled microspheres for oral cancer screening,” 2004.
- [31] B. Trobentar, S. Glode , and B. Zafosnik, “Gear tooth deflection of spur polymer gears,” P. B. T.-I. G. C. 2014: 26th–28th A. 2014 Vexex Lyon, Ed. Oxford: Chandos Publishing, 2014, pp. 129–137.
- [32] R. Raihan, M. R. P. Elenchezian, and V. Vadlamudi, “Durability of bonded composite systems,” in *Durability of Composite Systems*, 2020.
- [33] P. Hu, Z. W. Shi, X. X. Wang, W. D. Li, S. G. Zhou, and X. Han, “Strength degradation of adhesively bonded single-lap joints in a cyclic-temperature

- environment using a cohesive zone model,” *J. Adhes.*, vol. 91, no. 8, pp. 587–603, 2015, doi: 10.1080/00218464.2014.915754.
- [34] F. A. Stuparu, D. A. Apostol, D. M. Constantinescu, C. R. Picu, M. Sandu, and S. Sorohan, “Cohesive and XFEM evaluation of adhesive failure for dissimilar single-lap joints,” *Procedia Struct. Integr.*, vol. 2, pp. 316–325, 2016, doi: 10.1016/j.prostr.2016.06.041.
- [35] C. Barile, C. Casavola, V. Moramarco, and C. Pappalettere, “Bonding Characteristics of Single- and Joggled-Lap CFRP Specimens : Mechanical and Acoustic Investigations,” *Appl. Sci.*, 2020.
- [36] M. F. S. F. de Moura, R. Daniaud, and A. G. Magalhães, “Simulation of mechanical behaviour of composite bonded joints containing strip defects,” *Int. J. Adhes. Adhes.*, vol. 26, no. 6, pp. 464–473, 2006, doi: <https://doi.org/10.1016/j.ijadhadh.2005.06.010>.
- [37] M. D. Banea, L. F. M. da Silva, and R. D. S. G. Campilho, “Effect of temperature on the shear strength of aluminium single lap bonded joints for high temperature applications,” *J. Adhes. Sci. Technol.*, vol. 28, no. 14–15, pp. 1367–1381, Jul. 2014, doi: 10.1080/01694243.2012.697388.
- [38] C. Bellini, G. Parodo, and L. Sorrentino, “Effect of operating temperature on aged single lap bonded joints,” *Def. Technol.*, vol. 16, no. 2, pp. 283–289, 2020, doi: <https://doi.org/10.1016/j.dt.2019.05.015>.
- [39] J. Na, Y. Liu, Y. Fan, W. Mu, X. Chen, and Y. Yan, “Effect of temperature on the joint strength of a silyl-modified polymer-based adhesive,” *J. Adhes.*, vol. 93, no. 8, pp. 626–639, Jul. 2017, doi: 10.1080/00218464.2015.1128330.
- [40] H. C. Mattos, L. Nunes, and A. H. Monteiro, “LOAD RATE EFFECTS IN ADHESIVE SINGLE LAP JOINTS BONDED WITH EPOXY/CERAMIC COMPOSITES,” *Lat. Am. J. Solids Struct.*, vol. 13, pp. 1878–1892, 2016.
- [41] S. Wang, W. Liang, L. Duan, G. Li, and J. Cui, “Effects of loading rates on mechanical property and failure behavior of single-lap adhesive joints with carbon fiber reinforced plastics and aluminum alloys,” *Int. J. Adv. Manuf. Technol.*, vol. 106, no. 5, pp. 2569–2581, 2020, doi: 10.1007/s00170-019-04804-w.
- [42] K. Wei, Y. Chen, M. Li, and X. Yang, “Strength and Failure Mechanism of Composite-Steel Adhesive Bond Single Lap Joints,” *Adv. Mater. Sci. Eng.*, vol. 2018, pp. 1–10, 2018, doi: 10.1155/2018/5810180.
- [43] M.-S. Seong, T.-H. Kim, K.-H. Nguyen, J.-H. Kweon, and J.-H. Choi, “A parametric study on the failure of bonded single-lap joints of carbon composite and aluminum,” *Compos. Struct.*, vol. 86, no. 1, pp. 135–145, 2008, doi: <https://doi.org/10.1016/j.compstruct.2008.03.026>.
- [44] L. F. M. da Silva and R. D. S. G. Campilho, “2 - Design of adhesively-bonded composite joints,” A. P. B. T.-F. and F. of A.-B. C. J. Vassilopoulos, Ed. Woodhead Publishing, 2015, pp. 43–71.
- [45] J. A. B. P. Neto, R. D. S. G. Campilho, and L. F. M. da Silva, “Parametric study of adhesive joints with composites,” *Int. J. Adhes. Adhes.*, vol. 37, pp. 96–101, 2012, doi: <https://doi.org/10.1016/j.ijadhadh.2012.01.019>.
- [46] L. F. M. da Silva, T. N. S. S. Rodrigues, M. A. V. Figueiredo, M. F. S. F. de Moura, and J. A. G. Chousal, “Effect of Adhesive Type and Thickness on the Lap Shear Strength,” *J. Adhes.*, vol. 82, no. 11, pp. 1091–1115, Nov. 2006, doi: 10.1080/00218460600948511.

- [47] R. Kahraman, M. Sunar, and B. Yilbas, “Influence of adhesive thickness and filler content on the mechanical performance of aluminum single-lap joints bonded with aluminum powder filled epoxy adhesive,” *J. Mater. Process. Technol.*, vol. 205, no. 1, pp. 183–189, 2008, doi: <https://doi.org/10.1016/j.jmatprotec.2007.11.121>.
- [48] A. P. Pisharody, B. Blandford, D. E. Smith, and D. A. Jack, “An experimental investigation on the effect of adhesive distribution on strength of bonded joints,” *Appl. Adhes. Sci.*, vol. 7, no. 1, p. 6, 2019, doi: 10.1186/s40563-019-0122-y.
- [49] Y. Boutar, S. Naïmi, S. Mezlini, and M. B. S. Ali, “Effect of surface treatment on the shear strength of aluminium adhesive single-lap joints for automotive applications,” *Int. J. Adhes. Adhes.*, vol. 67, pp. 38–43, 2016, doi: <https://doi.org/10.1016/j.ijadhadh.2015.12.023>.
- [50] K. Diharjo, M. Anwar, R. A. P. Tarigan, and A. Rivai, “Effect of adhesive thickness and surface treatment on shear strength on single lap joint Al/CFRP using adhesive of epoxy/Al fine powder,” *AIP Conf. Proc.*, vol. 1710, no. 1, p. 30030, Feb. 2016, doi: 10.1063/1.4941496.
- [51] C.-T. Hoang-Ngoc and E. Paroissien, “Simulation of Single-Lap Bonded and Hybrid (Bolted/Bonded) Joints with Flexible Adhesive,” *Int. J. Adhes. Adhes. - INT J ADHES ADHES*, vol. 30, pp. 117–129, Apr. 2010, doi: 10.1016/j.ijadhadh.2009.12.002.
- [52] D. Moreira and L. C. Nunes, “Comparison of simple and pure shear for an incompressible isotropic hyperelastic material under large deformation,” *Polym. Test.*, vol. 32, pp. 240–248, Apr. 2013, doi: 10.1016/j.polymertesting.2012.11.005.
- [53] Y. Boutar, S. Naimi, S. Mezlini, L. F. M. Silva, M. Hamdaoui, and M. Ali, “Effect of adhesive thickness and surface roughness on the shear strength of aluminium one-component polyurethane adhesive single-lap joints for automotive applications,” *J. Adhes. Sci. Technol.*, vol. 30, pp. 1–17, Apr. 2016, doi: 10.1080/01694243.2016.1170588.
- [54] J. Pirvics, “Two Dimensional Displacement-Stress Distributions in Adhesive Bonded Composite Structures,” *J. Adhes.*, vol. 6, no. 3, pp. 207–228, Jan. 1974, doi: 10.1080/00218467408075027.
- [55] I. U. Ojalvo and H. L. Eidinoff, “Bond Thickness Effects upon Stresses in Single-Lap Adhesive Joints,” *AIAA J.*, vol. 16, no. 3, pp. 204–211, Mar. 1978, doi: 10.2514/3.60878.
- [56] L. F. M. Silva, M. Costa, G. Viana, and R. Campilho, “Chapter 2. Analytical Modelling for the Single-Lap Joint,” 2016, pp. 8–46.
- [57] L. F. M. da Silva, P. J. C. das Neves, R. D. Adams, and J. K. Spelt, “Analytical models of adhesively bonded joints—Part I: Literature survey,” *Int. J. Adhes. Adhes.*, vol. 29, no. 3, pp. 319–330, 2009, doi: <https://doi.org/10.1016/j.ijadhadh.2008.06.005>.
- [58] D. A. Dillard, “Fundamentals of stress transfer in bonded systems,” *Adhes. Sci. Eng.*, pp. 1–44, 2002, doi: 10.1016/b978-0-444-51140-9.50028-7.
- [59] A. V. Pocius, “Mechanical Tests of Adhesive Bond Performance,” in *Adhesion and Adhesives Technology*, 2012, pp. 47–83.
- [60] L. D. R. Grant, R. D. Adams, and L. F. M. da Silva, “Experimental and numerical analysis of single-lap joints for the automotive industry,” *Int. J. Adhes. Adhes.*, vol. 29, no. 4, pp. 405–413, 2009, doi:

- <https://doi.org/10.1016/j.ijadhadh.2008.09.001>.
- [61] A. Kwakernaak, J. Hofstede, J. Poullis, and R. Benedictus, “8 - Improvements in bonding metals for aerospace and other applications,” in *Woodhead Publishing Series in Welding and Other Joining Technologies*, M. C. B. T.-W. and J. of A. M. Chaturvedi, Ed. Woodhead Publishing, 2012, pp. 235–287.
- [62] L. F. M. da Silva, E. A. S. Marques, and R. D. S. G. Campilho, “Design Rules and Methods to Improve Joint Strength BT - Handbook of Adhesion Technology,” L. F. M. da Silva, A. Öchsner, and R. D. Adams, Eds. Cham: Springer International Publishing, 2018, pp. 773–810.
- [63] D. B. Richardson, T. Z. Blanzymski, E. N. Gregory, A. R. Hutchinson, and L. M. Wyatt, “16 - Manufacturing methods,” E. H. B. T.-M. E. R. B. (Twelfth E. Smith, Ed. Butterworth-Heinemann, 1994, pp. 16–112.
- [64] R. D. Adams and V. Mallick, “The Effect of Temperature on the Strength of Adhesively-Bonded Composite-Aluminium Joints,” *J. Adhes.*, vol. 43, no. 1–2, pp. 17–33, Nov. 1993, doi: 10.1080/00218469308026585.
- [65] M. D. Banea and L. F. M. da Silva, “The effect of temperature on the mechanical properties of adhesives for the automotive industry,” *Proc. Inst. Mech. Eng.*, vol. 224, no. L2, pp. 51–62, 2010, [Online]. Available: <https://www.proquest.com/scholarly-journals/effect-temperature-on-mechanical-properties/docview/366313349/se-2?accountid=8555>.
- [66] J. Richeton, S. Ahzi, K. S. Vecchio, F. C. Jiang, and R. R. Adharapurapu, “Influence of temperature and strain rate on the mechanical behavior of three amorphous polymers: Characterization and modeling of the compressive yield stress,” *Int. J. Solids Struct.*, vol. 43, no. 7, pp. 2318–2335, 2006, doi: <https://doi.org/10.1016/j.ijsolstr.2005.06.040>.
- [67] G. M. Swallowe, “Strain Rate Effects BT - Mechanical Properties and Testing of Polymers: An A–Z Reference,” G. M. Swallowe, Ed. Dordrecht: Springer Netherlands, 1999, pp. 214–218.
- [68] X. Liu, X. Shao, Q. Li, and G. Sun, “Experimental study on residual properties of carbon fibre reinforced plastic (CFRP) and aluminum single-lap adhesive joints at different strain rates after transverse pre-impact,” *Compos. Part A Appl. Sci. Manuf.*, vol. 124, p. 105372, 2019, doi: <https://doi.org/10.1016/j.compositesa.2019.03.018>.
- [69] F. Zhang, X. Yang, Y. Xia, Q. Zhou, H.-P. Wang, and T.-X. Yu, “Experimental study of strain rate effects on the strength of adhesively bonded joints after hygrothermal exposure,” *Int. J. Adhes. Adhes.*, vol. 56, pp. 3–12, 2015, doi: <https://doi.org/10.1016/j.ijadhadh.2014.07.008>.
- [70] A. A. Bezemer, C. B. Guyt, and A. Vlot, “New impact specimen for adhesives: optimization of high-speed-loaded adhesive joints,” *Int. J. Adhes. Adhes.*, vol. 18, no. 4, pp. 255–260, 1998, doi: [https://doi.org/10.1016/S0143-7496\(97\)00032-8](https://doi.org/10.1016/S0143-7496(97)00032-8).
- [71] G. Amos, G. R. K., and R. G. D., “Strain Rate Sensitivity of Epoxy Resin in Tensile and Shear Loading,” *J. Aerosp. Eng.*, vol. 20, no. 2, pp. 75–89, Apr. 2007, doi: 10.1061/(ASCE)0893-1321(2007)20:2(75).
- [72] R. D. Adams and N. A. Peppiatt, “Stress analysis of adhesive-bonded lap joints,” *J. strain Anal.*, vol. 9, no. 3, pp. 185–196, 1974.
- [73] B. Duncan, “14 - Developments in testing adhesive joints,” in *Woodhead Publishing in Materials*, D. A. B. T.-A. in S. A. B. Dillard, Ed. Woodhead Publishing, 2010, pp. 389–436.

- [74] Matweb, “MatWeb, Material property data,” *MatWeb*, 2015.
- [75] S. Hassan, C. Santulli, M. Yahya, C. Gang, and B. Abu, “The potential of biomimetics design in the development of impact resistant material,” *FME Trans.*, vol. 46, pp. 108–116, Jan. 2018, doi: 10.5937/fmet1801108H.
- [76] D. Brewis, “4 - Surfaces: how to treat,” in *Woodhead Publishing Series in Welding and Other Joining Technologies*, R. D. B. T.-A. B. Adams, Ed. Woodhead Publishing, 2005, pp. 75–88.
- [77] A. A. Baker and J. Wang, “Chapter Six - Adhesively Bonded Repair/Reinforcement of Metallic Airframe Components: Materials, Processes, Design and Proposed Through-Life Management,” R. Jones, A. Baker, N. Matthews, and V. B. T.-A. S. and R. Champagne, Eds. Boston: Butterworth-Heinemann, 2018, pp. 191–252.
- [78] A. A. Baker, “2 - Repair of metallic airframe components using fibre-reinforced polymer (FRP) composites,” V. M. B. T.-R. of M. C. I. U. F. R. P. (FRP) C. Karbhari, Ed. Woodhead Publishing, 2014, pp. 11–59.
- [79] M. F. Bahbou, P. Nylén, and J. Wigren, “Effect of grit blasting and spraying angle on the adhesion strength of a plasma-sprayed coating,” *J. Therm. Spray Technol.*, vol. 13, no. 4, pp. 508–514, Dec. 2004, doi: <http://dx.doi.org/10.1361/10599630421406>.
- [80] H. C. J. Hoefsloot, D. J. Vis, J. A. Westerhuis, A. K. Smilde, and J. J. Jansen, “2.23 - Multiset Data Analysis: ANOVA Simultaneous Component Analysis and Related Methods,” S. D. Brown, R. Tauler, and B. B. T.-C. C. Walczak, Eds. Oxford: Elsevier, 2009, pp. 453–472.
- [81] N. R. Smalheiser, “Chapter 11 - ANOVA,” N. R. B. T.-D. L. Smalheiser, Ed. Academic Press, 2017, pp. 149–155.
- [82] E. A. Campo, “2 - Mechanical Properties of Polymeric Materials,” in *Plastics Design Library*, E. A. B. T.-S. of P. M. Campo, Ed. Norwich, NY: William Andrew Publishing, 2008, pp. 41–101.
- [83] H. Ren, X. Chen, and Y. Chen, “Chapter 3 - Aircraft Reliability and Maintainability Analysis and Design,” in *Aerospace Engineering*, H. Ren, X. Chen, and Y. B. T.-R. B. A. M. O. and A. Chen, Eds. Academic Press, 2017, pp. 37–78.
- [84] H. Nezhad and D. Stratakis, “PERFORMANCE OF AEROSPACE COMPOSITES IN THE PRESENCE OF PROCESS-INDUCED DEFECTS,” 2017.
- [85] F. Asgari Mehrabadi, “Experimental and Numerical Failure Analysis of Adhesive Composite Joints,” *Int. J. Aerosp. Eng.*, vol. 2012, p. 925340, 2012, doi: 10.1155/2012/925340.
- [86] N. M. Rahman and C. T. Sun, “Strength calculation of composite single lap joints with Fiber-Tear-Failure,” *Compos. Part B Eng.*, vol. 62, pp. 249–255, 2014, doi: <https://doi.org/10.1016/j.compositesb.2014.03.004>.
- [87] B. Kim *et al.*, “A Comparison Among Neo-Hookean Model, Mooney-Rivlin Model, and Ogden Model for Chloroprene Rubber,” *Int. J. Precis. Eng. Manuf.*, vol. 13, May 2012, doi: 10.1007/s12541-012-0099-y.
- [88] Z. Guo and L. J. Sluys, “Application of a new constitutive model for the description of rubber-like materials under monotonic loading,” *Int. J. Solids Struct.*, vol. 43, no. 9, pp. 2799–2819, 2006, doi: <https://doi.org/10.1016/j.ijsolstr.2005.06.026>.

- [89] T. V Korochkina, E. H. Jewell, T. C. Claypole, and D. T. Gethin, “Experimental and numerical investigation into nonlinear deformation of silicone rubber pads during ink transfer process,” *Polym. Test.*, vol. 27, no. 6, pp. 778–791, 2008, doi: <https://doi.org/10.1016/j.polymertesting.2008.06.003>.